UNIVERSITY OF CALIFORNIA,
IRVINE

Bacterial Stress Response and Antibiotic Tolerance

THESIS

submitted in partial satisfaction of the requirements
for the degree of

Doctor of Philosophy

in Chemical and Biomolecular Engineering

by

Saba Ranjbar

Thesis Committee:
Associate Professor Allon Hochbaum, Chair
Professor Nancy Da Silva
Assistant Professor Han Li
Assistant Professor Albert Siryaporn

2020

DEDICATION

To

My Family and the Love of My Life

in Recognition of Their Worth

TABLE OF CONTENTS

LIST OF FIGURES

LIST OF TABLES

ACKNOWLEDGEMENTS

I would like to express my deep and sincere gratitude to my research supervisor Professor Allon Hochbaum, who has the attitude and the substance of a genius: he continually and convincingly conveyed a spirit of adventure and critical thinking in regard to research, and an excitement in regard to encouraging me to pursue my goals in my professional life. Without his guidance and persistent help this dissertation would not have been possible.

I would like to thank my committee members, Professor Nancy Da Silva, Professor Han Li, and Professor Albert Siryaporn whose continued encouragement and constructive feedbacks always helped me make this path more professional and successful.

I thank my fellow lab-mates for the stimulating discussions, the sleepless nights we were working together, and for all the fun we have had in the recent years.

Financial support was provided by Air Force Office of Scientific Research award FA9550-17-1-0193, NSF award CHE-1808332, and the Bridge Fellowship.

Special thanks to all my friends living all around the world who have given me their friendship, empathy, and practical help.

I am extremely grateful for my family and their love and support through all these years. They are the main reason for where I am standing today. I would also thank Kamyar for his love, extreme support, and patience throughout this entire process and for making countless sacrifices to help me get to this point.

VITA

Saba Ranjbar
Torrance, CA
Sranjba1@uci.edu

EDUCATION

University of California, Irvine, Irvine, CA, US
Doctor of Philosophy in Chemical and Biomolecular Engineering — Dec 2020

University of California, Irvine, Irvine, CA, US
Master of Science in Chemical and Biochemial Engineering — June 2018

Amirkabir Univesity of Technology, Tehran, Iran
Master of Science in Chemical Engineering-Biotechnology — Sep 2015

Isfahan University of Technology, Isfahan, Iran
Batchelor of Science in Chemical Engineering — Feb 2013

RESEARCH PROJECTS

University of California, Irvine — Oct 2016 – Present

- Studied the role of osmotic stress and use of an enzyme inhibitor to prevent bacterial infection
  - *Confocal Fluorescence Microscopy:* live cell imaging, biovolume quantification with Volocity and Imaris
  - *Microfluidic Device:* device fabrication, flow cell setup design
  - *Mass Spectrometry Analysis:* cell lysis, protein quantification, LC-MS setup optimization (Triple Quadrupole)
- Studied intestinal bacteria functions during iron scavenging conditions
  - *CFU Measurements:* dilution plating, use of CFU counter, data analysis with ImageJ
- Designed wound meat model to investigate the role of reactive oxygen species and antibiotics on bacterial infections
  - *Mammalian Cells:* host microbiota analysis, characterization of bacterial growth on muscle tissue
- Investigated the role of a bacterial metabolite in preventing bacterial infection on medical devices
  - *Biofilm Characterization:* bacterial biofilm development on substrates, quantification with CV staining assay
  - *Microscope Imaging:* epifluorescence microscope imaging of biofilms

Janssen, Pharmaceutical Companies of Johnson & Johnson — Jun 2019 – Sep 2019

- Developed a novel labeling technique for ADC analysis using quantitative proteomics
  - *Sample Preparation:* TMT labeling, protocol design, drug conjugation chemistries
  - *Large Mass-Spectrometric Dataset Analysis:* data dependent MS/MS workflows using Q-Exactive and Fusion Lumos instrumentation, manual interpretation of peptide MS/MS spectra, large scale automated database searches of peptides and modifications using maxQuant, data analysis by Perseus

Amirkabir University of Technology — Sep 2013 – Sep 2015

- Studied biological phenol degradation by using airlift reactor
  - *Quantification:* phenol and biomass analysis
  - *Hydrodynamics of Reactor:* gas holdup, mixing time and gas-liquid

mass transfer determination of the reactor
- *Data Analysis:* fitting models to biological and hydrodynamics data using nonlinear regression in Graphpad Prism

Isfahan University of Technology Sep 2008 – Feb 2013

- Studied the process of biodiesel production from microalgae.
  - *Microalgal Culturing:* photobioreactor design and microalgae cultivation
  - *Cell Harvest to Biodiesel Production:* solvent extraction, transesterification process, liquid-liquid separation.
- Supervised a research group of 4 to study biodiesel production to establish a pilot unit.
- Designed and evaluated cost of biogas power plant using Isfahan municipal wastewater.

RELEVANT WORK EXPERIENCE

Bioprocess Research & Development Intern /PBS Biotech Sep 2020 – Present

- Knowledge of cell therapy manufacturing process development, process optimization, and scale up
- Experiment design, execution, and data processing, to perform cell culture operations in bioreactors up to 80 liters
- Collaborate with engineering department for aeration optimization for iPSCs

Research Assistant /University of California, Irvine Sep 2016 – Sep 2020

- Perform different research projects and submit scientific journal papers
- Supervise six students by training members on lab rules, experimental procedures, and theoretical history
- Manage students' projects, timelines, and lab equipment

COOP Scientist /Janssen (Johnson & Johnson) Jun 2019 – Sep 2019

- Utilized quantitative proteomics methodologies to determine drug conjugation efficiency for early discovery programs
- Collaborated with Targeted Therapeutics Discovery group to analyze ADCs and explore new technologies
- Managed experimentation to deliver all projects within rigorous timelines and establish a new MS-workflow that is submitted for IP
- Created new protocols to automate ADC analysis

Teaching Assistant/University of California, Irvine Jan 2019– Jun 2019

- Co-Instructed multiple sections of Chemical Engineering Design I & II equating to eight hours per week
- Provided assistance to approximately 90 students through in-class learning and one-on-one mentoring

Laboratory Assistant/Amirkabir University of Technology Sep 2014 – Dec 2014

- Tutored 12 graduate students for experimental works in Biotechnology Laboratory course

Engineering Intern/Isfahan Oil Refinery May 2012 – Sep 2012

- Monitored daily processes including starting materials and final product's quality and quantity
- Addressed inefficiencies and energy loss within the system
- Checked process units for environmental compliance

PUBLICATIONS

- Joann Phan, **Saba Ranjbar**, Miki Kagawa, Matthew Gargus, Allon Hochbaum, Katrine Whiteson. "Thriving under stress: *Pseudomonas aeruginosa* outcompetes the background polymicrobial community under treatment conditions in a novel chronic wound model" Frontiers in Cellular and Infection Microbiology, no.10 (2020).
- Arunima Bhattacharjee, Martina Sassone-Corsi, **Saba Ranjbar**, Manuela Raffatellu, Allon Hochbaum. "Inhibition of Bacterial Biofilm Formation by Microcin-Mediated Iron Competition" mBio (Under editorial process.)
- William Thrift, Antony Cabuslay, **Saba Ranjbar**, Allon Hochbaum, Regina Ragan.

”Surface-Enhanced Raman Scattering-Based Odor Compass: Locating Multiple Chemical Sources and Pathogens” ACS Sensors 4, no. 9 (2019): 2311-2319.

- Monfared, Mohammad, Saeed Taghizadeh, Alireza Zare-Hoseinabadi, Seyyed Mojtaba Mousavi, Seyyed Alireza Hashemi, **Saba Ranjbar**, and Ali Mohammad Amani” Emerging frontiers in drug release control by core–shell nanofibers: a review.” Drug metabolism reviews (2019): 1-23.
- Nguyen, Cuong Quoc, William John Thrift, Arunima Bhattacharjee, **Saba Ranjbar**, Tara Gallagher et al.” Longitudinal Monitoring of Biofilm Formation via Robust Surface-Enhanced Raman Scattering Quantification of *Pseudomonas aeruginosa*-Produced Metabolites” ACS applied materials & interfaces 10, no. 15 (2018): 12364-12373.
- **Saba Ranjbar**, Hoda Khesali Aghtaei, Elham Jalilnejad, and Farzaneh Vahabzadeh. ” Application of an airlift reactor with a net draft tube in phenol bio-oxidation using *Ralstonia eutropha*” Desalination and Water Treatment 57, no. 54 (2016): 25972-25984.

HONORS & AWARDS

- PhD bridge fellowship award (2017-18) — Sep 2017
- Credited as the 1st author of 4 for article in “Desalination and Water Treatment Journal” — Sep 2015
- Ranked 3rd in the class of 2015 in department of Chemical Engineering — Sep 2015
- 4-Year national undergraduate fellowship award — Sep 2008

ABSTRACT OF THE THESIS

Bacterial Stress Response and Antibiotic Tolerance

by

Saba Ranjbar

Doctor of Philosophy

University of California, Irvine, 2020

Associate Professor Allon Hochbaum, Chair

Antibiotic resistant pathogens cause more than 2.8 million infections and 35000 deaths in the United States each year. We need unique and effective therapies that will eradicate bacterial colonization, reduce patient suffering, and improve our ability to deliver necessary medications with reduced complications. Unfortunately, making new classes of antibiotics will not solve the antibiotic resistant problem.

Bacteria face different stressful conditions which have an adverse effect on the physiological welfare of bacterial cells. Stress response mechanisms protect cells against stress and make them tolerant to antibiotics. As a result, tolerant cells might be

a source of resistance. Targeting the stress response mechanisms can be a good tool to prevent tolerance.

Throughout this research, different analytical and characterization methods were used to investigate different stress responses from pathogens in different environmental conditions. Additionally, the effects of stress response mechanisms on making cells tolerant to antibiotics was studied. Consequently, this approach was used to develop some strategies for preventing infection. For example, a small molecule was found to be effective against bacterial survival in some stressful environments, and one type of probiotic strain was used to interact with pathogens and prevent the growth by using its stress response mechanism. Using this knowledge, we can find the ways tolerance arises to target mechanisms of tolerance to combat antibiotic resistance as a more time saving strategy.

Chapter 1
Introduction

1.1. Overview

Bacteria face different stressful conditions which have an adverse effect on the physiological welfare of bacterial cells, leading to growth rate reduction, or in more extreme circumstances, to inhibition and/or death [1]. The molecular response mechanisms are triggered by a variety of environmental stimuli, from changes in temperature, pH, nutrient availability, or osmolarity, to host responses to infection by pathogens, and addition of toxic molecules which manifest adaptive and protective responses from the cell. They can repair the damage or return the cell to homeostasis by generation of resistance mutations, alterations to the membrane barrier functions, or promotion of resistant growth modes, such as in biofilms [2].

The attachment of microbial communities to different surfaces is a well-known problem having detrimental effects. The bacterial colonization is recognized to be involved in a variety of critical issues such as, clogging of membrane, corrosion of industrial equipment, infection from implants, and chronic wounds[1] [3].

Biomedical devices such as artificial joint, dental implants, and catheters have become important approaches to save human lives and improve the life quality of patients. On the other hand, bacterial infection is a serious issue related to these devices. Bacteria evidently colonize surfaces of these synthetic materials and cause fatality secondary to antibiotic resistance due to the ineffective and excessive use of antibiotics [4], [5].

These infections often are not detected at an early stage and pose a substantial health risk to patients, the need of reoperation and device replacement which apply considerable costs to the healthcare system [5]. According to Centers of Disease Control and Prevention (CDC) 2019

[1] Chronic wound: A type of that has failed to progress through the phases of healing in an orderly and timely fashion.

report, antibiotic resistant bacteria and fungi cause more than 2.8 million infections and 35000 deaths in the united states each year. This number means that at least one infection every 11 seconds and nearly one death from antibiotic resistance is occurred every 15 minutes [6]. These bacterial infections could be acquired within the intensive care unit; gastrointestinal tract (GI), urinary tract, or wound colonization [7]. These are problems that surgeons and healthcare workers deal with on a daily basis [8]. We need unique and effective therapies that will eradicate bacterial colonization, reduce patient suffering, and improve our ability to deliver necessary medications with reduced complications [8]. Antimicrobial-coated or impregnated catheters, applications of lactic acid bacteria and their antibacterial peptides as probiotics in GI tract, use of bacteriophages, are among the top strategies which have been worked on recently [8], [9].

In addition to medical misuse, inappropriate use of antibiotics in the agricultural setting, results in antibiotic residues in animal-derived products and has a major role in the increase of antibiotic-resistant bacteria. Antibiotics in agriculture are used as growth-promoting agents (90% of the use), improved feed conversion efficiency, or routine disease prevention [10], [11]. In terms of annual applications of antibiotics in the United States agri-food industry, over 8 million kg is for animals and 22000 kg for fruit trees and spraying of the corps. Emergence of antibiotic-resistant bacteria from agricultural products, could spread to humans and cause worse consequences [11].

Regarding undesired industrial problems made by accumulation of bacteria on surfaces, biofouling has a detrimental impact on piping systems, naval industry, and heat exchangers and leads to both economic and environmental issues [12], [13]. For example, marine fouling on ship hulls increases the hydrodynamic drag forces and fuel consumption causing emission of harmful compounds. High rate surface corrosion, protective coatings damages, and increase of cleaning maintenance will cost billions of dollars a year to the maritime industry ($200 M annual cost for the US Navy fleets). Therefore, development of new materials to solve the biofouling problem is of immediate importance [13].

Pathogenic bacteria experience stress from the first moment of contact with the host. Hence, they activate their adaptive responses and regulate the expression of virulence genes to withstand diverse host conditions during infection. The Virulence factors include toxins, adhesins, and iron-acquisition system and polysaccharide coats which commensal strains do not usually have [14].

Biofilm-forming pathogens play a key role in establishing infections. They can switch from the planktonic (freely swimming) state to biofilm state by regulating the gene expression. First stage of bacterial colonization is adhesion to biological and non-biological surfaces [15], [16]. Different types of pilus and adhesins help motile and non-motile cells for next steps in adherence [14], [17]. They make the thick extracellular matrix to facilitate the adaptation and survival. Although this matrix is a mixture of exopolysaccharides, DNA, proteins, and other extracellular polymeric substances to stabilize the biofilm structure, and play protective roles, it can apply osmotic stress to the cells and trigger other stress responses[18]. During the infection development and biofilm maturation, other complex mechanisms are involved to trigger proper responses leading cells to their maximum potential to adapt and survive host-derived stressors. These responses include two component systems, sigma factors, various decarboxylases and genes involved in central metabolism, and membrane composition of the pathogens [19].

Some stressful conditions that bacteria adapt to during infection are the oxygen tension in the gut, anaerobic environment of intestinal lumen [20], osmotic stress environment of urine [21], host-derived antimicrobial compounds, including bactericidal peptides produced by epithelial cells [22], nutrient availability which is high in mammalian gut, and limited in intracellular environments (**Figure *1.1***) [23].

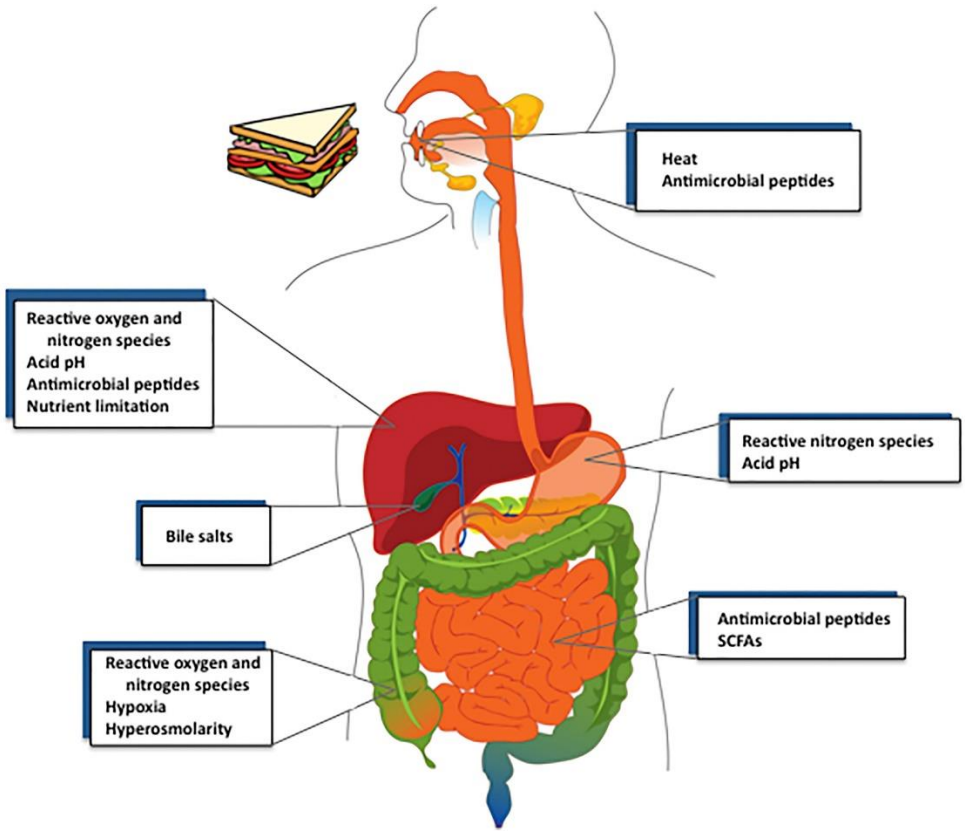

Figure 1.1- Stresses faced by a typical foodborne enteric pathogen (adapted from [23])**.**

Consequently, a better understanding of bacterial strategies for dealing with stresses can provide targets for the development of infection therapeutics, reduce costs of infections/contamination, and improve patient outcomes.

Bacteria use a combination of strategies to counteract stressful environmental stimuli by countering the stress agent, repairing cell damage, or inducing a general stress response to render the bacteria robust to the culture conditions [24], [25]. These physiological changes help microorganisms maintain in a proper condition and survive the stressful condition [25], [26], [27]. The response mechanisms range from synthesis/uptake of new metabolites, expression of protective shock proteins, or change of the cell structure [28], [29], [30]. Bacterial stress response typically takes one of two forms, (1) a stringent response to nutrient deprivation or oxidative stress,

or (2) a cell envelope stress response to changes in environmental conditions, such as high/low temperature, low pH, and osmotic stress.

The stringent response is a stress response of bacteria (and plant chloroplasts), which is activated through starvation for any single nutrient [31], [32]. This response is responsible for fortifying cells against deprivation of nutrients, such as C [32], N [33], amino acids [34], and iron [31]. Stress is sensed via RelA/SpoT homologues to fine-tune the cellular levels of the guanosine pentaphosphate or tetraphosphate, (p)ppGpp, which ensures the survival and adaptation by regulating growth, persistence, cell division, and activation of stress coping mechanisms[32], [35] (**Figure *1.2*-A**)**.** RelA catalyzes the (p)ppGpp synthesis and SpoT has a strong hydrolase and weak synthetase activity [32]. *relA/spoT* deletion for several strains showed that this system helps cells to inhibit primary metabolism including DNA replication, transcription, and translation; carbohydrate and energy metabolism; and ion transport and metabolism and activate secondary metabolism [36]. For example, during normal conditions σ^{70} guides RNA-Polymerase to transcribe genes in growing cells to keep essential genes and pathways operating [2]. However, during the stringent response, ppGpp binding to RNA Polymerase makes conformational changes and prevents genes transcription through σ^{70} promoter. As a result, other σ factors which induce stress response mechanisms get activated (**Figure *1.2*-B**) [35].

During low concentrations of carbon, accumulation of (p)ppGpp represses most of the genes, like tRNA and rRNA resulting in limitation of unnecessary activities [34], [37]. It is shown that the carbon type affects (p)ppGpp regulation. In good carbon (glucose) concentration the (p)ppGpp level is low and uncontrolled accumulation can cause severe growth inhibition or cell death [37]. However, in poor carbon (casamino acids or succinate) SpoT hydrolysis function is stimulated and RelA synthesizes the (p)ppGpp to balance its concentration. As a result, cells can

[2] Sigma factor: A protein needed for initiation of transcription in bacteria.

adapt to the fluctuations in carbon source. Another example is the environment with nitrogen limitation in which, RelA expression is integrated into the Ntr stress response to protect N-starved enteric bacteria through (p)ppGpp synthesis [33]. Iron limited environment makes cells increase their capacity to take up iron. Stringent response mechanism stimulates the expression of the enterochelin system (scavenges ferric ions) and at least one alternative (non-enterochelin) iron uptake system by ppGpp accumulation. All these, in turn help relieve the iron limitation. Correspondingly, relA/spoT mutation makes cells severely handicapped by downregulating iron carrier biosynthesis and iron utilization, in iron limited condition as a result of (p)ppGpp absence [38].

The cell envelope stress response is activated by two-component systems (TCS) a dominant form of bacterial signal transduction. This protein family has been implicated to control a remarkable number of cellular functions including motility, metabolism, developmental switches, in response to membrane stressors [39], [26].

Effective stress response allows cells to survive stress and grow (active cell division), or tolerate stress longer (e.g. by spore formation, or forming biofilms) [40]. Nutrient limitation, and exposure to stress factors divert cell resources away from growth/division. Hence, complex regulatory networks including stringent response regulators, the RpoS factor and the quorum sensing factor will be activated [40]. Comparative functional genomic studies have shown that 46% of genes dependent on RpoS are expressed to varying degrees in the immobilized cells of biofilms, suggesting their formation is another reaction to stress factors [40], [41].

A)

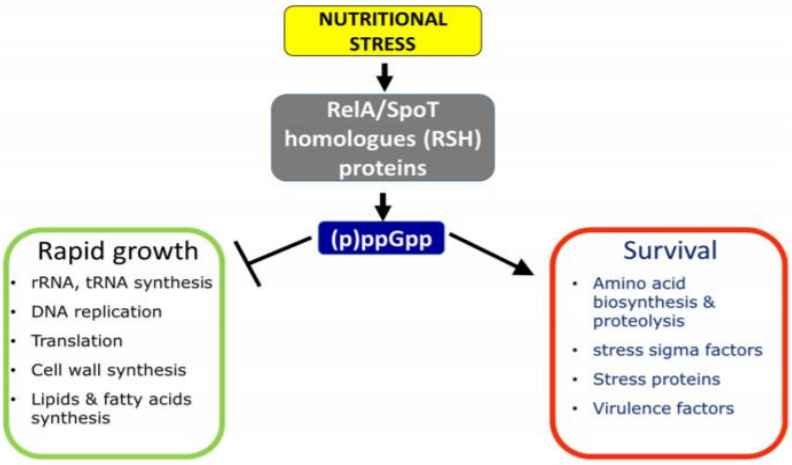

B)

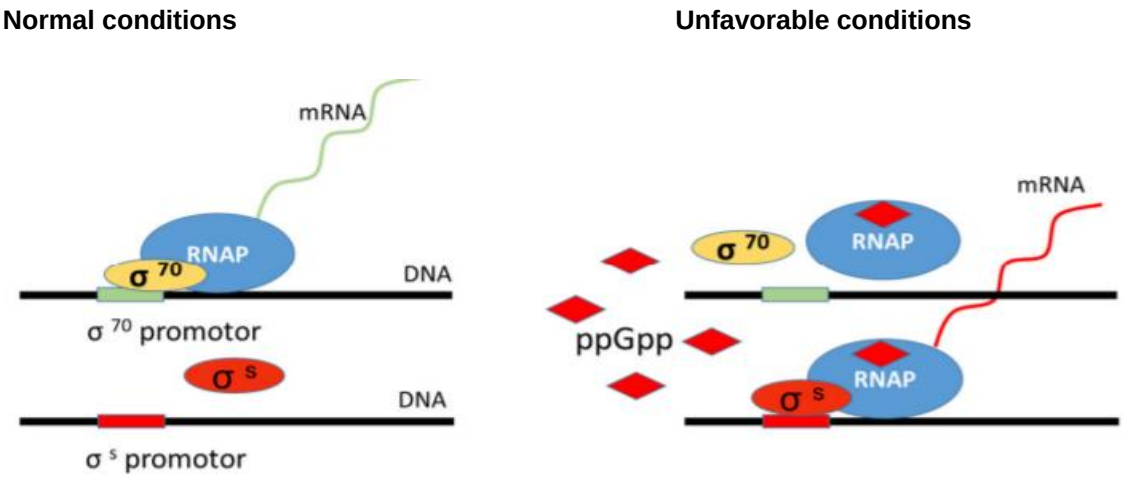

Figure 1.2 - Stringent response through (p)ppGpp in bacteria (adapted from [35]) A) (p)ppGpp role in inhibiting rapid growth or activating stress responses. B) (p)ppGpp role in *σ* factor regulation during unfavorable conditions.

The cell envelope response responding to stress by modifying the phosphorylation state of a cognate regulatory protein is called two-component system. These systems are the most prevalent form of signal transduction mediating the bacterial response to environmental signals.

Environmental signal is relayed by a sensor, which is a histidine kinase (HK) present in the inner membrane, to a cytoplasmic response regulator (RR) (**Figure 1.3**).

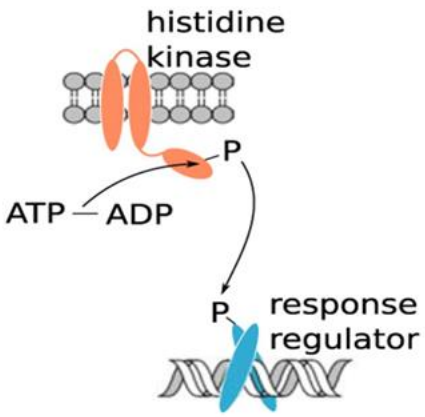

Figure 1.3 - Two-component system signalling in the histidine kinase-response regulator system.
(adapted from[42]).

Genes regulated by RRs and input signals triggering sensors, are different across two-component systems. Input signals enhance sensor phosphorylation which is considered as a substrate for phosphorylating RRs. Additionally, this signal can repress the phosphatase activity of the sensor. Other molecules such as acetyl phosphate can influence the sensitivity of the adaptive response and phosphorylate the regulator as well [26], [43].

EnvZ/OmpR, a two-component regulatory system, controls remarkable number of cellular functions such as expression of OmpF and OmpC porins which are outer membrane beta-barrel proteins (OMP) altering the cell membrane permeability [44], [45]. These porins provide a means for cells to balance the need for nutrients and the need for protection against toxins [46], and are therefore heavily involved in the envelope stress response to a variety of environmental stressors [47]. EnvZ functions as a membrane-bound HK, an OmpR phosphotransferase, and as a phospho-OmpR (OmpR-P) phosphatase by responding to changes in the extracellular osmolarity. It is proposed that the signal regulating the ratio of the kinase to the phosphatase activity of EnvZ

is osmotic level in the cell environment. Phosphorylation of OmpR often increases its affinity for DNA leading to transcriptional activation or repression of OMPs such as *ompC* and *ompF,* depending on the mode of action. Growth temperature, antibiotic exposure, oxidative stress, nutrients availability are among the signals affecting OmpF and OmpC production [48]. Within the context of envelope stress by oxidative stress, metal stress, osmotic stress, and heat shock, outer membrane proteins have generally been associated with the σ^E pathway and make changes in the membrane [46], [49], [50], [51].

Various two-component systems are triggered by antibiotic reagents as stress applicators. For example, PhoP/PhoQ TCS can sense the availability of antimicrobial peptides to regulate expression of virulence genes to protect cells or VbrK/VbrR TCS regulate beta-lactamase expression and lead cells to antibiotic resistance. Other than activating TCSs, bacteria alter the permeability of the outer membrane, or increase the efflux pump activity in order not to let antibiotics reach their target [52].

In the following chapters, bacterial response to stress factors including nutrient deprivation (Fe) and osmotic and antibiotic stress will be discussed.

Iron limitation in many bacterial species leads to induction of Ferric Uptake Regulator (Fur) regulon to activate more siderophore biosynthesis and iron transporters to scavenge iron [53]. On the other hand, the osmotic stress response of *E. coli* includes accumulation of K^+, glutamate, proline, glycine betaine, or trehalose. Proline, glycine betaine, and trehalose are effective compatible solutes transported and synthesized by *proU*, *proP*, and *otsA/otsB* gene expression respectively which are regulated by cytoplasmic K^+ [54], [55]. RpoS, the responsible sigma factor for several genes during stationary phase, and other stress has been shown to be responsible for transcribing trehalose synthases [56].

Previously, it is shown that RpoS which is a general stress response regulator provides the ability to survive stressful conditions for *E. coli*. Sometimes stressors sharing common induced proteins, lead to cross-protection against each other [57], [58]. For example, RpoS sigma factor regulating genes in nutrient starvation during stationary phase, cross protect cells against osmotic stress by trehalose synthesis [59]. Another example is for osmotically stressed *E. coli* which are less susceptible to tetracycline antibiotic due to AcrAB-TolC efflux pump[3] expression [60].

This thesis shows that *in-vitro* biofilm models can be used to study interaction between pathogens and host microbiota, and recognize the biomarkers evolved by these interactions and use of different medical treatments. Also, it gives us the insight into targeting stress response strategies used by *E. coli* as a new direction for combating bacterial infections and their antibiotic resistance characteristics.

1.2. References

[1] M. A. S. Mcmahon *et al.*, “Environmental Stress and Antibiotic Resistance in Food-Related Pathogens,” *Appl. environmen*, vol. 73, no. 1, pp. 211–217, 2007.

[2] P. Mañas, S. Condón, and R. Pagán, “International Journal of Food Microbiology Role of general stress-response alternative sigma factors σ S (RpoS) and σ B (SigB) in bacterial heat resistance as a function of treatment medium pH,” *Int. J. Food Microbiol.*, vol. 153, no. 3, pp. 358–364, 2012.

[3] L. Deschênes and T. Ells, “Bacteria-nanoparticle interactions in the context of nanofouling,” *Adv. Colloid Interface Sci.*, vol. 277, pp. 102–106, 2020.

[4] A. Nerurkar, P. Solanky, S. S. Naik, M. D. M. Associate, G. M. College, and B.

[3] Efflux pumps: Transport proteins involved in the extrusion of toxic substrates

West, “Bacterial pathogens in urinary tract infection and antibiotic susceptibility pattern,” *J Pharm Biomed Sci*, vol. 21, no. 21, pp. 2010–2012, 2012.

[5] J. Cook, “Antibacterial surfaces for biomedical devices,” vol. 6, no. 5, pp. 553–567, 2009.

[6] U. S. Centers and D. Control, “Antibiotic Resistance Threats in the United States, 2019,” 2019.

[7] J. C. Marshall, N. V. Christou, and J. L. Meakins, “The Gastrointestinal Tract, The ‘Undrained Abscess’ of Multiple Organ Failure,” *Ann. Surg.*, vol. 218, no. 2, pp. 111–119, 1993.

[8] B. Haymond, “Targeting Biofilms in Translational Research, Device Development, and Industrial Sectors,” D. L. Williams, Ed. Cham: Springer International Publishing, 2019, pp. 97–105.

[9] N. Principi, E. Silvestri, and S. Esposito, “Advantages and Limitations of Bacteriophages for the Treatment of Bacterial Infections,” *Bacteriophages Bact. Infect.*, vol. 10, no. 5, pp. 1–9, 2019.

[10] I. Consequential and P. H. Implications, “Antibiotic Use in Agriculture and Its Consequential Resistance in Environmental Sources : Potential Public Health Implications,” *Molecules*, vol. 23, no. 4, p. 795, 2018.

[11] G. G. Khachatourians, “Agricultural use of antibiotics and the evolution and transfer of antibiotic-resistant bacteria,” vol. 159, no. 9, pp. 1129–1136, 1998.

[12] T. S. Rao, A. J. Kora, P. Chandramohan, and B. S. Panigrahi, “Biofouling and

microbial corrosion problem in the thermo-fluid heat exchanger and cooling water system of a nuclear test reactor," vol. 7014, no. May, 2009.

[13] B. Eslami *et al.*, "Stress-localized durable anti-biofouling surfaces," *Soft Matter*, no. 70, pp. 6014–6026, 2019.

[14] M. Kostakioti, M. Hadjifrangiskou, and S. J. Hultgren, "Bacterial Biofilms: Development, Dispersal, and Therapeutic Strategies in the Dawn of the Postantibiotic Era," *Cold Spring Harb. Perspect. Med.*, vol. 3, pp. 1–23, 2013.

[15] C. M. Toutain, N. C. Caizza, M. E. Zegans, and G. A. O. Toole, "Roles for flagellar stators in biofilm formation by Pseudomonas aeruginosa," vol. 158, pp. 471–477, 2007.

[16] S. M. Soto, "Importance of Biofilms in Urinary Tract Infections : New Therapeutic Approaches," vol. 2014, 2014.

[17] A. M. Edwards, R. C. Massey, and S. R. Clarke, "Molecular mechanisms of *Staphylococcus aureus* nasopharyngeal colonization," vol. 27, pp. 1–10, 2012.

[18] P. S. Stewart, M. J. Franklin, K. S. Williamson, J. P. Folsom, L. Boegli, and A. James, "Contribution of Stress Responses to Antibiotic Tolerance in *Pseudomonas aeruginosa* Biofilm," vol. 59, no. 7, pp. 3838–3847, 2015.

[19] H. Flemming *et al.*, "The EPS Matrix: The 'House of Biofilm Cells " *J. Bacteriol.*, vol. 189, no. 22, pp. 7945–7947, 2016.

[20] V. Sperandio, "Pathogens ' adaptation to the human host," vol. 115, no. 38, pp. 9342–9343, 2018.

[21] S. T. Chambers and M. Leverb, “Betaines and Urinary Tract Infections,” pp. 1–10, 1996.

[22] V. Pathology and V. Medicine, “Collectins and Cationic Antimicrobial Peptides of the Respiratory Epithelia,” vol. 612, pp. 595–612, 2006.

[23] F. C. Fang, E. R. Frawley, T. Tapscott, and V.-T. Andres, “Bacterial Stress Responses during Host Infection,” vol. 2, pp. 133–143, 2016.

[24] R. Hengge, *The General Stress Response in Gram-Negative Bacteria*. 2011.

[25] K. Shimizu, “Regulation Systems of Bacteria such as *Escherichia coli* in Response to Nutrient Limitation and Environmental Stresses,” *Metabolites*, vol. 4, pp. 1–35, 2014.

[26] E. A. Groisman, “Feedback Control of Two-Component Regulatory Systems,” *Annu. Rev. Microbiol. 2016.*, vol. 70, pp. 103–124, 2016.

[27] K. Poole, “Bacterial stress responses as determinants of antimicrobial resistance,” no. May, pp. 2069–2089, 2012.

[28] J. E. Purvis, L. P. Yomano, and L. O. Ingram, “Enhanced Trehalose Production Improves Growth of *Escherichia coli* under Osmotic Stress Enhanced Trehalose Production Improves Growth of *Escherichia coli* under Osmotic Stress,” *Appl. Environ. Microbiol.*, vol. 71, no. 7, pp. 3761–3769, 2005.

[29] D. Kapfhammer, E. Karatan, K. J. Pflughoeft, and P. I. Watnick, “Role for Glycine Betaine Transport in Vibrio cholerae Osmoadaptation and Biofilm Formation within Microbial Communities,” *Appl. Environ. Microbiol.*, vol. 71, no. 7, pp. 3840–3847,

2005.

[30] S. I. Miller, “Antibiotic Resistance and Regulation of the Gram-Negative Bacterial Outer Membrane Barrier by Host Innate Immune Molecules,” vol. 7, no. 5, pp. 5–7, 2016.

[31] M. Miethke, H. Westers, E. Blom, O. P. Kuipers, and M. A. Marahiel, “Iron Starvation Triggers the Stringent Response and Induces Amino Acid Biosynthesis for Bacillibactin Production in Bacillus subtilis,” *J. Bacteriol.*, vol. 188, no. 24, pp. 8655–8657, 2006.

[32] J. Lee, Y. Park, and Y. Seok, “Rsd balances (p) ppGpp level by stimulating the hydrolase activity of SpoT during carbon source downshift in *Escherichia coli*,” vol. 115, no. 29, 2018.

[33] D. R. Brown, G. Barton, Z. Pan, M. Buck, and S. Wigneshweraraj, “Nitrogen stress response and stringent response are coupled in Escherichia,” *Nat. Commun.*, vol. 5, p. 4115, 2014.

[34] K. Potrykus and M. Cashel, “(p)ppGpp : Still Magical?,” *Annu. Rev. Genet.*, vol. 62, pp. 35–51, 2008.

[35] I. Dzhygyr, “Functional Studies of *Escherichia coli* Stringent Response Factor RelA,” 2018.

[36] L. Wu, Z. Wang, Y. Guan, and X. Huang, “The (p) ppGpp-mediated stringent response regulatory system globally inhibits primary metabolism and activates secondary metabolism in Pseudomonas protegens H78,” pp. 3061–3079, 2020.

[37] V. Jain, M. Kumar, and D. Chatterji, “ppGpp : Stringent Response and Survival,” vol. 44, no. 1, pp. 1–10, 2006.

[38] D. Vinella, C. Albrecht, M. Cashel, and R. D. Ari, “Iron limitation induces SpoT-dependent accumulation of ppGpp in *Escherichia coli*,” vol. 56, pp. 958–970, 2005.

[39] W. J. Gooderham and R. E. W. Hancock, “Regulation of virulence and antibiotic resistance by two-component regulatory systems in Pseudomonas aeruginosa,” *FEMS Microbiol Rev*, vol. 33, pp. 279–294, 2009.

[40] A. Święciło and I. Zych-wężyk, “Bacterial Stress Response as an Adaptation to Life in a Soil Environment,” vol. 22, no. 6, pp. 1577–1587, 2013.

[41] P. Landini, “Cross-talk mechanisms in biofilm formation and responses to environmental and physiological stress in *Escherichia coli*,” *Res. Microbiol.*, vol. 160, no. 4, pp. 259–266, 2009.

[42] N. A. Held, M. R. Mcilvin, D. M. Moran, M. T. Laub, and A. Saito, “Unique Patterns and Biogeochemical Relevance of Two-Component Sensing in Marine Bacteria,” vol. 4, no. 1, pp. 1–16, 2019.

[43] W. R. Mcclearys and J. B. Stock, “Acetyl Phosphate and the Activation of Two-component Response Regulators*,” vol. 269, no. 50, 1994.

[44] M. Pagès, “Porins and small- molecule translocation across the outer membrane of Gram-negative bacteria,” *Nat. Rev. Microbiol.*, vol. 18, no. March, 2020.

[45] C. Prigent-combaret, O. Vidal, C. Dorel, and P. Lejeune, “Abiotic Surface Sensing and Biofilm-Dependent Regulation of Gene Expression in *Escherichia coli*,” vol.

181, no. 19, pp. 5993–6002, 1999.

[46] E. Batchelor, D. Walthers, L. J. Kenney, and M. Goulian, “The Escherichia coli CpxA-CpxR Envelope Stress Response System Regulates Expression of the Porins OmpF and OmpC The *Escherichia coli* CpxA-CpxR Envelope Stress Response System Regulates Expression of the Porins OmpF and OmpC,” *J. Bacteriol.*, vol. 187, no. 16, pp. 5723–5731, 2005.

[47] A. Siryaporn and M. Goulian, “Cross-talk suppression between the CpxA – CpxR and EnvZ – OmpR two-component systems in E . coli,” vol. 70, no. September, pp. 494–506, 2008.

[48] L. A. Pratt, W. Hsing, K. E. Gibson, and T. J. Silhavy, “From acids to osmZ multiple factors influence synthesis of the OmpF and OmpC porins in *Escherichia coli*,” *Mol. Microbiol.*, vol. 20, no. 5, pp. 911–917, 1996.

[49] J. Mecsas, P. E. Rouviere, J. Erickson, I. D, and C. A. Gross, “The activity of sigmaE an *Escherichia coli* heat-inducible sigma-factor, is modulated by expression of outer membrane proteins,” *Genes Dev.*, vol. 7, pp. 2618–2628, 1993.

[50] G. Klein and S. Raina, “Small regulatory bacterial RNAs regulating the envelope stress response,” vol. 0, no. January, pp. 417–425, 2017.

[51] M. Egler, C. Grosse, G. Grass, and D. H. Nies, “Role of the Extracytoplasmic Function Protein Family Sigma Factor RpoE in Metal Resistance of *Escherichia coli* †,” vol. 187, no. 7, pp. 2297–2307, 2005.

[52] L. Li, H. Ge, D. Gu, H. Meng, Y. Li, and M. Jia, “The role of two-component

regulatory system in β -lactam antibiotics resistance," vol. 215, no. June, pp. 126–129, 2018.

[53] C. Metallomics, P. Cornelis, Q. Wei, C. Andrews, T. Vinckx, and P. Cornelis, "Iron homeostasis and management of oxidative stress response in bacteria," *Metallomics*, vol. 3, pp. 540–549, 2011.

[54] S. Grothe, R. L. Krogsrud, D. J. Mcclellan, J. L. Milner, and J. M. Wood, "Proline Transport and Osmotic Stress Response in *Escherichia coli* K-12," vol. 166, no. 1, pp. 253–259, 1986.

[55] H. M. Giaiver, O. B. Styrvold, and I. Kaasen, "Biochemical and Genetic Characterization of Osmoregulatory Trehalose Synthesis in *Escherichia coli*," *J. Bacteriol.*, vol. 170, no. 6, pp. 2841–2849, 1988.

[56] D. E. Culham, A. Lu, M. Jishage, K. A. Krogfelt, A. Ishihama, and J. M. Wood, "The osmotic stress response and virulence in pyelonephritis isolates of *Escherichia coli*: contributions of RpoS, ProP, ProU and other systems," *Microbiology*, vol. 147, pp. 1657–1670, 2001.

[57] M. Zhu and X. Dai, "High Salt Cross-Protects *Escherichia coli* from Antibiotic Treatment through Increasing Efflux Pump Expression," *mSphere*, vol. 3, no. 2, pp. 1–8, 2018.

[58] D. E. Jenkins, J. E. Schultz, and A. Matin, "Starvation-Induced Cross Protection against Heat or H202 Challenge in *Escherichia coli*," *J. Bacteriol.*, vol. 170, no. 9, pp. 3910–3914, 1988.

[59] D. E. N. Rangel, “Stress induced cross-protection against environmental challenges on prokaryotic and eukaryotic microbes,” *World. J. Microbiol. Biotechnol.*, vol. 27, pp. 1281–1296, 2011.

[60] M. Zhu and X. Dai, “High Salt Cross-Protects *Escherichia coli* from Antibiotic Treatment through Increasing Efflux Pump Expression,” *mSphere*, vol. 3, no. 2, pp. 1–9, 2018.

Chapter 2
Bacterial Microcins Mediate Iron Competition in Coculture Biofilms[4]

2.1. Introduction

Competition for resources represents a common interaction that can determine biofilm development. In the case of bacterial infections, effective competition can allow commensal or probiotic bacterial populations to inhibit pathogen colonization or eliminate existing infection. Iron is one such nutrient that sustains microbial life and the requirement for iron drives competition between several gut microorganisms. Bacteria require iron for essential processes like respiration, DNA replication, transcription, biofilm formation [1], [2]. As a result, bacteria have evolved strategies to recruit and compete for scarce iron from their surrounding environment. Such scarcity occurs during infections, when the host releases iron-scavenging proteins, including transferrin, Lipocalin-2, and ferritin, to limit pathogen growth (**Figure *2.1***) [1], [3], [4]. Microbes respond to iron starvation by releasing small molecules, including siderophores such as enterobactin and salmochelin, which have greater iron binding affinities than several host secreted proteins (**Figure *2.1***) [2], [3], [5]. Competition for iron between bacterial species in the mammalian gut is critical to determining whether pathogens can establish an infection. For example, the probiotic *Escherichia coli Nissle* 1917 (EcN) strain uses multiple iron uptake pathways to inhibit and abolish established *Salmonella enterica* serovar Typhimurium (STm) infections in murine models [6], [7], [8]. A better understanding of such evolved strategies used by probiotic bacteria to combat pathogen gut colonization promises to identify new targets for species-specific antimicrobials and provide insight into population dynamics of the gut microbiota.

[4] This work was done originally by Arunima Bhattacharjee. I was responsible to apply CFU counting method and redo all the biofilm imaging to compare the biofilm quantification methods together.

A

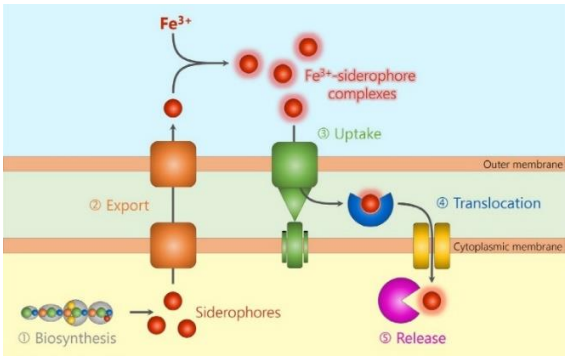

B

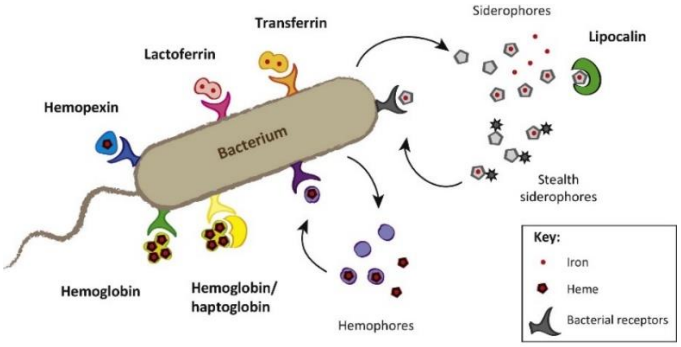

Figure 2.1- Iron uptake mechanisms in bacteria. A) Schematic showing iron uptake by siderophores in *E. coli*. high-affinity surface receptor proteins (green) bind iron-loaded siderophores. Periplasmic-binding proteins (blue) and ATP-driven transporters (yellow) that are in the cytoplasmic membrane are facilitating transport into the cell (adapted from [9]). B) Schematic showing different mechanisms in a bacterial cell to sequester iron from host proteins [5].

Once secreted by producing cells, siderophores are public goods that can be used cooperatively by other producers, or they can be exploited by non-producing cells [10], [11], [12]. Bacteria have evolved anti-cheating strategies to curb siderophore use by non-producers, such as the development of chemically distinct siderophores [11] and the production of siderophore-conjugated antimicrobial peptides, called microcins. Microcins are small peptides (< 10 kDa) produced in many Enterobacteriaceae, and some are post-translationally conjugated to siderophores as a strategy to dominate polymicrobial iron competition in the gut [13], [14], [15]. EcN produces two microcins, H47 and M, as part of an iron competition strategy against enteric pathogens [16]. STm is one such pathogen that causes acute gastroenteritis [17], [18], [19], and EcN production of microcin M was recently shown to inhibit intestinal colonization of

enteropathogens and pathobionts like STm [6]. Microcin production confers a critical competitive advantage to EcN, and they are thought to act by post-translational conjugation to the siderophore salmochelin [20]. Like the process of intestinal colonization and infection *in vivo*, bacterial biofilm formation is dependent on iron recruitment from the environment [21], [22], and iron competition plays a critical role in the development and maintenance of polymicrobial biofilms. For instance, biofilm-associated bacteria, use siderophores produced by their counterparts for cross-feeding in mutualistic communities [21], [23]. On the other hand, the use of siderophores by cheaters, biofilm constituents that provide no mutual benefit in return, can threaten the fitness of a community by making it more susceptible to bactericidal compounds [21]. Few studies have explored competition mediated by siderophores within multispecies biofilms [24], [25], and microcin based anti-cheating strategies in biofilms have not been previously investigated.

In this work, we develop a set of *in vitro* biofilm models for EcN and STm cocultures to provide insights into siderophore and microcins based iron competition and population dynamics. Both EcN and STm produce enterobactin and salmochelin siderophores, which are candidates for cross-feeding or piracy within these coculture biofilms. Moreover, EcN microcins are thought to be conjugated to salmochelin and confer a competitive advantage over enteric pathogens, including STm [20]. EcN wild type, but not the mutant unable to produce microcins, outcompetes STm in co-inoculated static biofilm models. Moreover, this phenotype was only observed under iron limiting conditions. These biofilm models recapitulate results from murine models indicating that microcin production is key to EcN domination of cocultures with STm, supporting the hypothesis that they inhibit biofilm colonization when STm exploits microcin conjugated EcN salmochelin [20]. In an instance of siderophore piracy, an EcN *entC* mutant, which lacks the ability to synthesize enterobactin, still out-competes STm in biofilms, possibly via the utilization of STm siderophores. In static cultures of EcN wild-type supernatant, the growth of STm is unaffected by the presence or absence of microcins. Instead, STm biofilm growth is inhibited only when grown

in a microfluidic device, in which the concentration of EcN supernatant components, including microcins, are constant. These results suggest that EcN domination of STm cocultures is independent of contact dependent inhibition mechanisms, but that the constant proximal production of microcin-conjugated siderophores is likely required.

2.2. Materials and Methods

2.2.1. Bacterial Strains

Strains of the probiotic *Escherichia coli* Nissle 1917 (EcN; Mutaflor, DSM 6601) and the pathogen *Salmonella enterica* serovar Typhimurium (STm, [IR715]) utilized in this study are listed in Table 1. EcN was kindly provided by Ardeypharm Gmb, Herdecke, Germany. IR715 is a fully virulent, nalidixic acid-resistant derivative of STm wild-type isolate ATCC 14028. Plasmids expressing GFP (pGFPuv) or mCherry (pFPV-mCherry) were used to distinguish bacterial strains during competition in biofilm growth. The pFPV-mCherry was a gift from Dr. Olivia Steele-Mortimer (Addgene plasmid # 20956). All the mutants in this chapter were constructed by Dr. Matina Sassone-Corsi. Mutants in EcN were constructed as described previously [20] using the lambda red recombinase system.

2.2.2. Static Biofilm Growth Conditions

All bacterial strains were revived from frozen stocks by streaking on LB agar plates. A single colony was inoculated into 2 mL Lysogeny Broth (LB) media (Fisher scientific) and growth shaking at 37 ºC for 6 h. Bacteria from these shaking cultures were diluted in 10 g/L Bacto tryptone media (BD) to an OD of 0.02. 18x18 mm glass cover slips in 6 well plates were inoculated with 2 mL of the diluted cultures in TB for static growth biofilm imaging. The plates were left to grow on the bench top for 24 h, unless otherwise noted, at 22 ºC. To grow biofilms in iron limited media, 200 μM 2,2'-bipyridyl (Sigma) was added to tryptone broth. At the end of the growth time, biofilms

were rinsed with phosphate buffered saline (PBS) and taken for imaging using confocal microscopy.

2.2.3. Supernatant Preparation

EcN WT and EcN *mcmA mchB* were revived from frozen stocks by streaking on LB agar plates. Single colonies from the LB plates were inoculated in 2 mL LB media and grown by shaking at 37 ºC for 6 h. 100 µL of the shaking culture was added to 100 mL of TB supplemented with 2,2'-bipyridyl and grown by shaking at 37ºC for 24 h. The final supernatant samples were obtained after these cultures were centrifuged at 15,000 x *g* and filtered using a 0.2 µm membrane filter.

2.2.4. Planktonic Growth Assay in the Presence of EcN Supernatant

EcN WT and EcN *mchDEF* were grown in shaking Nutrient Broth supplemented with 200 µM 2,2'-bipyridyl at 37 ˚C overnight. Approximately 5 x 10^3 CFU/mL from an overnight culture was inoculated into 15 mL of tissue culture medium (DMEM/F12 with 10% fetal bovine serum (FBS); Invitrogen), and grown for 12 h. After 12 h EcN WT and EcN *mchDEF* supernatants were filtered with a 0.2 µm membrane filter and concentrated by centrifugation using 3 kDa centrifugal filter (Millipore). Then, 10 or 20 µL of the concentrated supernatant were added to DMEM/F12 with 10% fetal bovine serum containing 5 x 10^3 CFU/mL of STm WT and grow aerobically at 37 °C. OD_{600} was then read at 10 h post-inoculation.

2.2.5. Microfluidic Device Construction

Microfluidic flow channel devices incorporating glass coverslip and polydimethylsiloxane (PDMS) (Dow chemicals) were used to image biofilm development in real-time. Microfluidic devices with 4 consecutive channels, each one configured as shown in (**Figure *2.7*-A**), with channel dimensions 10 x 0.5 x 0.25 mm (*l* x *w* x *h*) were fabricated using PDMS.

Flow channels were molded by curing PDMS on lithographically defined SU-8 (microchem) patterns on silicon wafers. A hole puncher was used to make holes for the inlet and

outlet lines. The PDMS was bonded to 24 x 50 mm glass coverslips by plasma cleaning both the surfaces.

2.2.6. Biofilm Growth in Microfluidic Flow Cells

All bacterial strains were revived from frozen stocks by streaking on LB agar plates. A single colony was inoculated into 2 mL LB media and grown by shaking at 37 ºC for 6 h. Ampicillin was added to cultures for STm pEmpty, STm pMchI and STm pMcmI at a concentration of 100 µl/mL to maintain the plasmids. Biofilms of all strains were seeded in the flow cells by flowing the planktonic culture of each strain into separate microfluidic channels and arresting flow for 2 h. Biofilms were grown by switching the feed line to each microfluidic channel to sterile supernatant supplemented with 100 µl/mL ampicillin and 5 µM of the membrane stain SynaptoRed C2 (FM4-64, Biotium) was then flowed through the channels at 2.5 mL/h for 15 h.

2.2.7. Crystal Violet (CV) Assay for Biofilm Biomass Quantification

Biofilms were rinsed in PBS and then incubated with 1 mL of 0.1 % aqueous CV for 15 min at room temperature. The stained wells were rinsed with PBS and growth substrates were transferred to another clean well to quantify biomass accumulated on the substrates only. 2 mL of ethanol was added to the clean wells and incubated for 5 min at room temperature. The optical density of the dissolved CV in ethanol was obtained at 600 nm (OD_{600}) and measured using a Biowave CO8000 cell density meter. All absorbance values were obtained from triplicate or greater number of samples and normalized to a self-consistent control within each experiment.

2.2.8. Laser Scanning Confocal Microscopy (CLSM) Imaging of Biofilms

All confocal images were obtained using a Zeiss LSM780 inverted confocal microscope with 63X oil immersion objective. Dichroic beam splitters were used to reflect laser lines 488/561 nm. Green fluorescent protein (GFP) and mCherry expressing biofilms were excited with 488 nm and 561 nm laser lines, respectively. The SynaptoRed C2 membrane stain was excited using 561

nm laser line as well. In the case of coculture biofilms, both color channels were imaged using alternating line averaging to avoid blurring of the image due to sample drift.

These adjustments reduced fluorescence cross-talk to undetectable levels in two-color imaging experiments. Confocal images were obtained with a *z* interval of 1 μm and a pinhole size of 1 airy unit.

The 3D coculture and monoculture microfluidic biofilm images were reconstructed using Volocity (Perkin Elmer). The biofilm-associated volume of cells (“biovolume”) was quantified using the "select objects" function on the fluorescence intensity images.

2.3. Results

2.3.1. EcN Outcompetes STm in Biofilms Only During Iron Starvation

Competition between STm and EcN under iron limiting condition has been demonstrated in mouse models and planktonic cultures [6], but details of their competition in biofilms have not been studied. Using biofilm models, it was found that the competition between EcN and STm is only observed in iron limiting conditions. No significant difference was observed between population fractions of wild type EcN and STm within 24 h coculture biofilms grown in iron rich, tryptone media. On the other hand, in biofilms grown in tryptone media supplemented with an iron chelator, 2,2’-bipyridyl, EcN WT is able to outcompete STm, comprising a much larger fraction of the biofilm (**Figure *2.2*-A**). Population fractions were calculated from biovolume measurements of confocal fluorescence microscopy images (see Materials and Methods). These values and ratios are consistent with those obtained from viable cell counts of these coculture biofilms **(Figure *2.3*)**. This indicate that iron limitation is a necessary condition to observe competition between STm and EcN during biofilm growth.

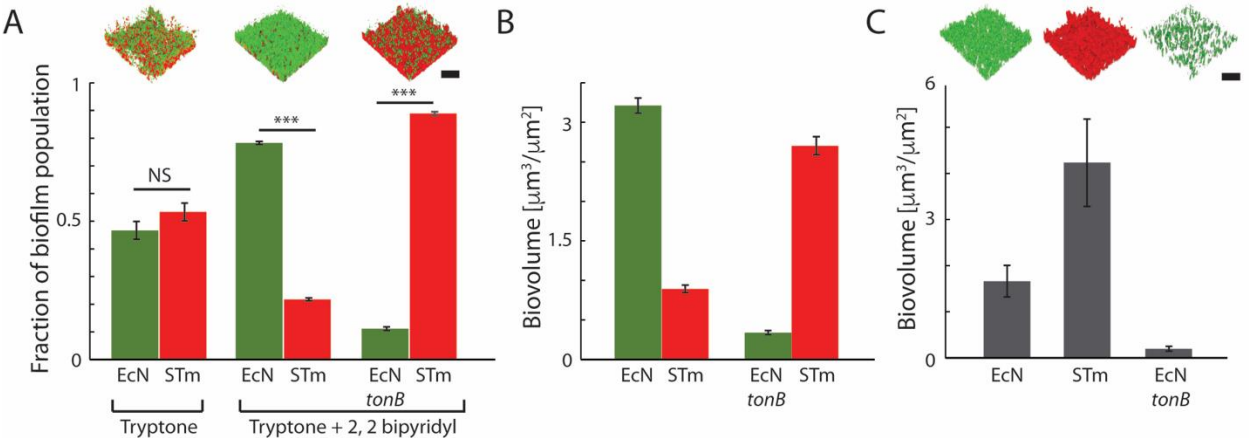

Figure 2.2- EcN inhibits STm growth in coculture biofilms during iron starvation. A) Population fractions of coculture biofilms of wild type EcN and STm grown in tryptone media, and EcN-STm and EcN tonB-STm cocultures grown in tryptone media supplemented with 2,2'-bipyridyl. B) Biofilm volumes (biovolume) of coculture biofilms of willd type EcN-STm and EcN tonB-STm grown in tryptone media supplemented with 2,2'-bipyridyl. C) Monoculture biofilms of EcN, STm, and EcN tonB grown in tryptone media supplemented with 2,2,'-bipyridyl. Scale bars are 20 μm. *** represents p value < 0.001 and NS represents no significant difference.

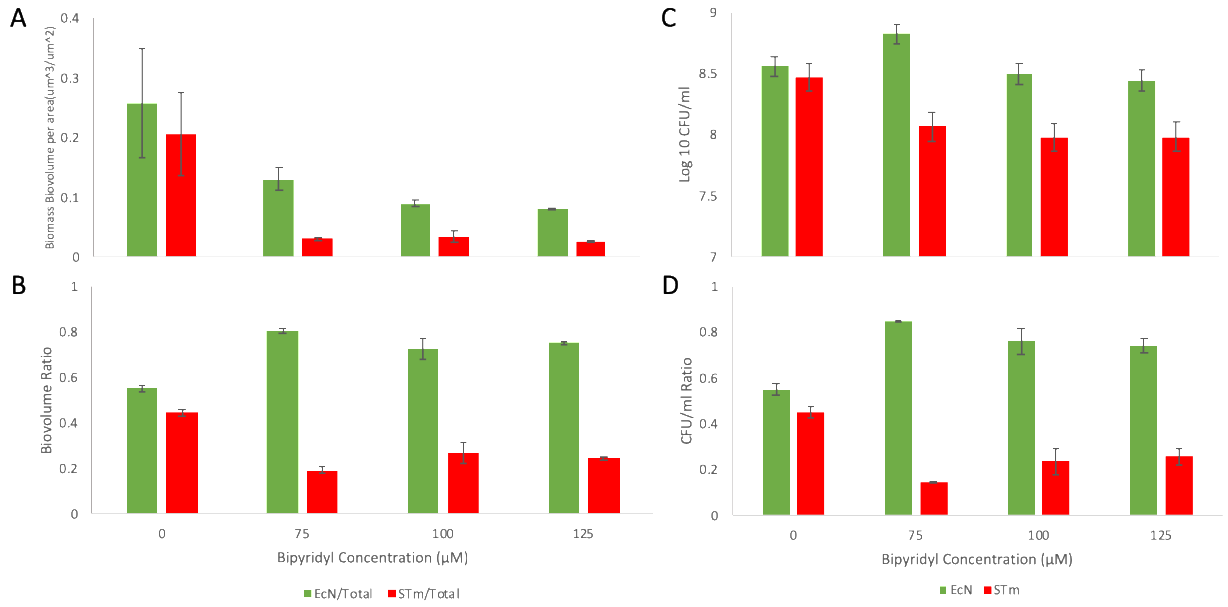

Figure 2.3 - ***Growth competition of EcN WT and STm WT quantified by confocal microscopy and viable cell counts.*** *A) Raw area-normalized biovolume, from confocal fluorescence microscopy, of EcN WT (green) and STm WT (red) in coculture biofilms at different 2,2'-bipyridyl concentrations, and B) biovolume ratios of the same. C) Viable cell counts of EcN WT (green) and STm WT (red) from coculture biofilms at different 2,2'-bipyridyl concentrations, and D) ratios of the same. 2,2'-bipyridyl concentrations are different from those reported in the main text due to the use of a newer batch of bacto tryptone with evidently different iron content.*

The EcN *tonB* mutant, incapable of transporting iron-bound siderophores across the cell membrane, grows poorly both in monoculture and in competition with STm (**Figure *2.2*-B**). EcN grows biofilms with less biovolume than STm WT in monocultures (**Figure *2.2*-C**), but

outcompetes STm by a significant margin in terms of relative biovolume in coculture biofilms (**Figure *2.2*-B**). These results indicate the importance of iron scavenging mechanisms in mediating the outcome of competition between these two species. Apart from producing two additional, chemically distinct siderophores compared to STm, EcN produces two antimicrobial microcins, H47 and M, which play a significant role during competition in the gut [6], [20]. Consequently, these microcins may play an essential role in competition between EcN and STm in this biofilm model.

2.3.2. EcN Microcins Inhibit STm Biofilms

EcN microcins exhibit antibacterial activity against enteric pathogens in iron-limited medium and in the inflamed gut [20]. To determine whether STm inhibition by EcN is microcin-dependent we cocultured STm with EcN *mcmA mchB*, a mutant deficient in microcin production [20]. There was no significant difference between population fractions of EcN *mcmA mchB* and STm WT in biofilms grown in tryptone medium, but in tryptone supplemented with 2,2'-bipyridyl, STm outcompeted EcN *mcmA mchB* (**Figure *2.4*-A, B**). Monoculture biofilms grown under iron limiting conditions show that both EcN *mcmA mchB* and STm WT have comparable biofilm growth rates when cultured alone (**Figure *2.4*-C**), suggesting that microcins provide EcN an advantage in iron competition over STm in in biofilms, consistent with results from *in vivo* models [20].

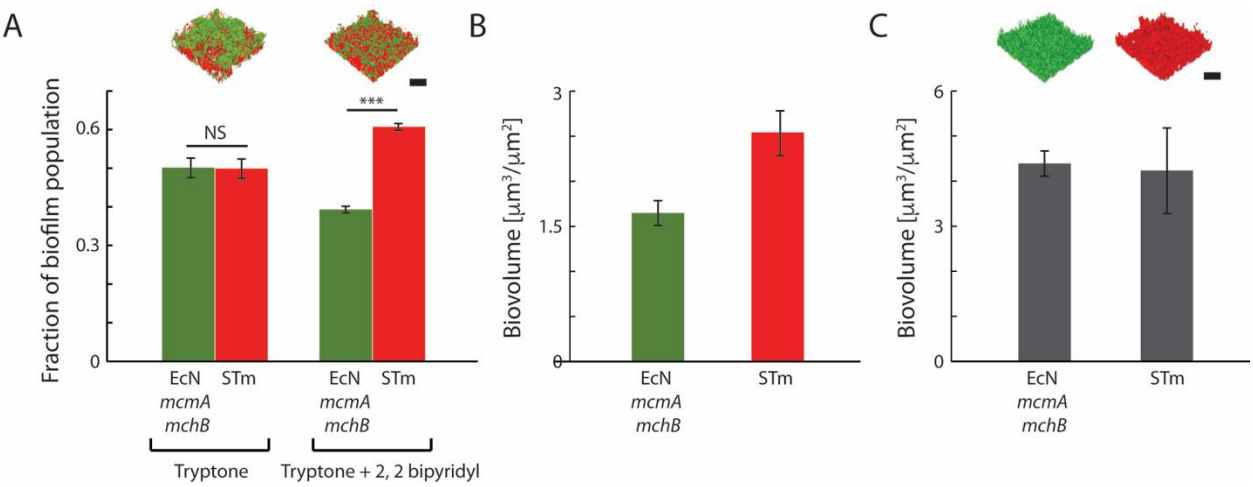

Figure 2.4 - *STm outcompetes EcN mcmA mchB in coculture biofilms under iron starvation.* *A) Population fractions of coculture biofilms of EcN mcmA mchB and STm grown with and without 2,2'-bipyridyl in tryptone media. B) Biovolume of coculture biofilms of EcN mcmA mchB and STm grown in tryptone media supplemented with 2,2'-bipyridyl. C) Monocultures of EcN mcmA mchB grown in tryptone media supplemented with 2,2'-bipyridyl. Scale bars are 20 μm. *** represents p value < 0.001 and NS represents no significant difference.*

2.3.3. EcN Uses STm Enterobactin to Outcompete STm in Coculture Biofilms

Class IIb microcins have been characterized as Trojan horse antimicrobial peptides since it was described that microcin MccE492 produced by *Klebsiella Pneumoniae* can be post-translationally conjugated to siderophores [27], [28]. It is suspected that also EcN microcins are post-translationally modified to bind salmochelin. Data in ***Figure 2.2*** and ***Figure 2.4*** are consistent with a mechanism by which EcN outcompetes STm in coculture as a result of STm using microcin-conjugated siderophores produced by EcN. STm produces, and can presumably exploit from the environment, the siderophores enterobactin and salmochelin. Under conditions where EcN is unable to conjugate microcins to siderophores, I expect the competition dominance by EcN to be diminished. To study the competition dynamics under conditions where EcN produces microcins but is unable produce its own enterobactin and salmochelin, we cocultured EcN *entC* and EcN *iroBC* with STm (**Figure 2.5**). EcN *entC* is an enterobactin biosynthesis mutant, and therefore cannot make its own salmochelin. EcN *iroBC* can produce enterobactin, but it lacks the biosynthetic and transporter genes for salmochelin. Surprisingly, EcN *entC* outcompetes STm in coculture biofilm experiments (**Figure 2.5-A, B**), while in monoculture biofilms, it grows

significantly less biovolume than STm. Like STm, these results suggest that EcN exploits enterobactin from the environment and grows poorly when it is not present. In the case of EcN *entC*-STm cocultures, only STm produces enterobactin, and EcN *entC* is apparently able to use STm enterobactin to produce microcin-conjugated siderophores with resulting effects on iron competition similar to those of EcN WT. EcN *iroBC*, on the other hand, grows comparable biovolume biofilms as STm in monoculture, and it is outcompeted by STm when grown in coculture biofilms. These results suggest that *iroBC* are involved in salmochelin production and/or conjugation of microcins to siderophores. The consequence of this deletion renders EcN *iroBC* unable to compete with STm, and further establish the role of microcin-conjugated siderophores in EcN-STm iron competition in biofilms.

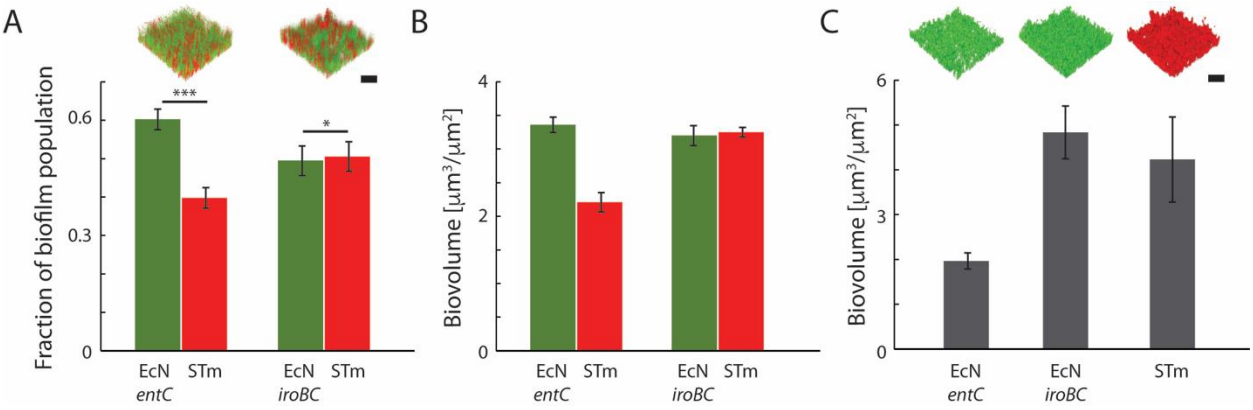

Figure 2.5- EcN uses STm-derived enterobactin to outcompete STm in coculture biofilms. A) Population fractions of coculture biofilms of EcN entC and STm, EcN iroBC and STm grown in tryptone media supplemented with 200 μM 2,2'-bipyridyl. B) Biofilm volume per scan area of coculture biofilms of EcN entC and STm WT, EcN iroBC and STm WT tryptone media supplemented with 2,2'-bipyridyl. C) Monoculture biofilm biovolumes of EcN entC, EcN iroBC and STm WT grown in tryptone media supplemented with 200 μM 2,2'-bipyridyl. Scale bars are 20 μm. * and*** represents p value < 0.01 and 0.001 respectively.

2.3.4. EcN Supernatant Inhibits STm Biofilms in Microfluidic Devices

To isolate the effect of microcins alone, STm shaking cultures and biofilms were exposed to EcN, *mcmA mchB,* and *mchDEF* supernatants. EcN *mchDEF* is a mutant deficient in transporter genes for microcins. Both EcN *mcmA mchB* and EcN *mchDEF* exhibit the same phenotype in cocultures with STm [20]. **Figure 2.6-A** shows statically grown STm biofilms in EcN

WT and EcN *mcmA mchB* supernatant. The biomass was normalized to STm biofilms grown in iron limited media which served as a control. There was no significant difference between the biofilms grown in EcN WT and EcN *mcmA mchB* supernatant. STm shaking cultures grown at 37°C to a cell density of 5 x 10^3 CFU/mL and exposed to different concentrations of EcN and EcN *mchDEF* supernatant showed no inhibition in growth after 10 h static culture (**Figure 2.6-B, C**). These observations indicate that the concentration of microcins was not sufficient to inhibit STm WT growth as seen in the in vitro biofilm cocultures of EcN and STm (**Figure *2.2*** and **Figure *2.4***), suggesting an effectively diminished concentration of microcins, possibly due to degradation, consumption, sequestration, or other mechanisms to reduce their overall effectiveness.

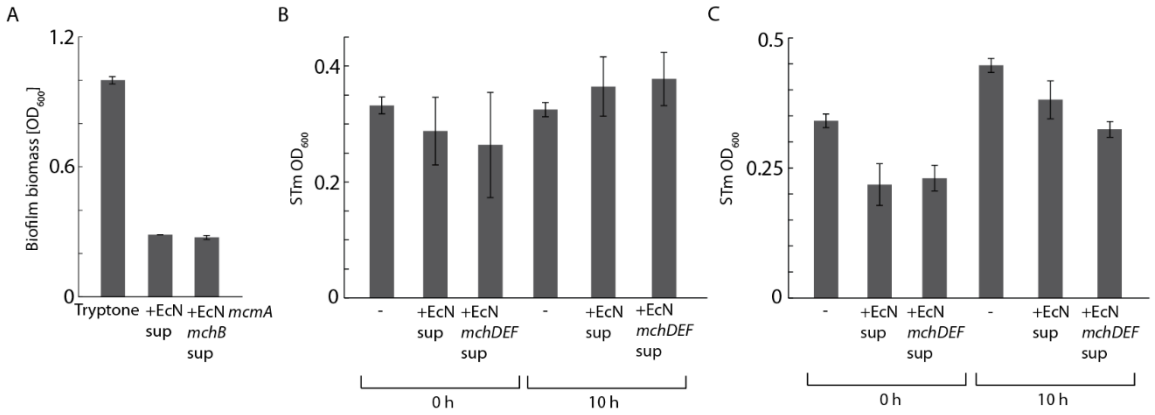

Figure 2.6-STm static biofilm and shaking culture growth in EcN WT and microcin mutant STm static biofilm and shaking culture growth in EcN WT and microcin mutant supernatant. A) Biofilm biomass of STm grown in tryptone media supplemented with 2,2'-bipyridyl, and in EcN or EcN mcmA mchB supernatant (sup). B) Cell density of STm grown in shaking cultures in DMEM+10% FBS media (-), DMEM+10%FBS media + 10 µL EcN supernatant, and DMEM+10% FBS media + 10 µL EcN mchDEF supernatant for 0 and 10 h. C) Cell density of STm grown in shaking cultures in DMEM+10% FBS media (-), DMEM+10%FBS media + 20 µL EcN supernatant and DMEM+10% FBS media + 20 µl EcN mchDEF supernatant for 0 and 10 h.

In contrast to the batch culture conditions used for planktonic and static biofilm growth, we hypothesized that EcN biosynthetic products, such as microcins, are produced continuously in cocultures and therefore may exist in higher effective concentrations. In order to mimic the constant production of microcin-conjugated siderophores in EcN-STm cocultures while controlling for contact-dependent inhibition mechanisms, the growth of STm in a microfluidic flow cell device as a function of exposure to EcN mutant supernatants was monitored. EcN WT or EcN *mcmA mchB* cell free supernatant was flowed through the growth channels continuously for the growth

period of 15 h, providing a constant concentration of microcin, or lack thereof. STm biofilms grown in the presence of EcN WT supernatant grew significantly less biomass than STm biofilms exposed to EcN *mcmA mcmB* supernatant (**Figure *2.7***).

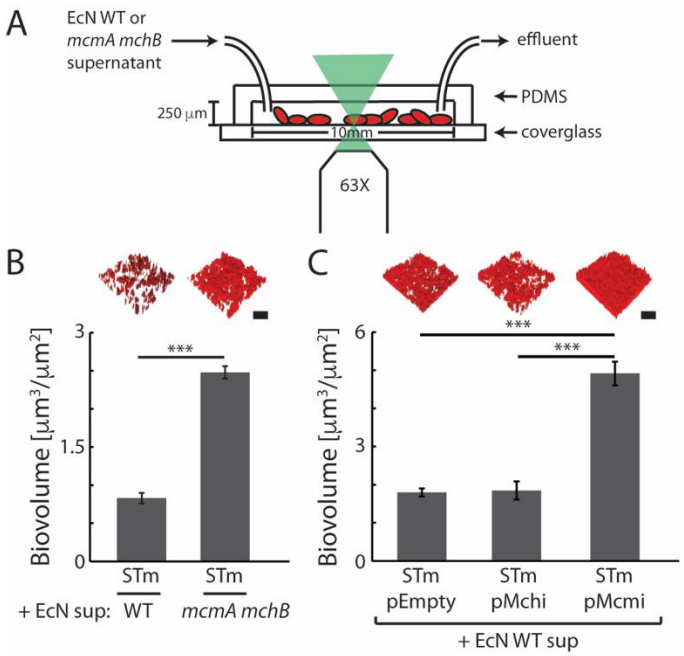

Figure 2.7-EcN microcin M inhibits STm biofilm growth in microfluidic devices. A) Schematic cross-section of the microfluidic channel used for STm biofilm growth in the presence of EcN wild-type and mutant planktonic culture supernatants. B) STm biofilms grown for 15 h in microfluidic device in EcN wild-type and mcmA mchB supernatant (sup). Insets are representative 3D fluorescence confocal images of the STm biofilms. C) STm pEmpty, STm pMchI and STm McmI biofilms grown for 15 h in microfluidic device in EcN wild-type supernatant. Scale bars in (B) and (C) insets are 20 μm. *** represents $p < 0.001$

To show that the growth inhibition effect is due to microcin production, the STm WT strain was transformed with plasmids bearing microcin immunity genes [20]. These were pMchI, which provides immunity to microcin H47, to which STm is naturally immune [20]; pMcmI, which provides immunity to microcin M; and pEmpty, the empty plasmid. When these three strains were grown in continuously flowing EcN WT supernatant, I observed biofilm growth inhibition in STm pEmpty and STm pMchI, which both provide no additional immunity to EcN microcins beyond that already present in the STm WT. However, STm pMcmI grown in EcN WT supernatant grew significantly more biofilm in comparison to STm pEmpty and STm pMchI (**Figure *2.7*-C**). These flow cell outcomes are recapitulated in biofilm coculture experiments with EcN WT and STm pMchI and pMcmI (**Figure 2.8**). These results indicate that growth inhibition in STm WT biofilms is primarily

due to microcin M, though a constant concentration of microcins in the growth environment is required observe it. In cocultures of EcN with STm, microcins are maintained at a constant concentration by EcN present in the biofilms, which results in STm biofilm inhibition.

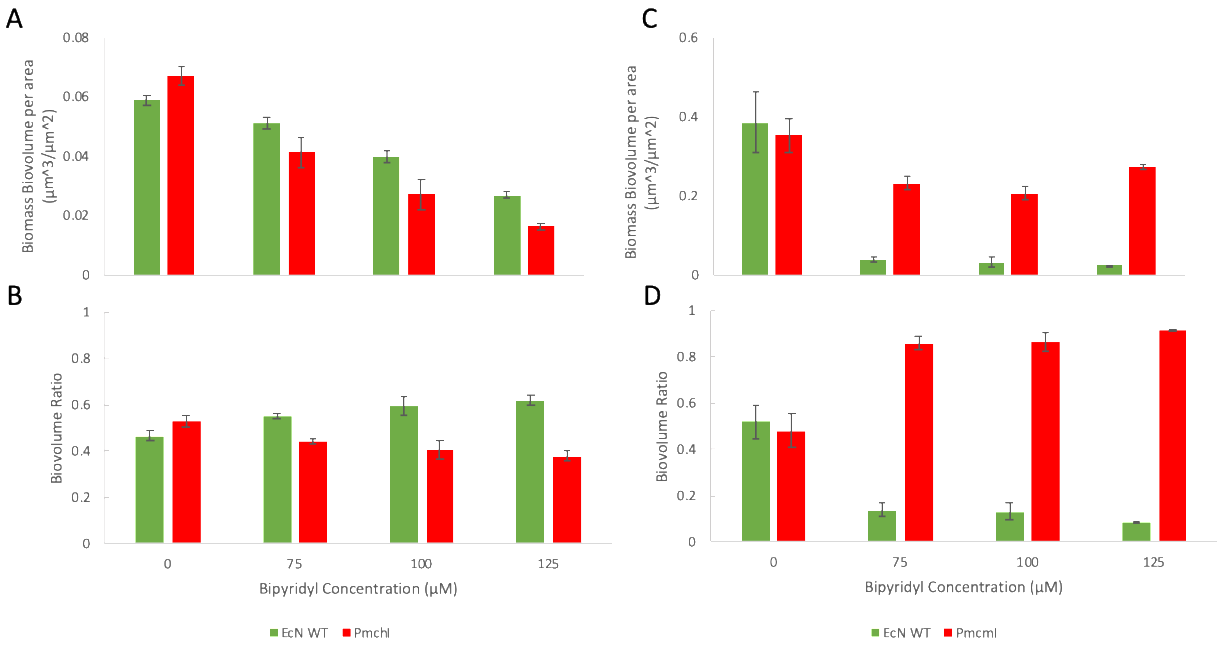

Figure 2.8-Growth competition of EcN WT and STm with microcin immunity plasmids. A) Raw area-normalized biovolume, from confocal fluorescence microscopy, of EcN WT (green) and STm pMchI (red) in coculture biofilms at different 2,2'-bipyridyl concentrations, and B) biovolume ratios of the same. C) Raw area-normalized biovolume of EcN WT (green) and STm pMcmI (red) in coculture biofilms, and (D) biovolume ratios of the same. While pMchI confers redundant immunity to STm WT, pMcmI confers additional immunity against the M microcin, greatly enhancing the competitiveness of STm with EcN under iron-limiting conditions.

2.4. Discussion

In this paper, we developed an *in-vitro* biofilm model that recapitulates the competition dynamics between EcN and STm as shown previously in murine models [6], [20]. The essential role of microcins during EcN and STm iron competition in biofilms was demonstrated. The results in this chapter show that microcin mediated inhibition of gut pathogen is not contact dependent, though microcins are required at a constant concentration to inhibit STm biofilm growth, which was achieved using microfluidics devices. Microcins are metabolically costly products and are produced in minimum quantities by the bacteria which makes their extraction and purification process difficult [29]–[32]. STm growth inhibition is mediated by microcins with post-translational modification to conjugate siderophores, which requires extractions of modified microcins from the

pool for modified and unmodified microcin making the extraction process tedious [27], [28]. The static and microfluidic *in vitro* biofilm models, on the other hand, simplify the study of competition mediated by microcins and siderophores, and they provide well resolved temporal and spatial information about community structure that is difficult to acquire through *in vivo* studies. Previous studies provide evidence that microcins M and H47 are post-translationally modified, however there is no information regarding the compound conjugated after the modification [33]. My results indicate that both microcins and *iroBC* genes are required for growth inhibition of STm. In contrast, an EcN *entC* mutant can outcompete STm, suggesting that EcN could be using STm enterobactin and salmochelin for post-translational modification of microcins. Previous work on *Klebsiella pneumonia* shows that the presence of unmodified microcins and salmochelin in supernatant is not enough to produce an antibacterial effect [34]. This has not been proven in the case of microcin M of EcN and the data in this chapter provides indirect evidence that *iroBC* may be required for post-translational modification of microcin in EcN.

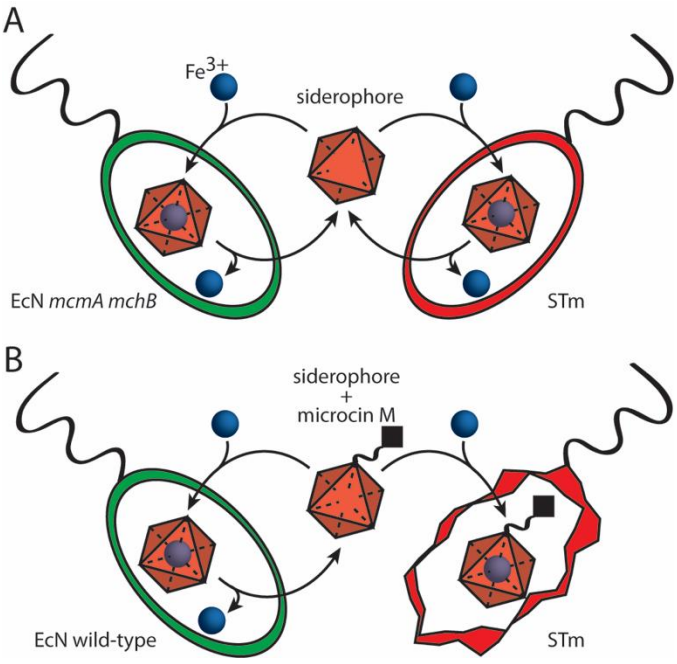

Figure 2.9- Schematic showing the proposed anti-cheating mechanism of the siderophore-microcin conjugate.

2.5. Conclusion

In conclusion, these results provide evidence that *in vitro* biofilm models can be used to study competition dynamics of *Enterobacteriaceae*. The data in this chapter agree with previous *in vivo* findings and provide evidence supporting the hypothesis that microcins act as an anti-cheating device of EcN [20] (**Figure *2.9***). Using microfluidic devices, it is shown that microcins are required at a constant concentration to induce pathogen growth inhibition, while growth assays and static biofilm growth in supernatant could not provide this information. Biofilm competition models in static and microfluidic devices will further our understanding of multispecies interactions of *Enterobacteriaceae* in the gut by providing the ability to separate different signaling and metabolite-based interactions, which *in vivo* models do not. Elucidation of such dynamics will better our understanding of underlying mechanism of the complex relationship between host and microbiota and provide potential target for intervention strategies.

2.6. References

[1] L. D. Palmer and E. P. Skaar, “Transition Metals and Virulence in Bacteria,” *Annu. Rev. Genet.*, vol. 50, pp. 67–91, 2016.

[2] B. J. Cherayil, “The role of iron in the immune response to bacterial infection,” *Immunol. Res.*, vol. 50, no. 1, pp. 1–9, May 2011.

[3] V. I. Holden and M. A. Bachman, “Diverging roles of bacterial siderophores during infection,” *Metallomics*, vol. 7, no. 6, pp. 986–995, 2015.

[4] G. A. M. Kortman, M. Raffatellu, D. W. Swinkels, and H. Tjalsma, “Nutritional iron turned inside out: intestinal stress from a gut microbial perspective,” vol. 38, pp. 1202–1234, 2014.

[5] M. F. Barber and N. C. Elde, “Buried Treasure: Evolutionary Perspectives on Microbial Iron Piracy,” *Trends Genet.*, vol. 31, no. 11, pp. 627–636, Nov. 2015.

[6] E. Deriu *et al.*, “Probiotic Bacteria Reduce *Salmonella Typhimurium* Intestinal Colonization

by Competing for Iron," *Cell Host Microbe*, vol. 14, no. 1, pp. 26–37, Jul. 2013.

[7] M. Valdebenito, A. L. Crumbliss, G. Winkelmann, and K. Hantke, "Environmental factors influence the production of enterobactin, salmochelin, aerobactin, and yersiniabactin in *Escherichia coli* strain Nissle 1917," *Int. J. Med. Microbiol. IJMM*, vol. 296, no. 8, pp. 513–520, Dec. 2006.

[8] J. Behnsen, S. Jellbauer, C. P. Wong, R. A. Edwards, M. D. George, and W. Ouyang, "The Cytokine IL-22 Promotes Pathogen Colonization by Suppressing Related Commensal Bacteria," *Immunity*, vol. 40, no. 2, pp. 262–273, 2014.

[9] P. Martin, S. Tronnet, C. Garcie, and E. Oswald, "Interplay Between Siderophores and Colibactin Genotoxin in *Escherichia coli* Battle for Iron Between Host and," *Int. Union Biochem. Mol. Biol.*, vol. 69, no. 8, pp. 435–441, 2017.

[10] W. Lee, B. M. Van, and J. Vincent, "An evolutionary mechanism for diversity in siderophore-producing bacteria," *Ecol. Lett.*, vol. 15, pp. 119–125, 2012.

[11] Z. Dumas and R. Kümmerli, "Cost of cooperation rules selection for cheats in bacterial metapopulations," *J. Evol. Biol.*, vol. 25, no. 3, pp. 473–484, Mar. 2012.

[12] A. Leinweber, R. F. Inglis, and R. Kümmerli, "Cheating fosters species co-existence in well-mixed bacterial communities," pp. 1179–1188, 2017.

[13] S. Duquesne, V. Petit, J. Peduzzi, and S. Rebuffat, "Structural and Functional Diversity of Peptides from Enterobacteria," pp. 200–209, 2007.

[14] K. Zimmermann, J. Blom, A. Goesmann, C. Po, A. Zschu, and F. Gunzer, "Identification and Characterization of Microcin S , a New Antibacterial Peptide Produced by Probiotic Escherichia," vol. 7, no. 3, pp. 1–9, 2012.

[15] S. Rebuffat, "Microcins in action: amazing defence strategies of Enterobacteria," *Biochem.*

Soc. Trans., vol. 40, no. 6, pp. 1456–1462, Dec. 2012.

[16] S. I. Patzer, M. R. Baquero, D. Bravo, F. Moreno, and K. Hantke, “The colicin G , H and X determinants encode microcins M and H47 , which might utilize the catecholate siderophore receptors FepA , Cir , Fiu and IroN Printed in Great Britain,” pp. 2557–2570, 2003.

[17] M. Barman *et al.*, “Enteric salmonellosis disrupts the microbial ecology of the murine gastrointestinal tract,” *Infect. Immun.*, vol. 76, no. 3, pp. 907–915, Mar. 2008.

[18] B. Stecher *et al.*, “Salmonella enterica serovar typhimurium exploits inflammation to compete with the intestinal microbiota,” *PLoS Biol.*, vol. 5, no. 10, pp. 2177–2189, Oct. 2007.

[19] T. D. Lawley, D. M. Bouley, Y. E. Hoy, C. Gerke, D. A. Relman, and D. M. Monack, “Host Transmission of Salmonella enterica Serovar Typhimurium Is Controlled by Virulence Factors and Indigenous Intestinal Microbiota,” *Infect. Immun.*, vol. 76, no. 1, pp. 403–416, Jan. 2008.

[20] M. Sassone-Corsi *et al.*, “Microcins mediate competition among Enterobacteriaceae in the inflamed gut,” *Nature*, vol. 540, no. 7632, pp. 280–283, Dec. 2016.

[21] F. Harrison and A. Buckling, “Siderophore production and biofilm formation as linked social traits,” *ISME J.*, vol. 3, no. 5, pp. 632–634, Feb. 2009.

[22] M.-H. Lin, J.-C. Shu, H.-Y. Huang, and Y.-C. Cheng, “Involvement of Iron in Biofilm Formation by *Staphylococcus aureus*,” *PLoS One*, vol. 7, no. 3, p. e34388, Mar. 2012.

[23] P. Cornelis and J. Dingemans, “Pseudomonas aeruginosa adapts its iron uptake strategies in function of the type of infections,” *Front. Cell. Infect. Microbiol.*, vol. 3, 2013.

[24] A. Trejo-Hernández, A. Andrade-Domínguez, M. Hernández, and S. Encarnación,

"Interspecies competition triggers virulence and mutability in Candida albicans–*Pseudomonas aeruginosa* mixed biofilms," *ISME J.*, vol. 8, no. 10, pp. 1974–1988, Oct. 2014.

[25] L. M. Filkins *et al.*, "Coculture of *Staphylococcus aureus* with *Pseudomonas aeruginosa* Drives S. aureus towards Fermentative Metabolism and Reduced Viability in a Cystic Fibrosis Model," *J. Bacteriol.*, vol. 197, no. 14, pp. 2252–2264, Jul. 2015.

[26] I. Stojiljkovic, A. J. Ba, F. Heffron, O. F. California, O. Health, and S. Unversity, "Ethanolamine Utilization in *Salmonella typhimurium*: Nucleotide Sequence, Protein Expression, and Mutational Analysis of the cchA cchB eutE eutJ eutG eutH Gene Cluster," *J. Bacteriol.*, vol. 177, no. 5, pp. 1357–1366, 1995.

[27] E. M. Nolan, M. A. Fischbach, A. Koglin, and C. T. Walsh, "Biosynthetic tailoring of microcin E492m: post-translational modification affords an antibacterial siderophore-peptide conjugate," *J. Am. Chem. Soc.*, vol. 129, no. 46, pp. 14336–14347, Nov. 2007.

[28] E. M. Nolan and C. T. Walsh, "Investigations of the MceIJ-catalyzed posttranslational modification of the microcin E492 C-terminus: linkage of ribosomal and nonribosomal peptides to form 'trojan horse' antibiotics," *Biochemistry*, vol. 47, no. 35, pp. 9289–9299, Sep. 2008.

[29] C. García-Bustos, J. F., Pezzi, N. & Asensio, "Microcin 7: Purification and Properties," *Biochem. Biophys. Res. Commun.*, vol. 119, no. 2, pp. 779–785, 1984.

[30] V. De Lorenzo, "Isolation and characterization of microcin E 492 from Klebsiella pneumoniae," *Arch. Microbiol.*, vol. 139, pp. 72–75, 1984.

[31] A. Pons, N. Zorn, D. Vignon, A. Van Dorsselaer, and G. Cottenceau, "Microcin E492 Is an Unmodified Peptide Related in Structure to Colicin V," vol. 46, no. 1, pp. 229–230, 2002.

[32] G. Corsini *et al.*, “Purification and characterization of the antimicrobial peptide microcin N,” *FEMS Microbiol. Lett.*, vol. 312, pp. 119–125, 2010.

[33] D. Destoumieux-garzo, C. Lombard, S. Rebuffat, and J. Peduzzi, “Isolation and Characterization of Two Members of the Siderophore-Microcin Family, Microcins M and H47,” *Antimicrob. Agents Chemother.*, vol. 54, no. 1, pp. 288–297, 2010.

[34] G. Mercado, M. Tello, M. Marín, O. Monasterio, and R. Lagos, “The Production *in vivo* of Microcin E492 with Antibacterial Activity Depends on Salmochelin and EntF,” *J. Bacteriol.*, vol. 190, no. 15, pp. 5464–5471, Aug. 2008.

Chapter 3
Osmotic Stress and Trehalose Synthesis in Bacterial Biofilms

3.1. Introduction

Biofilms are groups of adherent microbes that colonize solid surfaces. They are responsible for biofouling of plumbing and contamination of medical implants such as artificial joints and catheters [1], [2], [3]. By accumulating in a biofilm, microbes form a cluster of cells that are more resistant to conditions in the external environment [4]. Recent research on approaches to treat biofilm infections has focused on signaling factors that encourage dispersal of the biofilm and a return to the planktonic state, as microbes growing in liquid culture are more susceptible to traditional antibiotics [5], [6]. However, an alternative approach would be to prevent establishment of the biofilm to avert biofilm infections.

Microbes in a biofilm typically embed themselves in Extracellular Polymeric Substance (EPS) soon after colonization of a solid surface. EPS is a mixture of polysaccharides, nucleic acids, and proteins (**Figure *3.1***). EPS provides protection from shear forces and diffusible toxins such as antibiotics [7], [8]. Genetic reprogramming of gene expression in biofilms results from changes in environmental physicochemical conditions such as higher-osmolarity. In order to prevent water loss due to osmosis, microbes in a biofilm will upregulate the accumulation and biosynthesis of molecules known as compatible solutes [9], [10], [11].

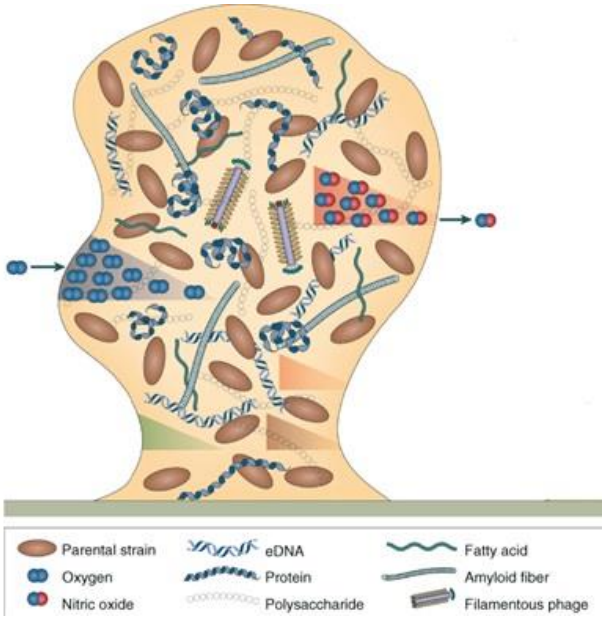

Figure 3.1 - Components of biofilms. Bacterial cells in the mature biofilm are characterized by and extracellular polymeric substance matrix which includes proteins, polysaccharides, proteins, and extracellular DNA (eDNA), and other compounds (adopted from [12]).

Compatible solutes are small organic compounds that can be accumulated in high concentrations without disturbing the function of macromolecules such as proteins and nucleic acids [13], [14]. By building up the intracellular concentration of compatible solutes, microbes are able to balance the solute concentration of both sides of the membrane and prevent loss of water. Compatible solutes have diverse structures and include substituted amines such as glycine betaine and sugars such as trehalose [14]. Based on bioinformatics studies demonstrating that *Pseudomonas aeruginosa* upregulated a glycine betaine transporter during biofilm formation, Mi et al. synthesized a panel of betaine precursors and tested their effect on *P. aeruginosa* biofilms. They found that one of the precursors, ethyl choline, inhibited biofilm formation but not planktonic growth. They hypothesized ethyl choline was transformed into ethyl glycine betaine, interfering with normal compatible solute recycling [15]. However, the authors noted the possibility for off-target effects in mammalian systems, as mammals utilize betaine in phospholipids of the plasma membranes and as a precursor for the neurotransmitter acetyl choline.

Trehalose is a much more attractive platform for targeting compatible solute inhibition. Mammals do not express proteins involved in trehalose biosynthesis or accumulation and have no known use for the sugar [16]. Recently, Wolber et al. synthesize a panel of trehalose analogs and tested them against mycobacterial biofilms [17]. Many of the trehalose analogs showed activity against mycobacterial biofilms at concentrations several orders of magnitude below the glycine betaine analogs from Mi et al's study. However, mycobacteria do not just use trehalose for osmo-protection, and require trehalose for formation of their cell wall [18]. While the authors did not observe any effect of the analogs on planktonic growth, the mycobacterial cells may just be more sensitive to cell wall disruption in a biofilm.

The commensal enteric microbe *Escherichia coli* also has a biosynthetic pathway for trehalose formation [19]. However, *E. coli* only uses trehalose for stress protection, and does not incorporate trehalose into the cell wall like mycobacteria. *E. coli* is genetically tractable, and pathogenic strains of *E. coli* have been isolated from biofilms of urinary catheters, making it a relevant experimental model for biofilm disruption [20].

In *E. coli*, trehalose is synthesized by the *otsBA* operon (**Figure *3.2***), and trehalose biosynthesis is controlled by the master stress regulator *rpoS*. Notably, *rpoS* knockouts of *E. coli* have severely impaired biofilm formation [21], [22]. However, *rpoS* controls the synthesis of more than 50 proteins, and a direct connection between trehalose and biofilm formation could not be conclusively drawn from these studies. Two bioinformatics studies of biofilm vs. planktonic gene expression gave conflicting results about the role of *otsBA* in biofilms. Ren et al. found no change in expression of *otsBA* in the *E. coli* JM109 strain, while Schembri et al. found that *otsB* expression decreased in a biofilm of *E. coli* MG1655 [23], [24]. Both sets of authors noted that their studies were limited to gene expression in two states: mid-log growth and well-established biofilms. Based on the importance of trehalose in the microbial stress response and the potential for compatible

solutes to be important in the full life cycle of biofilms, we decided to perform more focused tests on the significance of trehalose in *E. coli* biofilms.

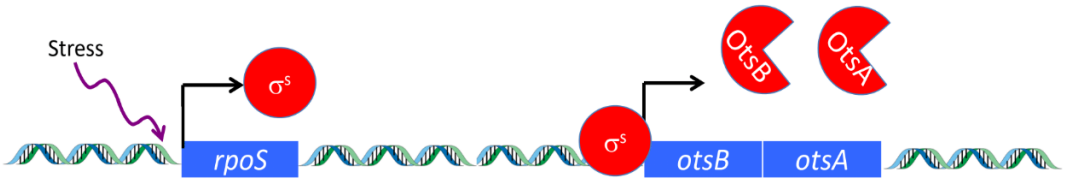

Figure 3.2 - Trehalose is synthesized from the enzymes OtsA and OtsB. Osmotic or thermal stress signals the transcription of the master stress regulator rpoS. The product of rpoS, activates transcription of otsA and otsB.

3.2. Materials and Methods

3.2.1. Bacterial Strains and Planktonic Culture Conditions

E. coli MC4100 was used in this study as a wild type strain when needed. The strain MDG131 [MC4100 ϕ(*ompF*$^{+}$-*yfp*$^{+}$) ϕ (*ompC*$^{+}$-*cfp*$^{+}$)], which contains operon fusions of *yfp* to *ompF* and *cfp* to *ompC*, was a gift from Albert Siryaporn (University of California, Irvine).

All strains were revived from frozen glycerol added stocks by streaking on lysogeny broth (LB) agar (1.5%) plates every 5 days. Single colonies were each inoculated in 3mL of 2% sterilized LB (2%) and placed on a rotating incubator at 37°C overnight and diluted with 1% tryptone broth (TB) to get to O.D. of 0.02.

Osmolarity was varied by supplementing with varying concentrations of sucrose. All chemicals were purchased from Fisher Scientific except dAdC which was from Sigma Aldrich.

3.2.2. Planktonic Culture Growth Curves

Overnight cultures of MDG131 strains were diluted by TB containing 0-15% sucrose. Each inner well of 96 well plate was filled with 200 µL of each solution and cell growth was tracked (optical density at 600 nm) for a day in shaking mode at 37°C. To analyze the dAdC effect on *E. coli* cells, 0-200 µM of dAdC added to the diluted cultures with the same protocol and growth curves were drawn for 24 hours of growth.

3.2.3. MDG131 Growth, *ompC/ompF* Expression

MDG131 overnight culture diluted 1:1000 into sucrose added M63 medium. 96 well plate filled with sucrose solutions (200 µL pipetted in inner wells) placed in the plate reader while continuously shaking in 37°C. YFP and CFP intensities were measured every 30 minutes using plate reader (BioTek Synergy H1) with excitation wavelengths of 500 nm and 420 nm and emission wavelengths of 540 nm and 485 nm respectively.

3.2.4. Biofilm Growth in Flow Cells

For biofilm growth in microfluidic devices, an overnight shaking culture of *E. coli yfp* or MDG131 was diluted in LB and seeded for 2 hours in channels without flow. The sterile tryptone with specific concentration of dAdC or sucrose was exchanged with inoculum and flowed into the channels through PTFE tubing (0.012” ID) with flowrate of 8 µL/h per channel by syringe pump. All dAdC solutions were prepared by dissolving dAdC in 1% Dimethyl Sulfoxide (DMSO).

3.2.5. Static Biofilm Characterization

2 mL of diluted overnight cultures of MC4100 and MDG131 were added to each well of sterile 6 well plates. One 18x18 mm coverslip submerged in each well and plates were kept in room temperature (22 °C) for 24 hours.

3.2.6. Crystal Violet Assay

To quantify biofilm formation, media was aspirated, the biofilms washed with Phosphate-*buffered* saline (PBS), and then stained with 0.1% aqueous crystal violet (CV) for 10 minutes. Excess stain was aspirated, the wells rinsed with PBS, and then stained biofilms were incubated with ethanol for 5 minutes to extract CV. CV was quantified by measuring the absorbance at 600 nm.

3.2.7. Confocal Microscopy

All biofilm samples were imaged by Zeiss LSM780 inverted confocal microscope. *E. coli* MC4100 *yfp* biofilms grown in microfluidic flow cells imaged with 63X oil immersion objective, Z intervals of 1 µm and a pinhole size of 101 µm. Cells were illuminated with a 488 nm laser and emission intensity was collected with 490-695 nm filter from YFP. For bio-volume quantification images were analyzed using the Volocity software. Each biofilm was imaged three times from different spots and final bio-volume values are the average of all for each treatment. Timeseries imaging was done through adjusting the settings to image 3 pre-selected spots on each channel every 30 minutes. The oil on the objective was refilled every 4 hours and the biomass biovolume levels for each spot in each time point was averaged to prepare the biofilm growth curve.

MDG131 strains used for static biofilm growth on 18x18 mm glass coverslips in tryptone media with and without sucrose addition for 24 hours. Each coverslip was rinsed by PBS to remove planktonic cells on the surface. Images were taken by 63x oil immersion objective, Z interval of 1 µm and a pinhole size of 50 µm from at least 3 different spots on each biofilm. YFP and CFP expressing cells were excited with 514 and 458 nm laser lines and 520-620 nm and 463-520 nm filters were used for YFP and CFP channels emission intensities. Z stacks were separated by ZEN lite black 2.3 SP1 software and intensity of each channel was quantified for each Z stack individually with Volocity.

3.2.8. Sample Analysis by LC-MS

3.2.8.1. Culture Growth Conditions

Trehalose biosynthesis levels were quantified for cells treated with sucrose and dAdC. Overnight cultures of wild type *E. coli* after dilution in 5 mL TB, incubated for 5 hours to reach mid-log phase and exposed to different concentrations of sucrose for 15 hours at 37°C in shaking incubator. But, for dAdC effect determination, the mid-log phase cells exposed to 5% sucrose and

0, 50, 100, and 200 µM dAdC for 0.5 and 1 hour. Each condition was prepared in three biological replicates.

3.2.8.2. *E. coli* Lysate Preparation

Before cell lysis, 50 µL of each treated sample was put aside and kept for CFU (Colony Forming Units) analysis. According to the method used for lysing cells before trehalose analysis, remaining cells were centrifuged (5000 rpm x 15 min), in conical tubes and the supernatant was removed. The cell pellet was resuspended in 5 mL PBS, centrifuged (5000 rpm x 15 min), and the supernatant was removed. This process was repeated one more time. After washing cells with PBS, each cell pellet was resuspended in 150 µL ultrapure water. These cell suspensions were heated at 97°C for 20 min, after which they were centrifuged (15000 rpm × 15 min) at 4°C. The supernatant was removed and kept frozen at −80°C until further use [25].

3.2.8.3. Deproteinization of Cell Lysates

For protein removal, 900 µL acetone which was kept in −80°C before use, was added to 100 µL of each lysed sample, vortexed for 30 seconds, and after 15 minutes centrifugation (15000 rpm), the supernatant was removed and located in speed-vac until complete evaporation. 100 µL of mobile phase used in LC-MS process, was added to each tube, vortexed and kept in -80°C until trehalose quantification process.

3.2.8.4. Liquid Chromatography−Mass Spectrometry (LC–MS) Conditions for Trehalose Quantification

Prepared deproteinized samples were analyzed at the UC Irvine Mass Spectrometry Core using a Waters Quattro Premier XE. LC separation was achieved using Waters high-performance C_{18} column. The mobile phase was composed of water containing 2 mM ammonium acetate (A_2) and 2 mM ammonium acetate with 3% acetonitrile (B_2). Analyte detection was achieved using an Agilent 6410B triple quadrupole mass spectrometer with an electrospray ionization source. The

mass spectrometer was operated in selected reaction monitoring (SRM) mode, monitoring for the trehalose transitions of 360-163 m/z and 360-85 m/z all in positive mode. Water MassLynx software version 4.1 was used to control all instruments.

3.2.8.5. Spot-Titer Culture Assay

CFU analysis was done with spot-titer culture assay. For each stock suspension, serial 10-fold dilutions were prepared started by adding 10 µL of sample to 90 µL of PBS in sterile 96-well plate. 5 µL from each dilution was spotted onto the LB-agar plate 5 times. After incubating plates in 37°C and enough growth of CFUs, they were counted, averaged, and reported as CFU/mL values.

3.2.8.6. Data Analysis and Trehalose Quantification

To calculate trehalose concentration per cell each sample was initially prepared in 3 biological replicates and each replicate was in a separate vial to be injected by the LC-MS autosampler needle 3 times to average three different quantified values for each biological replicate. According to the fact that cell lysates cause an error in analyte measurement, trehalose standard solutions were made in *otsA* mutant cell lysates background and trehalose levels were analyzed with the same LC-MS settings. These values were compared with the real trehalose added concentration and the correction factor was calculated (5.139). Considering the standard solutions made each time besides the real samples, 10 µL of each injection volume, and the correction factor, the concentration values read by the instrument were divided by the number of cells calculated for each sample the trehalose concentration per cell values were calculated and averaged for each proposed condition.

3.3. Results

3.3.1. Osmotic Stress Quantification in *E. coli* Biofilms

The relative expression levels of outer membrane porins, OmpC and OmpF is quantitatively indicative of osmotic stress experienced by *E. coli* cells. OmpC/OmpF ratio is increased by higher osmolarity in the media [26]. In order to show this behavior, MDG131 strains containing chromosomal transcriptional fusions of the gene for CFP to *ompC* and the gene for YFP to *ompF* were used and grown planktonically in sucrose added media. OmpC/OmpF ratio was increased by adding sucrose and it was measured by CFP and YFP intensities (**Figure *3.3***). Higher CFP/YFP ratio is showing more osmotic stress which is applied to the cells due to sucrose addition.

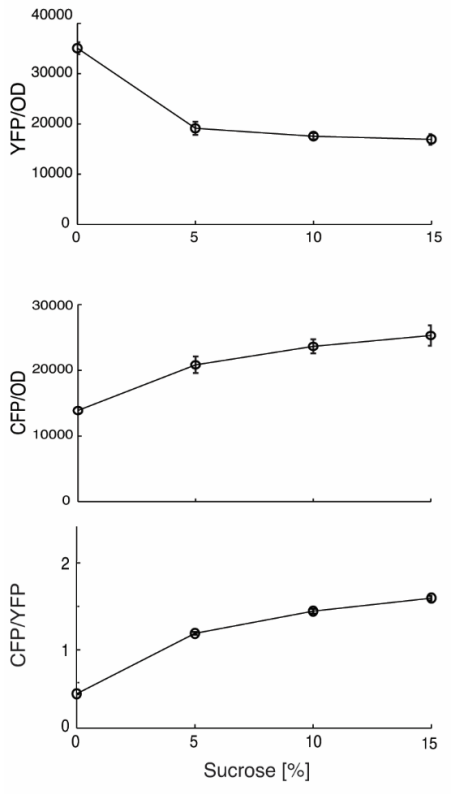

Figure 3.3 - Increasing sucrose concentration applies more osmotic stress to the planktonic cells. MDG131 planktonic cultures were grown in sucrose added media. Top) YFP/OD ratio is calculated for cultures grown in sucrose added m63. Middle) CFP/OD ratio is calculated for cultures grown in sucrose added m63. Bottom) CFP/YFP ratio is calculated for the same cultures for sucrose added m63. The fluorescent intensities and optical densities were

measured for sucrose added cultures, and were used to calculate YFP/OD, CFP/OD, and CFP/YFP ratios and averaged. For each condition, 3 biological replicates and 5 technical replicates for each were used. Error bars represent standard deviation values.

Additionally, MDG131 strains were grown as biofilms and imaged by confocal fluorescence microscopy to map the spatial distribution of osmotic stress. CFP/YFP values were higher for the cells deeper in the biofilm which are experiencing more osmotic stress due to higher solute concentration in that region. This data is in consistent with what is shown for planktonic cells in osmotically stressed media. It is a confirmation to show cells in biofilm environment are experiencing osmotic stress (**Figure *3.4***) [10], [27].

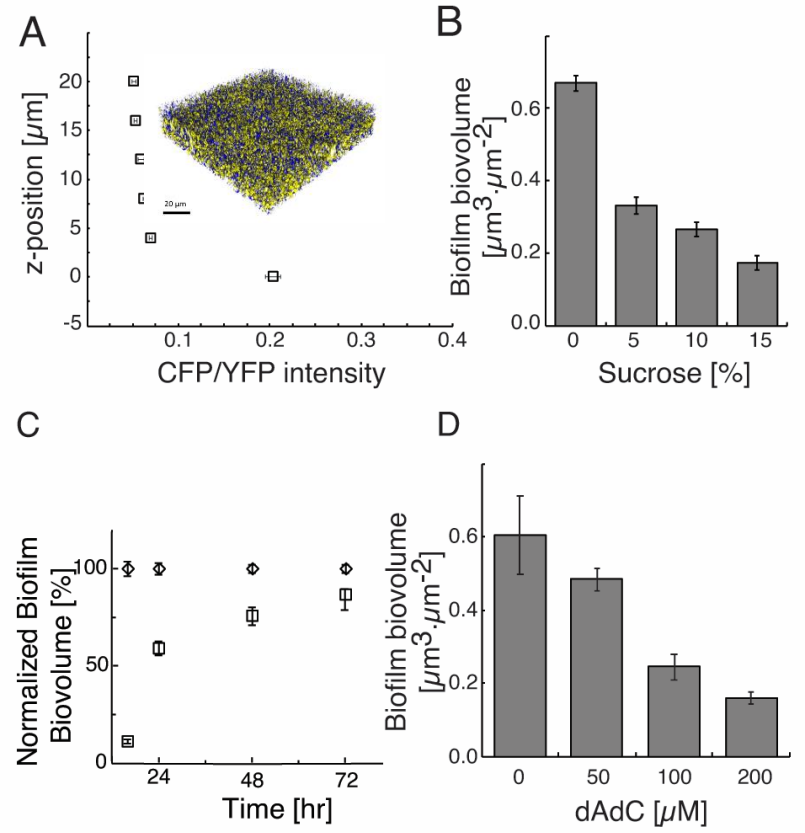

Figure 3.4 - A) There is a greater osmotic stress in the base layers of biofilm compared to the upper layers. CPF/YFP ratio for Z layers of 24-hour MDG131 biofilms were measured and averaged for three biological replicates and 3 technical replicates for each sample. Inset: 3D image of 24 h MDG131 biofilm grown in Tryptone media showing cells with YFP expression with yellow and CFP expression with blue to show osmotic stress applied to the cells in different layers of the biofilm. The scale shows 20 µm. **B) Increasing sucrose concentration inhibits *E. coli* biofilm growth.** *E. coli* YFP biofilm biovolume values were calculated by YFP intensity measurement for biofilms grown in flow cells fed by tryptone in the presence of different concentrations of sucrose for 24 hours. The biofilm biovolume values are averaged for 3 biological replicates for each concentration of sucrose. Three technical replicates were used for each sample. **C) dAdC loses its efficacy during 72 h biofilm growth.** Biofilm biovolume values of each static biofilm grown in the presence of only tryptone (diamond), and tryptone + 200 µM dAdC were

measured by CV assay and normalized by using the values of the same time point for the biofilms grown in tryptone only. Each value is the average of 3 biological replicates which are repeated three times technically each**. D) *E. coli* biofilm growth is inhibited in the presence of constant concentration of dAdC**. Biofilm biovolume values were measured for three biological replicates of *E. coli* YFP biofilms grown in flow cells fed by tryptone + 0-200 µM dAdC. Each biological replicate is repeated three times technically.

3.3.2. Osmotic Stress Inhibits *E. coli* Biofilm Growth

Osmotic stress applied to the cells inhibits the growth rate. *E. coli* planktonic growth rate is lowered by the increase in osmotic stress applied to the cells by adding up to 15% sucrose to the growth media (**Figure *3.5***). Accordingly, *E. coli* biofilms challenged with sucrose to increase osmotic stress, experienced inhibition in the growth (**Figure *3.4*-B**). This demonstrates that increasing osmotic stress can limit bacterial growth, even when the bacteria are protected in a biofilm.

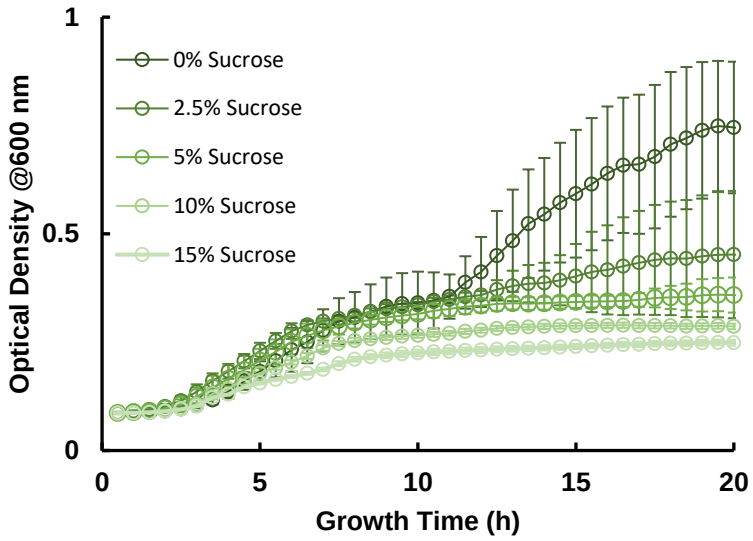

Figure 3.5 - Sucrose inhibits planktonic growth of *E. coli*. Optical density of *E. coli* cultures was measured for cells grown in LB + 0-15% sucrose. The optical density values are the average of 10 technical replicates and error bars represent standard deviations.

3.3.3. Involvement of *E. coli* Trehalose Synthesis Pathway in Biofilm Growth

In order to examine the effect of trehalose in biofilm formation, wild type MC4100 *E. coli* alongside a mutant where trehalose biosynthesis had been disabled (*otsA*$^{-}$) were grown. The OtsA protein combines glucose-6-phosphate and UDP glucose to make trehalose-6-phosphate,

while the OtsB protein has phosphatase activity that produces trehalose. Trehalose synthesis was disabled by transposon insertion in the *otsA* gene, as nonspecific phosphatase activity from other proteins could potentially complement an *otsB* knockout [28].

Wild type MC4100 *E. coli* and the MC4100 *otsA*⁻ mutant were grown in tryptone broth (TB) in 6 well plates. The *otsA*⁻ mutant had a severe biofilm formation defect (**Figure *3.6***). However, no difference in growth was observed in *otsA*⁻ planktonic cultures in TB (data not shown), in agreement with previous studies [29].

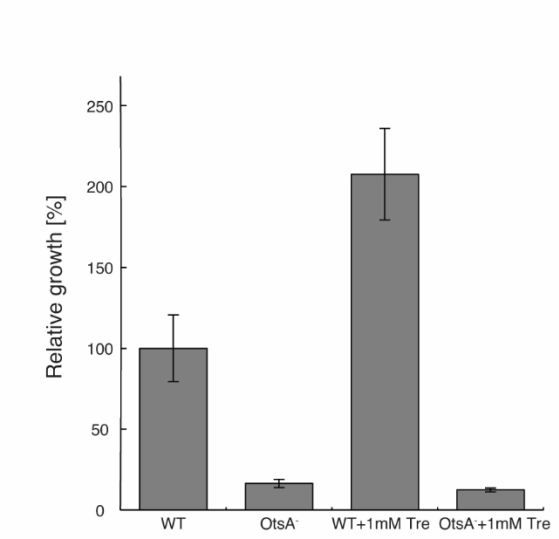

Figure 3.6 - Deficiency of MC4100 ΔotsA strain cannot be compensated for by exogenous trehalose. *The biofilm defect in MC4100 ΔotsA strain can be partially complemented by a plasmid containing otsA. Biofilms for three biological replicates of MC4100 (WT), and MC4100 ΔotsA (OtsA⁻) were grown in TB. The biofilms were measured with CV assay and the values are reported relative to the values from WT cells grown in only TB. Results are the averages of three biological replicates for each 3 technical replicates were used. Error bars represent standard deviations.*

The biofilm defect of the *otsA*⁻ mutant could not be recovered by adding trehalose to the media. *E. coli* has no known trehalose transporter, and trehalose cannot cross the plasma membrane [30]. Thus, exogenous trehalose could not complement the *otsA*⁻ mutant biofilms. However, high concentrations of trehalose increased the biomass in wild type MC4100 *E. coli* biofilms. *E. coli* expresses a periplasmic trehalase, which hydrolyzes trehalose into two glucose

molecules. *E. coli* has a glucose transporter, allowing these bacteria to import glucose and convert the carbon from trehalose into increased biomass.

In order to show that the biofilm defect of the *otsA*⁻ mutant was trehalose-specific, the *otsBA* pathway was cloned into an IPTG-inducible plasmid and transformed into the *otsA*⁻ mutant. When compared next to an empty vector treated MC4100 *otsA*⁻ mutant, the *otsBA*-complemented *otsA*⁻ mutant showed increased biomass under biofilm growth conditions. Empty vector MC4100 biofilm growth was unchanged, as expected (**Figure *3.7***).

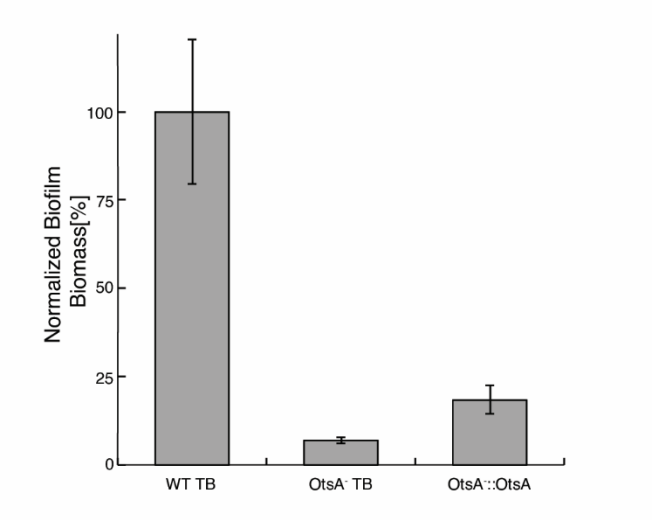

Figure 3.7 - The biofilm defect in MC4100 ΔotsA strain can be partially complemented by a plasmid containing otsA. Triplicate cultures of MC4100 (WT), MC4100 ΔotsA (OtsA⁻), and MC4100 ΔotsA transformed with a plasmid containing the otsBA operon (OtsA⁻OtsBA) were grown in TB to form biofilms. The biofilm growth was quantitated by CV assay and the values were normalized by the biofilm growth values from WT biofilms. Each biological replicate was done with three technical replicates and the obtained values are averaged. Error bars represent standard deviation.

The data from our *otsA*⁻ mutant experiments suggested that trehalose synthesis was important for biofilm growth. Next, we sought to determine if inhibition of trehalose biosynthesis in wild type *E. coli* could affect biofilm growth. Since the phosphatase activity of the OtsB protein could potentially be emulated by other proteins in the bacterium, we again focused our efforts on the OtsA protein.

3.3.4. Small Molecule Inhibition of Biofilm Growth

Small molecules can be selected to inhibit trehalose synthesis. Pan and Elbein performed a screen of purified mycobacterial OtsA and found that Novobiocin inhibited the protein in the millimolar range [31]. However, Novobiocin already has antimicrobial activity due to DNA gyrase inhibition in the micromolar range. While there are some Novobiocin-resistant mutants of *E. coli*, teasing apart gyrase vs. OtsA inhibition would be difficult. Errey et al. solved the structure of *E. coli* OtsA and created a transition state analog that functioned as a competitive inhibitor of OtsA [32]. This transition state analog inhibited OtsA in the millimolar range. While this could be improved to micromolar range by coincubation with UDP, the authors noted this was not practical for clinical settings. Kern et al. performed a high throughput screen to find inhibitors of insect OtsA proteins. Since insects rely on trehalose as a rapidly mobilizable carbon source, they proposed OtsA inhibitors could be potent insecticides [33]. They focused on the cat flea, *Ctenocephalides felis*, and the fruit fly, *Drosophila melanogaster*. There is a significant evolutionary divergence between OtsA from insects and microbes (**Figure *3.8***)**.** Insect OtsA proteins have an extended carboxy terminus that has no overlap with microbial OtsA proteins. However, the active sites of all the enzymes are highly conserved. Kern et al. measured IC_{50} values as part of their screen, so we were unable to determine whether the inhibitors they discovered function by binding the conserved regions or the unique carboxy termini. However, they identified several dozen compounds that inhibited insect OtsA proteins, some of which are inexpensive and commercially available.

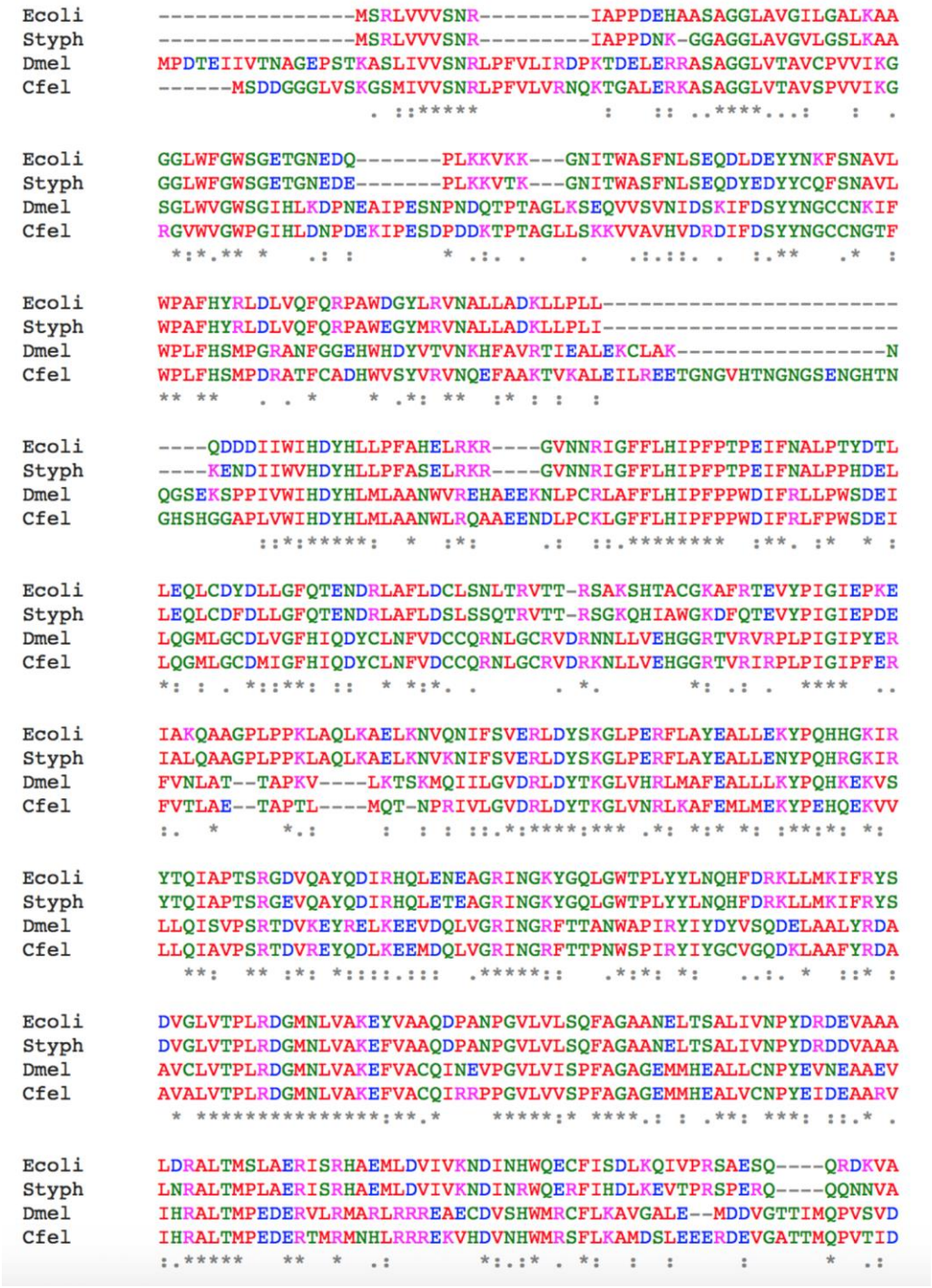

Figure 3.8 - OtsA multiple sequence alignment. *The first four hundred amino acids from E. coli (Ecoli), Salmonella enterica (Styph), Drosophila melanogaster (Dme), and Ctenocephalides felis (Cfe) were aligned using Clustal W. Colons denote similar amino acids, while stars denote identical amino acids. Fruit fly and cat flea have an additional 250 amino acids at their C termini with no identity to bacterial species (not shown)*

Most of the inhibitors discovered by Kern et al. have a 2,6 diamino 3, 5 di-carbonitrile thiopyran scaffold. Of the panel they examined, we decided to focus on one compound, 2,6-

diamino-4-cyclohexyl-4H-thiopuran-3,5-dicarbonitrile (dAdC). dAdC was active against both cat flea and fruit fly OtsA proteins, inhibiting them in the micromolar range. It has low/medium toxicity (LD_{50} of 150 mg/kg in rat) and is commercially available. To determine the effect of dAdC planktonic growth of *E. coli* was compared in presence of different concentrations of dAdC in TB. The growth rates were similar in absence and presence of dAdC and no inhibition in growth was observed (**Figure *3.9*).** Wild type MC4100 *E. coli* biofilms were grown in the presence and absence of 200 µM dAdC. After 16 hours, 80% inhibition of biofilm biomass was observed. The biofilm cultures were followed for several days, and dAdC-treated cultures still displayed a biofilm formation defect after three days (**Figure *3.4*-C**).

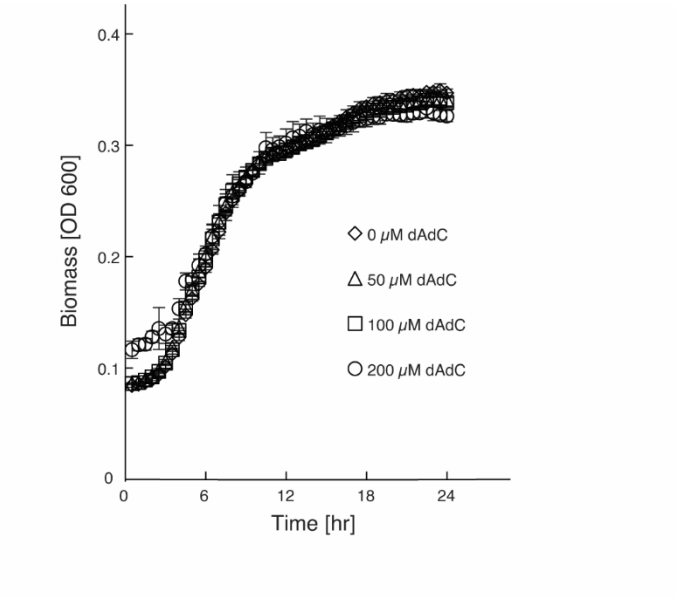

Figure 3.9 - dAdC does not inhibit MC4100 planktonic growth in TB. Optical density of cultures were averaged for all replicates during 24 hour growth in the presence of 0-200 µM dAdC in the TB. Each condition was done by three biological replicates for each 5 technical replicates were used. Error bars represent standard deviations.

In order to test whether the effects of dAdC were specific to the *E. coli* MC4100 strain, *Salmonella enterica* subsp. Typhimurium was incubated with dAdC. *S.* Typhimurium also synthesizes trehalose using the OtsBA pathway, and the active site of its OtsA protein is nearly identical to insect and *E. coli OtsA*. Biofilm formation in *S.* Typhimurium was inhibited by dAdC, although not to the same degree as the *E. coli* MC4100 strain (**Figure *3.10***). Additionally, *S.*

Typhimurium planktonic growth was unaffected by dAdC (data not shown), suggesting that, like *E. coli,* trehalose biosynthesis is only critical under biofilm growth conditions.

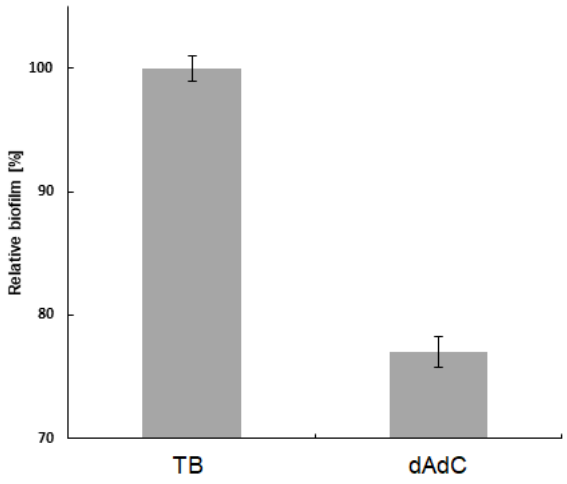

Figure 3.10 - *S. Typhimurium* biofilm growth is inhibited by dAdC. Biofilm growth of *S. Typhimurium* in TB only, and TB + 200 μM dAdC was quantitated and reported relative to values for TB only. Optical densities read for 3 biological replicates which have been technically repeated 3 times each, were averaged and reported. Error bars represent standard deviation.

While our studies suggested that dAdC was reducing biofilm growth by affecting OtsA, we decided to exclude the possibility that dAdC was acting against another target. dAdC effect was examined on a bacterial strain that does not require OtsA to synthesize trehalose. *P. aeruginosa* is a Gram-negative pathogen that synthesizes trehalose from the starch via the TreY/TreZ pathway. The TreY and TreZ enzymes show no similarity to OtsA, and thus we would not expect dAdC to have any activity against this bacterium. Cultures of *P. aeruginosa* incubated under biofilm formation conditions had identical biomass in the presence and absence of dAdC (data not shown).

dAdC appeared to lose efficacy over time, so we hypothesized the compound was being degraded by the bacteria. In order to address this possibility, MC4100 *E. coli* expressing Yellow Fluorescent Protein (YFP) was seeded in a continuous flow microfluidic device to initiate biofilm formation. In this system, the bacteria were constantly exposed to fresh dAdC and had no opportunity to degrade the drug. The seeded cells in every 4 channels were fed by similar

concentration of dAdC (0, 50,100, and 200 µM). The results show that there is a significant difference between average biomass biovolume grown in the channels in presence of dAdC and its absence (**Figure *3.4*-D**). Also, for making biofilm growth curve, the biofilms were imaged under a confocal microscope every thirty minutes, and biofilm biomass was reduced by 90% in the presence of 200 µM dAdC after 20 hours (**Figure *3.11***).

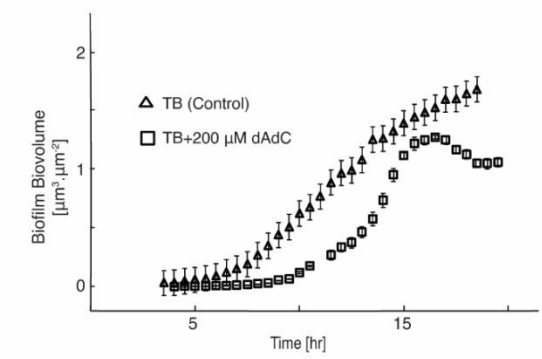

Figure 3.11 - MC4100 biofilm growth curve shows inhibition effect of dAdC during exponential phase of growth. Biofilm biovolume values for MC4100 YFP grown in flow cells, fed by TB only, or TB + 200 µM dAdC, were calculated during 20 h of growth by confocal images taken every 30 minutes. Reported values are the averages of 4 spots from two different channels. Error bars represent standard deviations of biofilm biovolumes.

Since planktonic cells grown in media containing dAdC had no growth defect, biofilm biomass reduction could be an indication of osmotic stress applied to the cells in this environment. The inhibitory effect of dAdC on trehalose biosynthesis would then result in an increase in osmotic stress. This can be confirmed by measuring trehalose made by *E. coli* in presence of dAdC during osmotic stress.

3.3.5. dAdC is an effective inhibitor of trehalose production in osmotic stress condition

Trehalose synthesis as a response to osmotic stress by *E. coli* can be lowered in presence of dAdC. MC4100 exposed to sucrose, induced osmotic stress, and showed lower growth with higher concentration of sucrose, as expected. We hypothesized that *E. coli* would upregulate trehalose biosynthesis when experiencing higher osmotic stress. Planktonic cultures

grown in TB did not produce significant amounts of trehalose, while cells exposed to 20% sucrose had five-fold higher trehalose accumulation than samples grown in 1% sucrose (**Figure *3.12*-A**). As expected, *otsA* $^{-}$ cells showed no accumulation of trehalose under any sucrose concentration and had impaired growth when cultured in sucrose added media (data not shown). Sucrose addition increased trehalose synthesis by *E. coli* cultures as a result of stress application to the cells.

A)

B)

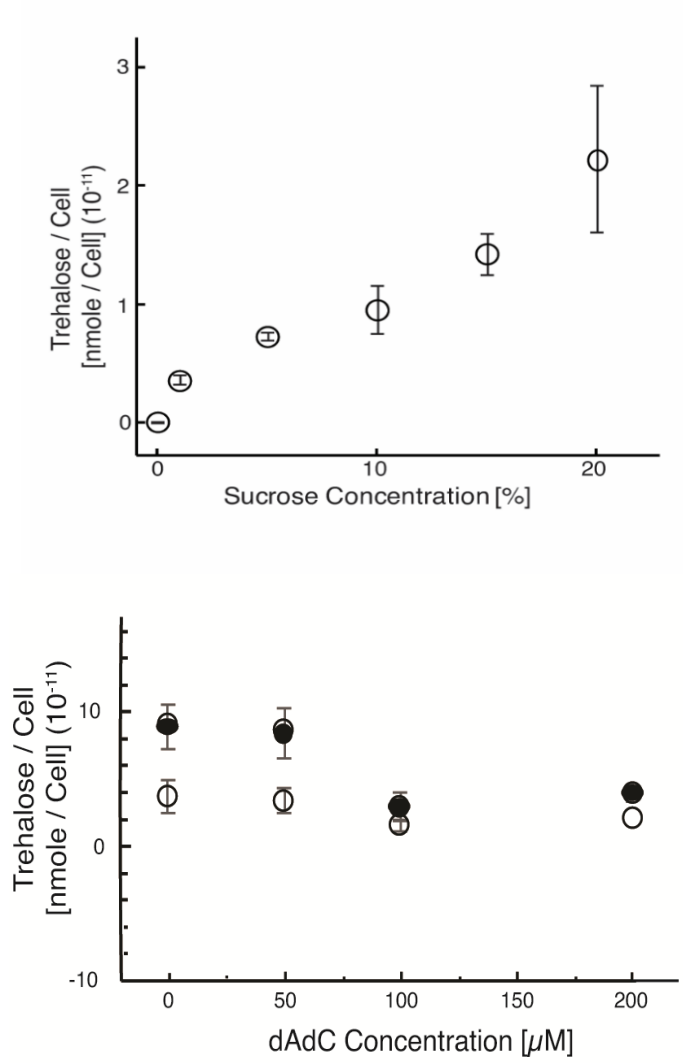

Figure 3.12 - *E. coli* trehalose synthesis is induced by osmotic stress and inhibited by dAdC. A) trehalose synthesis was measured for 3 biological replicates for each concentration of sucrose added to LB. **B)** osmotically stressed cells were exposed to dAdC for 0.5 h (open circle), and 1 h (closed circle). Each trehalose concentration is the average of 3 biological replicate for which we had 3 reads of trehalose concentration.

Based on the obtained data, 5% sucrose was added to media to induce osmotic stress in the cells which will be challenged with dAdC. Addition of 100 and 200 µM dAdC caused significant decrease in trehalose production (**Figure *3.12*-B**). We could attribute this effect specifically to

OtsA inhibition by dAdC, as OtsA mutant cells were unable to make trehalose in varying concentrations of sucrose.

3.4. Discussion

Infections of medical implants are costly complications of surgical procedures. Previous attempts to intervene in the establishment of biofilms by targeting the microbial stress response have met with little success due to the overlap between some microbial compatible solutes and mammalian biomolecules. In this study, we have demonstrated that the compatible solute trehalose is critical for establishment of biofilms in *E. coli* MC4100 and may be significant in other bacterial pathogens. As mammals have no known uses for this compatible solute, pharmaceuticals targeting trehalose, or its biosynthesis could be a new method to target biofilm formation.

It is unclear why our study found a correlation between trehalose and biofilm formation, whereas bioinformatics studies found the expression of trehalose biosynthetic pathways decreased in mature biofilms. Biofilm formation is a complex metabolic process, and it is possible that microbes early in the establishment of a biofilm are more sensitive to osmotic stress, or that established biofilms switch to using a different compatible solute. The creation of reporter strains to track compatible solute synthesis helps to reconcile these disparate sets of data.

At this point it is unclear how dAdC affects the trehalose biosynthetic protein OtsA. Kern et al. only used IC_{50} values to assay OtsA inhibition, and more detailed enzyme kinetics studies will be necessary to be done to find the precise mechanism of inhibition. However, there are other compounds with the same 2,6 diamino 3, 5, di-carbonitrile thiopyran scaffold as dAdC, and some of them may have greater efficacy against microbial OtsA.

dAdC is relatively hydrophobic and needed to be dissolved in DMSO in order to be present in high enough concentration to affect biofilm formation. However, that does not preclude its use

in a clinical setting. It may be possible to imbue medical implants with dAdC so that it can slowly diffuse out and delay or prevent the establishment of a biofilm. In this case, concentrating dAdC at the point where it is most needed would solve the problem of its low water solubility.

Trehalose biosynthesis has been targeted in microbes that require trehalose for cell wall biosynthesis. However, it is usually ignored in microbes that only require it for stress response. While dAdC may not be the most ideal candidate for inhibiting OtsA, this work clearly establishes trehalose biosynthesis in general, and OtsA function, in particular, as a promising drug target to prevent biofilm formation.

3.5. References

[1] D. Feraco, M. Blaha, S. Khan, J. M. Green, and B. J. Plotkin, “Host environmental signals and effects on biofilm formation,” *Microb. Pathog.*, vol. 99, pp. 253–263, 2016.

[2] A. Ogawa, K. Takakura, K. Sano, and H. Kanematsu, “Microbiome Analysis of Biofilms of Silver Nanoparticle-Dispersed Silane-Based Coated Carbon Steel Using a Next-Generation Sequencing Technique,” *Antibiotics*, vol. 7, no. 91, pp. 1–10, 2018.

[3] M. Chen, Q. Yu, and H. Sun, “Novel Strategies for the Prevention and Treatment of Biofilm Related Infections,” pp. 18488–18501, 2013.

[4] N. M. Vega and J. Gore, “Collective antibiotic resistance: mechanisms and implications,” *Curr. Opin. Microbiol.*, vol. 21, pp. 28–34, 2014.

[5] A. Bhattacharjee, T. D. Nusca, and A. I. Hochbaum, “Rhamnolipids Mediate an Interspecies Bio fi lm Dispersal Signaling Pathway,” *ACS Chem. Biol.*, vol. 11, pp. 3068–3076, 2016.

[6] M. Y. Galperin and M. Gomelsky, “Cyclic di-GMP: the First 25 Years of a Universal Bacterial Second MEssenger,” *Microbiol. Mol. Biol. Rev.*, vol. 77, no. 1, pp. 1–52, 2013.

[7] H. G. Brink and W. Nicol, “The influence of shear on the metabolite yield of Lactobacillus rhamnosus biofilms,” *N. Biotechnol.*, vol. 31, no. 5, pp. 460–467, 2014.

[8] C. Martin *et al.*, “Strategies for Antimicrobial Drug Delivery to Biofilm,” *Curr. Pharm. Des.*, vol. 21, no. 1, pp. 43–66, 2015.

[9] P. S. Stewart, M. J. Franklin, K. S. Williamson, J. P. Folsom, L. Boegli, and A. James, “Pseudomonas aeruginosa Biofilms,” vol. 59, no. 7, pp. 3838–3847, 2015.

[10] C. Prigent-combaret, O. Vidal, C. Dorel, and P. Lejeune, “Abiotic Surface Sensing and Biofilm-Dependent Regulation of Gene Expression in *Escherichia coli*,” vol. 181, no. 19, pp. 5993–6002, 1999.

[11] D. Kapfhammer, E. Karatan, K. J. Pflughoeft, and P. I. Watnick, “Role for Glycine Betaine Transport in Vibrio cholerae Osmoadaptation and Biofilm Formation within Microbial Communities,” *Appl. Environ. Microbiol.*, vol. 71, no. 7, pp. 3840–3847, 2005.

[12] D. Mcdougald, S. A. Rice, N. Barraud, P. D. Steinberg, and S. Kjelleberg, “Should we stay or should we go : mechanisms and ecological consequences for biofilm dispersal,” *Nat. Publ. Gr.*, vol. 10, no. January, 2012.

[13] P. H. Yancey, “Organic osmolytes as compatible , metabolic and counteracting cytoprotectants in high osmolarity and other stresses,” *J. Exp. Biol.*, vol. 208, pp. 2819–2830, 2005.

[14] N. Empadinhas and M. S. Costa, “Diversity and biosynthesis of compatible solutes in hyper/thermophiles,” *Int. Microbiol.*, vol. 9, pp. 199–206, 2006.

[15] L. Mi, G. A. Licina, and S. Jiang, “Nonantibiotic-Based Pseudomonas aeruginosa Biofilm Inhibition with Osmoprotectant Analogues,” *ACS Sustain. Chem. Eng.*, vol. 2, pp. 2448–2453, 2014.

[16] J. Argu, “Why Can’t Vertebrates Synthesize Trehalose ?,” *J Mol Evol*, vol. 79, pp. 111–116, 2014.

[17] J. M. Wolber *et al.*, “The trehalose-specific transporter LpqY-SugABC is required for antimicrobial and anti-biofilm activity of trehalose analogues in Mycobacterium smegmatis,” *Carbohydr. Res.*, vol. 450, pp. 60–66, 2017.

[18] P. J. Woodruff *et al.*, “Trehalose Is Required for Growth of *Mycobacterium smegmatis*,” *J. Biol. Chem.*, vol. 279, no. 28, pp. 28835–28843, 2004.

[19] O. Kandror, A. Deleon, and A. L. Goldberg, “Trehalose synthesis is induced upon exposure of *Escherichia coli* to cold and is essential for viability at low temperatures,” *PNAS*, vol. 99, no. 15, pp. 9727–9732, 2002.

[20] A. R. Eberly *et al.*, “Biofilm Formation by Uropathogenic *Escherichia coli* Is Favored under Oxygen Conditions That Mimic the Bladder Environment,” *Int. J. Mol. Sci.*, vol. 18, pp. 1–12, 2017.

[21] J. L. Adams and R. J. C. McLean, “Impact of rpoS Deletion on *Escherichia coli* Biofilms,” *Appl. envrionmental Microbiol.*, vol. 65, no. 9, pp. 4285–4287, 1999.

[22] A. Ito, T. May, K. Kawata, and S. Okabe, “Significance of rpoS During Maturation of *Escherichia coli* Biofilms,” *Biotechnol. Bioeng.*, vol. 99, no. 6, pp. 1462–1471, 2008.

[23] D. Ren, L. A. Bedzyk, S. M. Thomas, R. W. Ye, and T. K. Wood, “Gene expression in *Escherichia coli* biofilms,” *Appl. Microbiol. Biotechnol.*, vol. 64, no. 4, pp. 515–524, 2004.

[24] M. A. Schembri, K. Kjaergaard, and P. Klemm, “Global gene expression in *Escherichia coli* biofilms,” *Mol. Microbiol.*, vol. 48, no. 1, pp. 253–267, 2003.

[25] G. A. Hayner, S. Khetan, and M. G. Paulick, “Quantification of the Disaccharide Trehalose from Biological Samples: A Comparison of Analytical Methods,” *ACS Omega*,

vol. 2, pp. 5813–5823, 2017.

[26] E. Batchelor and M. Goulian, “Robustness and the cycle of phosphorylation and dephosphorylation in a two-component regulatory system,” *PNAS*, vol. 100, no. 2, pp. 691–696, 2003.

[27] A. C. Graf *et al.*, “Virulence Factors Produced by *Staphylococcus aureus* Biofilms Have a Moonlighting Function Contributing to Biofilm Integrity Authors Virulence Factors Produced by *Staphylococcus aureus* Biofilms Have a Moonlighting Function Contributing to Biofilm Integrity,” *Mol. Cell. Proteomics*, vol. 18, pp. 1036–1053, 2019.

[28] H. M. Giaiver, O. B. Styrvold, and I. Kaasen, “Biochemical and Genetic Characterization of Osmoregulatory Trehalose Synthesis in *Escherichia coli*,” *J. Bacteriol.*, vol. 170, no. 6, pp. 2841–2849, 1988.

[29] J. L. Willis, M. S. Shultz, and P. J. Woodruff, “Chromate reduction is expedited by bacteria engineered to produce the compatible solute trehalose,” *Biotechnol Lett*, vol. 35, pp. 1291–1296, 2013.

[30] W. Boos, U. Ehmann, E. Bremer, and A. Middendorf, “Mapping and cloning of its structural gene and identification of the enzyme as a periplasmic protein induced under high osmolarity growth conditions,” *J. Biol. Chem.*, vol. 262, no. 27, pp. 13212–13218, 1987.

[31] Y. T. Pan and A. D. Elbein, “Inhibition of the Trehalose-P Synthase of Mycobacteria by Various Antibiotics,” *Arch. Biochem. Biophys.*, vol. 335, no. 2, pp. 258–266, 1996.

[32] J. C. Errey *et al.*, “Mechanistic Insight into Enzymatic Glycosyl Transfer with Retention of Configuration through Analysis of Glycomimetic Inhibitors,” *Angew. Chem. Int. Ed*, vol. 49, pp. 1234–1237, 2010.

[33] C. Kern *et al.*, “Trehalose-6-phosphate synthase from the cat flea Ctenocephalides felis and Drosophila melanogaster: gene identification, cloning, heterologous functional expression and identification of inhibitors by high throughput screening,” *Insect Mol. Biol.*, vol. 21, no. 4, pp. 456–471, 2012.

Chapter 4
Pseudomonas aeruginosa Outcompetes the Background Polymicrobial Community Under Treatment Conditions in a Novel Chronic Wound Model[5]

4.1. Introduction

Opportunistic pathogens such as *Pseudomonas aeruginosa* typically dominate the microbial community in chronic infections, yet the underlying mechanisms are not well understood. In the earlier stages of infection, commensal microbes and host physiology play an important role in establishing a favorable environment for the opportunistic pathogen. For example, in cystic fibrosis, anaerobes present in the airways break down mucins to produce amino acids and short chain fatty acids that *P. aeruginosa* uses as a carbon source to grow and colonize [1]. Cross-feeding between commensal bacteria and *P. aeruginosa* has also resulted in changes in antibiotic tolerance [2]. However, the dynamic between the commensal microbes and opportunistic pathogens is missing in many chronic wound and infection models. Several wound studies indicate multispecies biofilms have negative impacts on wound healing and antimicrobial efficacy [3], [4]. In an *in vivo* murine chronic wound model, oxidative stress and community composition alone do not characterize the microbial community metabolism [5]. Similarly, tissue models, including an *ex vivo* porcine lung model, investigate only the growth of a single pathogen at a time [6]–[9]. To better understand chronic infections, it is important to consider the entire microbial community.

In order to model a polymicrobial community in a biologically relevant context, we developed a perfusion wound meat model that could support the growth of a native meat microbial background and *P. aeruginosa* (**Figure 4.1**). Based on an *ex vivo* porcine lung model for cystic

[5] This work was done in collaboration with Whiteson's lab. I participated in model design, characterizing the biofilm growth on meat surface, growth quantification, and fluorescent imaging.

fibrosis [6], [7], our *in vitro* model adds liquid flow via media perfusion and a native meat microbial community. Dumigan et al. included perfusion in the *ex vivo* porcine lung model but investigated the pathogenesis of a single pathogen – *Klebsiella pneumoniae* without the presence of a native microbiota [8]. Oates et al. developed a basally perfused model that successfully supports the growth of a multispecies community, but lacks a biological host component [4]. Our perfused meat model incorporates nutrient flow through a meat matrix that supports the growth of a multispecies biofilm. Just as human skin harbors a native microbial community, the meat microbial community was used to replicate a non-sterile environment of a wound or chronic infection.

To study changes in metabolite profiles in these microbial communities, volatile molecules were detected using vacuum assisted sorbent extraction (VASE). VASE involves extracting volatile molecules under vacuum, which results in greater detection sensitivity than methods that actively absorb the volatiles from the headspace of a sample (i.e. solid phase microextraction). The measurement of volatile molecules provides a non-invasive approach that could be widely used for detecting biomarkers in health and disease. Other studies have incorporated surveying volatile molecules to identify biomarkers of chronicity in wounds [10]–[12]. Therefore, elucidating the metabolism within the polymicrobial communities in wounds in response to antibiotic treatment and ROS from the host may reveal important information on treatment efficacy, microbial persistence, and host outcome.

We used the perfusion meat model to address the following questions: 1) how does the microbial community composition and viability shift in response to common wound therapies of antibiotics and hydrogen peroxide? and 2) how do metabolic signatures of this community change in response to these therapies? The overall technological goal and impact was to understand the community, metabolite, and pathogen dynamics in bacterial infections.

4.2. 4.2. Materials and Methods

4.2.1. Strains and Growth Conditions

Pseudomonas aeruginosa UCBPP-PA14 and clinical isolate PaFLR01 were used in this study. Clinical isolate PaFLR01 was isolated from the sputum of an individual with cystic fibrosis. The genome sequencing and assembly can be found with BioProject Accession PRJNA434465 on NCBI. Published studies involving PaFLR01 include [13] and [14]. *P. aeruginosa* strains were inoculated into Luria-Broth (LB for PA14; Sigma-Aldrich) or Todd-Hewitt broth (TH broth for PaFLR01; Sigma-Aldrich) and grown overnight on a shaker at 37°C. PaFLR01 does not grow well in LB, thus requiring a richer media for growth. Optical density measurements to estimate bacterial culture concentrations were made at 500 nm, rather than the standard 600 nm, in order to avoid overlapping signals from pigments including pyocyanin produced by *P. aeruginosa*. The meat microbial background was native to the meat.

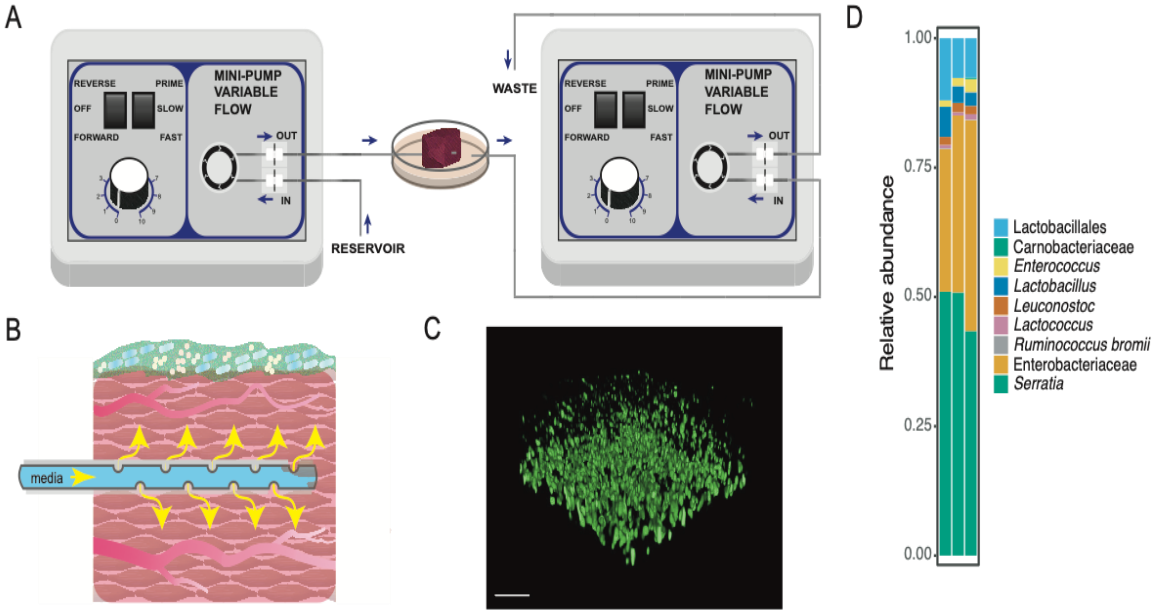

Figure 4.1-Schematic for the perfusion wound meat model. A) Perfusion setup with two flow regulators as described in the Methods. Briefly, the purpose of each of the flow regulators was to introduce flow of nutrients through the tissue and to remove excess media waste. Perforated tubing was threaded through the tissue to provide nutrients to the surrounding tissue. The end of the tube was capped, allowing the media to be released only through the pores

on the tubing in the meat (also displayed in B) A closer look at the tissue with flow and biofilm growth from the perfusion model. C) A confocal image of the PA14-YFP biofilm on the surface of the tissue. The biofilm image was taken from the static model after 24 hours of growth. Bar = 20 µm. The tissue had a native microbial community, meat background (MB control), whose bacterial members are displayed in D). The microbial community sequenced in D) was from the static meat model because we were only able to harvest enough cells from the static model for 16S rRNA amplicon sequencing.

4.2.2. Perfusion Meat Model

Meat for the perfusion model was from a packaged New York Strip Steak from a commercial source (beef, Trader Joe's). Steak tissue was cut into approximately 1-inch cubes and stored in phosphate buffered saline (PBS) at -20°C and thawed at 4°C before use. At the start of the experiment, the tissue was submerged in *P. aeruginosa* from an overnight culture diluted in LB to $OD_{500\ nm}$ = 0.05, or sterile LB as a control, in a 50 mL tube for 2 h at 37°C before setting up the perfusion model. At the end of this incubation, the tissue was transferred to a 30 mm petri dish for the perfusion setup.

The setup consisted of tubing, two flow regulators, a 30 mm petri dish, an autoclave tub, tissue, and 500 mL glass bottles to store media or collect waste (**Figure 4.1-A** and **Figure *4.2***). To pass the tubing through the 30 mm petri dish, a heated 16 ½ G needle was used to make holes on opposite sides of the dish. We pipetted 4 mL of LB into the 30 mm petri dish, threaded tubing that was perforated and sealed at one end through one side of the petri dish and tissue. The tubing that collected waste or excess media was pulled through the opposite side of the petri dish and the end of the tube was placed where the outward flow would not be disrupted. The threading process was performed with autoclaved dissection tweezers. Liquid media continuously flowed through the tube at the rate of 0.2 mL/min. Waste collection was also set at the rate of 0.2 mL/min. The perfusion setup was incubated for 24 hours in a temperature-controlled room set at 37°C.

Figure 4.2- Images of perfusion experiment A) Picture of the entire perfusion setup. Each pump controls the flow of either the waste or input media. B) A closeup of the perfused meat. One end of tubing is going through the meat tissue. The tubing on the lower left corner is removing the waste.

Perturbation conditions included the following additions to the input media: 50 µg/mL carbenicillin, 20 µg/mL gentamicin, or various concentrations of hydrogen peroxide. The concentrations of gentamicin and hydrogen peroxide were selected based on concentrations found in the literature relevant to chronic wounds and wound treatments summarized in Table 2. At the conclusion of each perfusion experiment, half of the tissue was saved for enumeration of colony forming units (CFUs) and the other half was saved for analysis of volatile compounds.

Sterilization of the materials used in the perfusion model consists of bleach, ethanol, and autoclaving. The tubing is submerged in a 10% bleach solution for at least 2 hours, rinsed and drained with water, dried, and autoclaved. The surgical tweezers used for manipulation of the tubing and meat are sprayed with bleach and autoclaved prior to each experiment. During the perfusion setup, the tweezers are sprayed with a bleach solution and then an ethanol solution to prevent cross- contamination when preparing multiple experiments. The petri dishes are purchased as sterile.

Table 4.1- Concentrations of biologically and treatment relevant hydrogen peroxide and antibiotics.

Molecule	Model	Concentration	Result	Reference
Hydrogen peroxide	C57/BL6 mice (excision wounds)	10 mM or 166 mM	Low concentrations of exogenous H_2O_2 promoted wound closure but high concentrations of it delay wound closure	[15]
Hydrogen peroxide	C57BL/6 mice	~225 µM after 2 days and ~150 µM after 5 days	Concentration of H_2O_2 measured in wound fluid	[16]
Hydrogen peroxide	C57BL/6 mice	~330 µM in wound fluid after 2 days	Concentration of H_2O_2 measured in wound fluid	[17]
Gentamicin	Healthy human	18.0 ± 4.0 mg · liter^{-1} in serum, 6.7 ± 2.0 mg · liter^{-1} in subcutaneous tissue	Concentration of gentamicin in serum and subcutaneous tissue	[18]
Gentamicin	Human, irrigation in joint replacement surgery	≤ 2 µg/mL in serum 4 and 24 hours post-surgery	Concentration of gentamicin in serum after surgery with an initial dose of 320 mg gentamicin (diluted with 40 mL saline)	[19]
Gentamicin ointment	Inoculated cellulose disks with PAO1	0.1% with gauze	Gentamicin ointment prevents formation of *P. aeruginosa* biofilm.	[20]

4.3. Static Meat Model

The basis of this experimental setup was modeled after the *ex vivo* porcine lung model in Harrison et al. [6]–[8]. The differences, however, included the tissue source and media, and our model did not use antibiotics to clear the native microbial community from the tissue. Tissue for the static model was the same as used for the perfusion model. The static model was performed in a 12-well plate and stored at 37°C for 24 hours. The tissue was submerged in a diluted overnight bacterial culture (OD_{500} 0.05) or sterile LB as a control in a 50 mL tube and incubated for 2 hours prior to the start of the plate experiment. After the 2-hour incubation, each cube was placed in an individual well in the 12-well plate. Media was added to each well to cover the tissue. Each well contained about 2 mL media with or without antibiotic or hydrogen peroxide and the tissue. At the conclusion of each static experiment, half of the tissue was saved for enumeration of CFUs.

4.3.1. Cell Viability and Relative Growth Analysis

Half of the tissue was vortexed with 1 mL of media for 30 seconds to remove cells adhered to the tissue surface. The liquid was then collected and used for dilution plating, where 10 µL of each dilution was spotted onto a LB or TH agar petri dish at least three times as technical replicates for each biological sample. LB agar plates were used for models with PA14, whereas TH agar plates were used for models with PaFLR01. Colonies of *P. aeruginosa* and meat background (MB) microbes were distinguished by phenotype. *P. aeruginosa* formed smaller and darker brown-green colonies while MB formed larger white colonies. All colonies that were not the *P. aeruginosa* phenotype were counted as MB.

4.3.2. Statistical Analyses

Analysis of variance (ANOVA) was performed with the aov function. Corrections for multiple comparisons following ANOVA were performed with the TukeyHSD function. Assumptions for ANOVA were tested with shapiro.test (normal distribution of residuals) and leveneTest (car package; homogeneity of variances) [21]. For data did not meet both assumptions for ANOVA, T tests were performed. The compare_means function from the ggpubr package in R was used to perform T tests to compare group means [22]. P values were adjusted with the Benjamini-Hochberg method (p.adjust.method = 'BH') for tests with multiple comparisons. Nonmetric multidimensional scaling (NMDS) was performed with the metaMDS function from the vegan package in R [23]. To generate clusters in the metabolic heatmap, a Bray-Curtis distance matrix of the sample normalized metabolite data was generated using the vegdist function in the vegan package [23]. The resulting matrix was then put into dist, hclust, and as dendrogram functions from the package stats [24].

4.3.3. Headspace Detection and Analysis

Volatile headspace analysis was performed using vacuum assisted sorbent extraction (VASE), the instrument and method developed by Entech Instruments (Simi Valley, California) were coupled with sample injection and thermal desorption on a gas chromatography mass spectrometer (GC-MS). The half of the tissue sections not used for viability and growth analysis were prepared by VASE for 1 hour at 70°C. Briefly, tissues stored at -80°C were thawed on ice for one hour and then placed into a pre-cleaned type 1 glass vial (VOA; Thermo Scientific). A VASE Sorbent Pen cartridge containing Tenax was placed into the vial and held in place by a lid liner. Air was removed from the vials using a vacuum pump and the vials were placed in a shaking incubator for 1 hour at 70°C. At the end of the extraction, vials were placed on a metal block equilibrated at -20°C for 15 minutes to remove water from the headspace. VASE pens were removed from the vials and their contents were run on an Agilent GC-MS (7890A GC and 5975C inert XL MSD with Triple-Axis Detector) with a DB-624 column. The splitless GC-MS method starts at 35°C with a 5-minute hold, ramps 10°C/min until 170°C, and ramps 15°C/min until 230°C with a total method runtime of 38 minutes. The corresponding Entech method has a 38-minute runtime with a preheat duration for 2 minutes at 260°C, desorption duration for 2 minutes at 260°C, bake-out duration for 33 minutes at 260°C, and post bake duration for 3 minutes at 70°C. Analysis and quantification of peaks were performed in the Agilent ChemStation software.

4.3.4. Meat Microbial Background Characterization

The meat microbial background was harvested from the control static meat model after 24 hours at 37°C. Microbial cells were collected from two sources: 1) the media the tissue was incubated in and 2) cells attached to the tissue collected by washing and vortexing the tissue with fresh media. Communities from three pieces of meat from the same steak were sequenced. All materials collected were combined, pelleted, and stored at -80°C until DNA extraction. DNA was extracted using the Quick-DNA Fecal/Soil Microbe Miniprep kit (D6010) from Zymo Research

(Irvine, CA). The 16S rRNA V4-V5 region was amplified using the 515F and 926R primers from the Earth Microbiome Project [151] and sequenced on an Illumina Miseq. The composition was determined using QIIME2 (https://qiime2.org/). The 16S rRNA data are available on the SRA at NCBI with BioProject ID PRJNA640161.

4.3.5. Visualization of PA14 Growth on Meat Tissue Surface

To visualize growth on the surface of the meat, we grew PA14-yfp in the static model for 24 hours. The tissue was rinsed gently with 1X PBS to wash off excess cells from the surface. Confocal laser scanning microscopy (Zeiss LSM780) with 63X oil immersion was used to visualize PA14-yfp growth on the surface of the tissue. Dichroic beam splitters were used to filter laser lines at 488 nm and emission intensity was collected from YFP at 493-598 nm. The images were processed in Volocity software to show the 3D image of PA14-yfp growth on the tissue

4.4. Results

4.4.1. Development of a Novel Perfused Meat Model

The goal of the perfused meat model was to create a three-dimensional *in vitro* model of bacterial community growth on an organic substrate resembling the wound environment to study the effects of antimicrobials on microbial growth and metabolism (**Figure 4.1**). Perfusing the tissue with nutrients mimics the role of vasculature found in wound tissue; the flow rate of media can be tailored to mimic different tissue types and could be infused with different compounds of interest such as host-derived factors and therapeutics, including the antibiotics and reactive oxygen species used in the present study. Pictures of the perfusion setup are shown in **Figure *4.2***. Visualization of PA14-yfp growth on the surface of the meat is shown in **Figure 4.1-C**. The use of steak as tissue provides important biological and structural or physical components that would not be present in a liquid culture model. Steak also has a native polymicrobial community, which was dominated in our samples by Enterobacteriaceae and *Serratia* (**Figure 4.1-D**) but also

included Lactobacillales, Carnobacteriaceae, *Enterococcus*, *Lactobacillus*, *Leuconostoc*, *Lactococcus*, and *Ruminococcus bromii*. In the following, we refer to this community as the meat background (MB). The microbes characterized in the meat background are also found as normal flora of the human gut, skin, oral cavity, and vagina, suggesting that the microbes native to the perfused meat model may represent relevant interactions for *P. aeruginosa* in infections in different types of communities.

In the meat model experiments described below, we grew and analyzed communities composed of either the MB alone or the MB inoculated with a *P. aeruginosa* lab strain (PA14, "PA14+MB") or clinical isolate (PaFLR01, "PaFLR01+MB"). We distinguish two populations in the pathogen inoculated PA14+MB (or PaFLR01+MB) community CFU analysis: the pathogen (PA14 or PaFLR01) and MB in the presence of the pathogen - "MB(PA14)" or "MB(PaFLR01)".

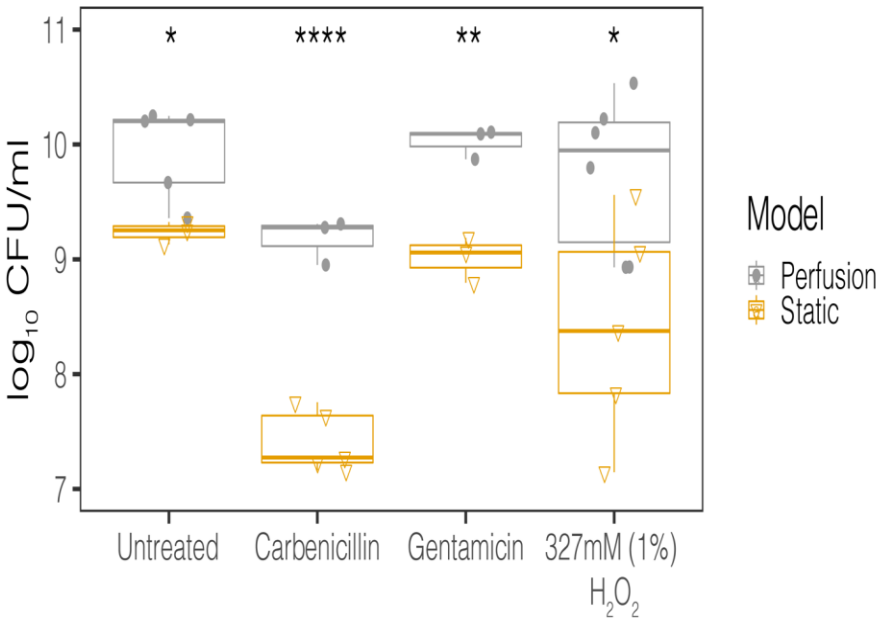

Figure 4.3- Perfusion and static model growth comparisons for the MB control community across antimicrobial treatments. The MB control community is the microbial background native to the meat. Treatments include control, 327 mM (1%) hydrogen peroxide, 50 µg/mL carbenicillin, and 20 µg/mL gentamicin. The closed circles represent the perfusion model and the open triangles represent the static model. Each point represents the average from at least three technical replicates from dilution plating for each biological replicate (N ≥ 3). Statistical testing was performed with ANOVA. Significance is indicated by asterisks. * $p < 0.05$; ** $p < 0.01$; **** $p < 0.0001$.

4.4.2. Impact of Antimicrobial Compounds on the Growth of the *P. aeruginosa* and Meat Microbial Background

In order to rationalize the use of media perfusion in our model, we first compared perfusion and static conditions for the MB control population in our meat model. The concentrations of antibiotics and hydrogen peroxide were chosen based on those used in therapeutic treatment and produced in physiological conditions (Table 2). The MB control population had significantly higher viable cell counts when grown in perfused media conditions compared to static conditions for all treatments – control, 327 mM (1%) hydrogen peroxide, carbenicillin, and gentamicin (**Figure *4.3***). All subsequent experiments were performed under perfused media conditions.

To measure the effects of antimicrobials on polymicrobial communities in the meat model, we perfused carbenicillin, gentamicin, gentamicin plus hydrogen peroxide, and hydrogen peroxide alone through meat with MB only or PA14+MB or PaFLR01+MB communities and measured colony forming units per mL (CFU/mL) after 24 hours of incubation (see Materials and Methods). In the control conditions, without any antimicrobial treatment, the viable cell density (CFU/mL) did not significantly differ between PA14 and its corresponding meat background community, MB(PA14), nor did CFU/mL differ between PaFLR01 and MB(PaFLR01), indicating that the growth of one population did not inhibit the growth of the other (**Figure *4.4***). There were also no differences in growth between the MB control (no PA) and the PA associated MB populations (**Figure *4.4***). However, with the addition of carbenicillin (50 µg/mL) at therapeutic concentrations, there was a significant decrease in the MB(PA14) population compared to PA14, but not in MB(PaFLR01) compared to PaFLR01. The addition of gentamicin (20 µg/mL) at therapeutic concentrations resulted in no differences between PA14 or PaFLR01 and their associated MB populations, MB(PA14) and MB(PaFLR01). H_2O_2 suppressed both MB(PA14) and MB(PaFLR01) growth relative to PA14 and PaFLR01, respectively. In carbenicillin, gentamicin, and 1 mM - 327 mM (1%) hydrogen peroxide antimicrobial conditions, MB(PA14 or PaFLR01) growth was significantly suppressed compared to the MB control (no PA) (**Figure *4.4*** and **Figure *4.5***).

For additional therapeutically relevant treatments with both gentamicin and hydrogen peroxide (1%), there was a significant decrease in the MB(PA14) population compared to PA14 and MB control (**Figure *4.5***) despite there being no significant difference for PA14 and MB(PA14) with gentamicin exposure alone. At H_2O_2 concentrations relevant to those naturally occurring in wounds during healing (0.05 – 0.5 mM) [15]–[17], there were no significant differences between PA14 and MB(PA14) populations (**Figure *4.5***). Significant differences between PA14 and MB(PA14) populations occurred at 1mM, 10 mM, 327 mM (1%), and 980 mM (3%) hydrogen peroxide (**Figure *4.5***).

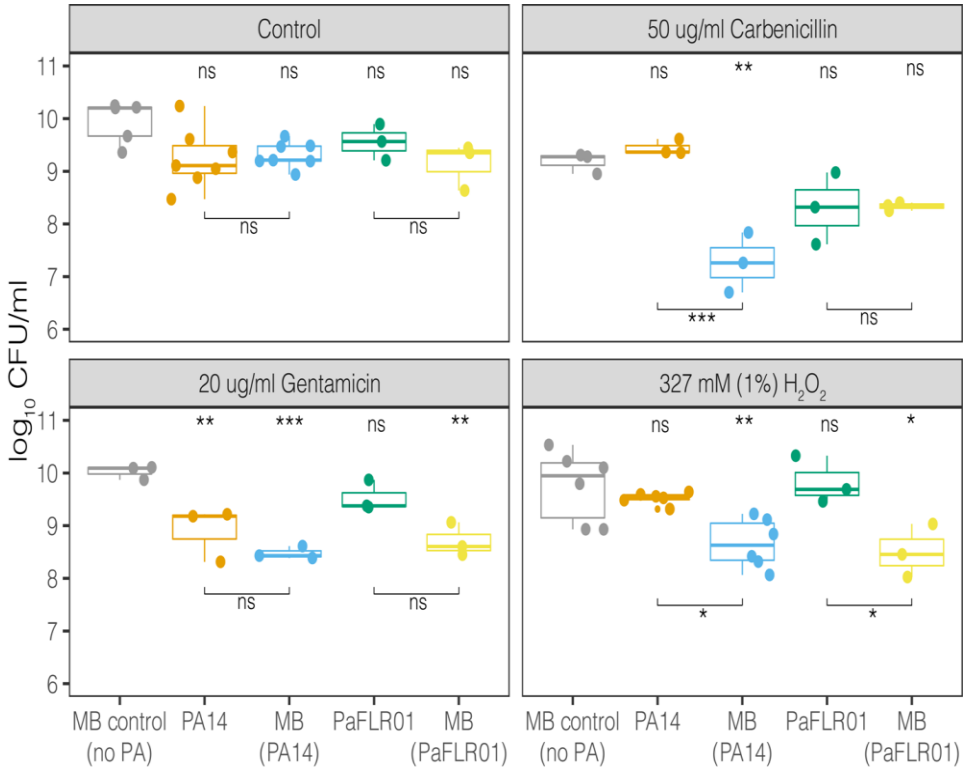

Figure 4.4- Growth, in CFU/mL, of MB alone, *P. aeruginosa* strains [PA14, PaFLR01] and their corresponding MB communities [MB(PA14), MB(PaFLR01)] in the perfused media meat model. Each point is a biological replicate and represents the average of > 3 technical replicates from dilution plating. N ≥ 3 biological replicates for all conditions. Statistical testing was performed with ANOVA with post-hoc Tukey tests. Significance is indicated by asterisks. The asterisk and "ns" indicators on the top of the graph are significance tests of each population versus the MB control (no PA). The asterisks and "ns" indicators with bars below the data are comparisons between the populations connected by the bars. ns $p > 0.05$; * $p < 0.05$; ** $p < 0.01$; ***$p < 0.001$.

4.4.3. Polymicrobial Community Volatile Metabolism

To probe the metabolism of the polymicrobial community when exposed to antimicrobials, we detected volatile metabolites with vacuum assisted sorbent extraction (VASE) and quantified relative abundances of the analytes on a gas chromatography-mass spectrometer (GC-MS). Because PA14 and MB(PA14) were grown on the same tissue, we could not determine whether PA14 or one of the native bacteria produced each volatile metabolite in these samples. However, we did measure the volatile molecules emitted from the MB control community as a baseline for identifying changes in metabolism associated with the addition of PA14 and antimicrobials. In addition, we expect the volatile molecules associated with fermentation such as acetic acid, 2,3-butanedione, ethanol, acetaldehyde and others, to be more commonly associated with the meat microbial background than PA14, which does not ferment unless in the absence of alternative anaerobic respiratory nutrients such as nitrate, nitrite, or arginine [25]–[27]. We also expected to detect core volatiles known to be produced by *P. aeruginosa*, including 2-nonanone, acetophenone, 2-aminoacetophenone, 2-butanone, dimethyl sulfide, dimethyl trisulfide, 2-heptanone, and others [28]–[30].

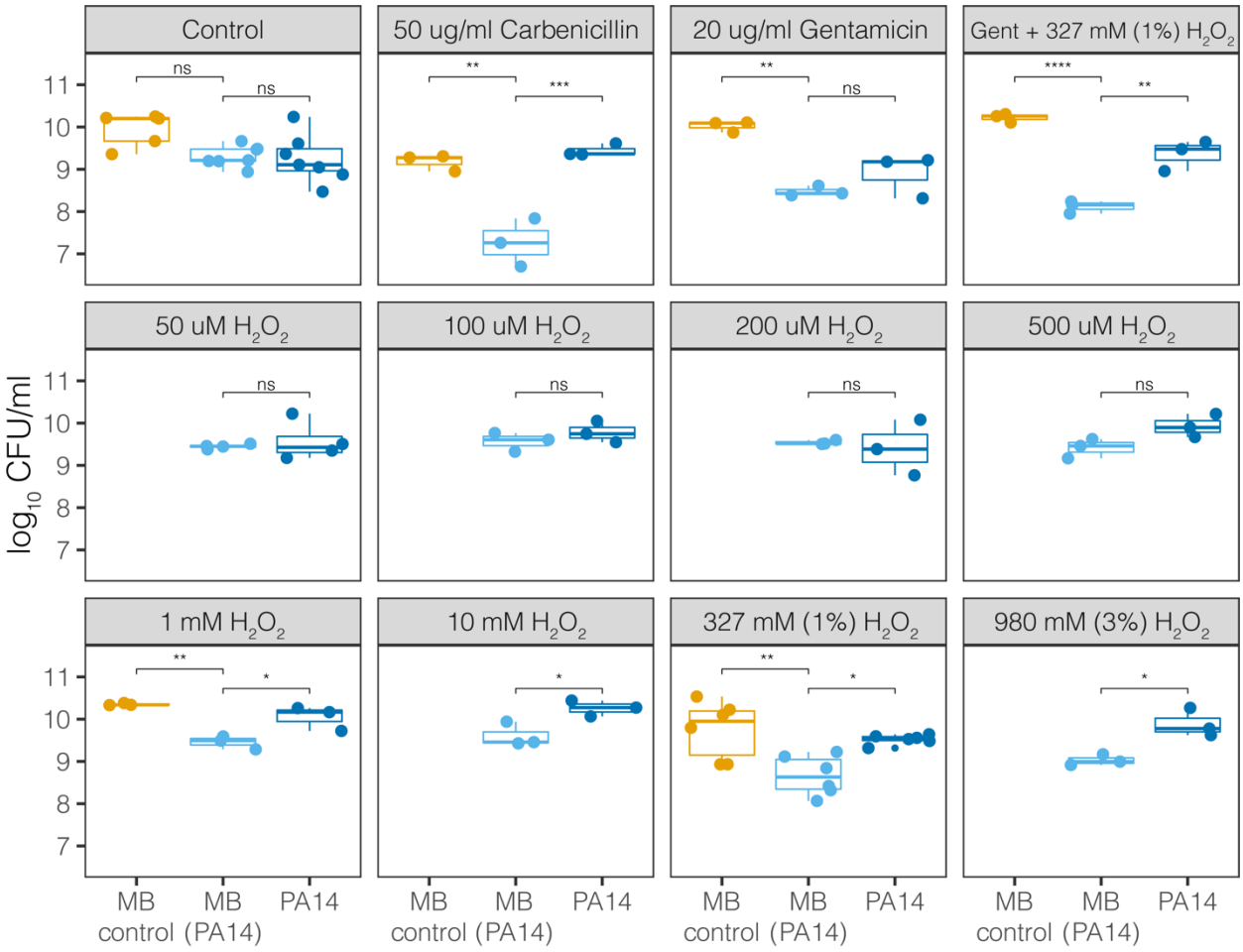

Figure 4.5- Growth summary of additional treatments for the perfusion model with MB control, PA14 and MB (PA14) populations. Note: MB control was not always included in these experiments. PA14 represents the colony counts of PA14 when grown with the meat background. MB (PA14) represents the colony counts of the meat microbial background when grown with PA14. MB(PA14) and PA14 colony counts come from the same tissue, but the counts for each do not overlap. MB control represents colony counts of the meat microbial background present on the meat. Each point represents the average from at least three technical replicates from dilution plating for each biological replicate. N>=3 biological replicates for all conditions. Significance testing is performed with ANOVA with post-hoc Tukey tests. Ns p>0.05; * p<0.05; *** p<0.001; ****p<0.0001.

We first used the VASE data to calculate the overall metabolite intensity for each treatment condition. In the control, carbenicillin, and hydrogen peroxide conditions, there were no significant differences in total ion intensity between MB control and PA14+MB communities (**Figure *4.6***). However, the total ion intensity of MB control was significantly higher than PA14+MB when exposed to gentamicin ($p = 2.2\times10^{-6}$) or gentamicin plus hydrogen peroxide ($p = 0.034$) (**Figure *4.6***). Interestingly, MB control growth was significantly higher than MB(PA14) with gentamicin and gentamicin plus hydrogen peroxide (**Figure *4.4*** and **Figure *4.5***). Because more of the volatile

signal may be coming from the MB control community, there may be changes in MB control growth associated with total ion intensity. For the PA14+MB community, low concentrations of hydrogen peroxide (50 – 100 µM) had the highest total ion intensity. As hydrogen peroxide concentrations increased, total ion intensity decreased (**Figure *4.6***). There was a negative correlation between the µM concentrations of hydrogen peroxide and total ion intensity for the PA14+MB communities (Pearson's correlation R = -0.9, p = 0.0024).

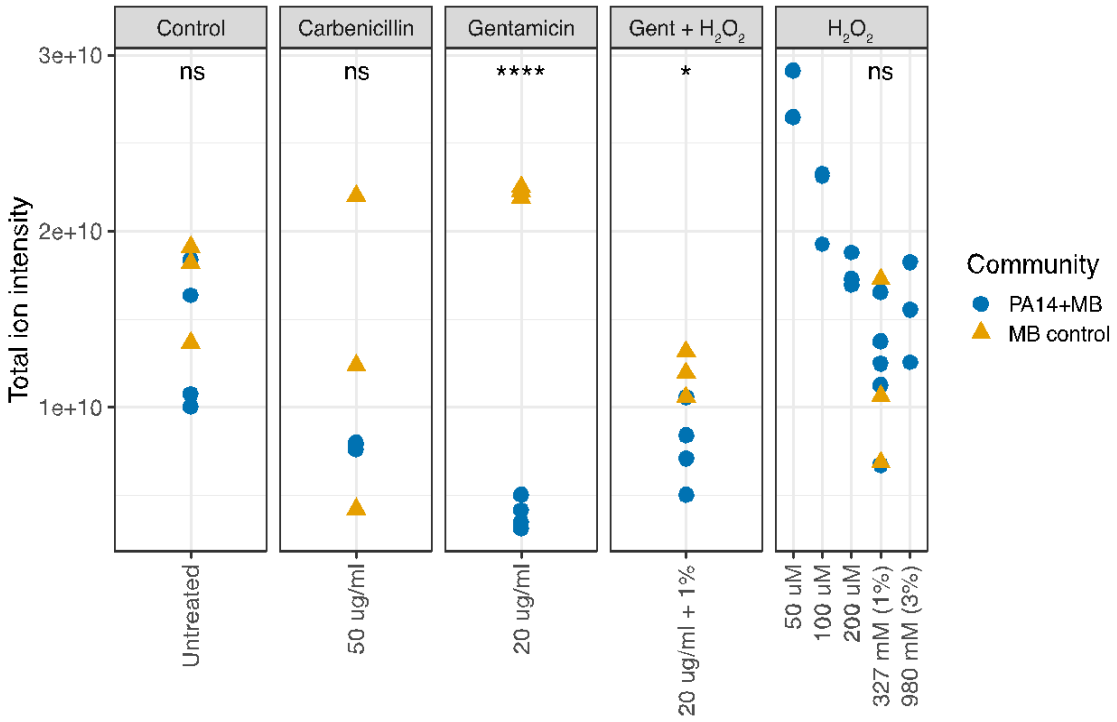

Figure 4.6-Total ion intensity of all volatile compounds. The PA14+MB community represents the microbial community on a meat sample with both PA14 and MB(PA14) populations. The MB control community is a meat sample with only the meat microbial background. Significant differences were found for gentamicin ($p = 2.2x10^{-6}$, T-test) and gentamicin + H_2O_2 ($p = 0.034$, T-test).

Next, we used nonmetric multidimensional scaling (NMDS) to visualize similarities in volatile signatures produced by the different treatment conditions. **Figure *4.6*-A shows** a comparison of volatile signatures from models treated with various concentrations of hydrogen peroxide. The control treatment for PA14+MB and MB control communities clustered together, with the exception of one outlier sample from PA14+MB on the bottom left. The MB control with 327 mM (1%) hydrogen peroxide was shifted away from the MB control treatment. PA14+MB with

327 mM (1%) and 980 mM (3%) hydrogen peroxide showed more distinct shifts away from the PA14+MB community control condition compared to PA14+MB community with lower concentrations of hydrogen peroxide (50-200 µM). One of the PA14+MB 50 µM hydrogen peroxide biological replicates, however, was more similar to PA14+MB 980 mM (3%) hydrogen peroxide than the control treatment.

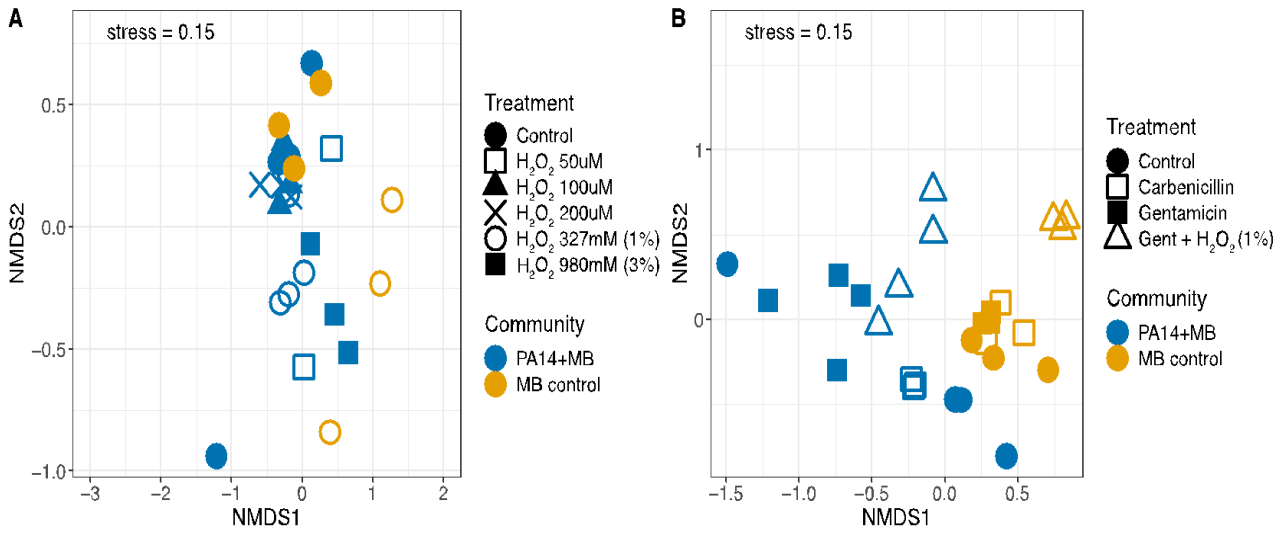

Figure 4.7- Nonmetric multidimensional scaling (NMDS) plot of volatile signatures from the perfusion model. A) hydrogen peroxide conditions and the control and B) the antibiotic conditions and the control. The PA14+MB community represents the microbial community on a meat sample with both PA14 and MB(PA14) populations. The MB control community is a meat sample with only the meat microbial background. Each point represents an individual sample. N ≥ 3 biological replicates for all treatments.

Antibiotic treatments distinctly altered the abundances of volatile compounds. Here, the PA14+MB and MB control communities formed distinct clusters. Within the MB control cluster, there was less movement with the addition of gentamicin or carbenicillin. MB control communities with the addition of gentamicin and hydrogen peroxide were shifted away from the main MB control cluster. Treatments for the PA14+MB community were more dispersed than the MB control. The PA14+MB community treated with antibiotics formed distinct clusters with biological replicates in close proximity to each other. PA14+MB with carbenicillin was more similar to the PA14+MB control than to gentamicin and gentamicin plus hydrogen peroxide. Similar to the NMDS with hydrogen peroxide and control treatments, PA14+MB control had one sample cluster closer to PA14+MB treated with gentamicin than to the control treatment samples. In summary,

antibiotics were driving changes in the volatile composition, whereas hydrogen peroxide did not appear to have as large of an impact.

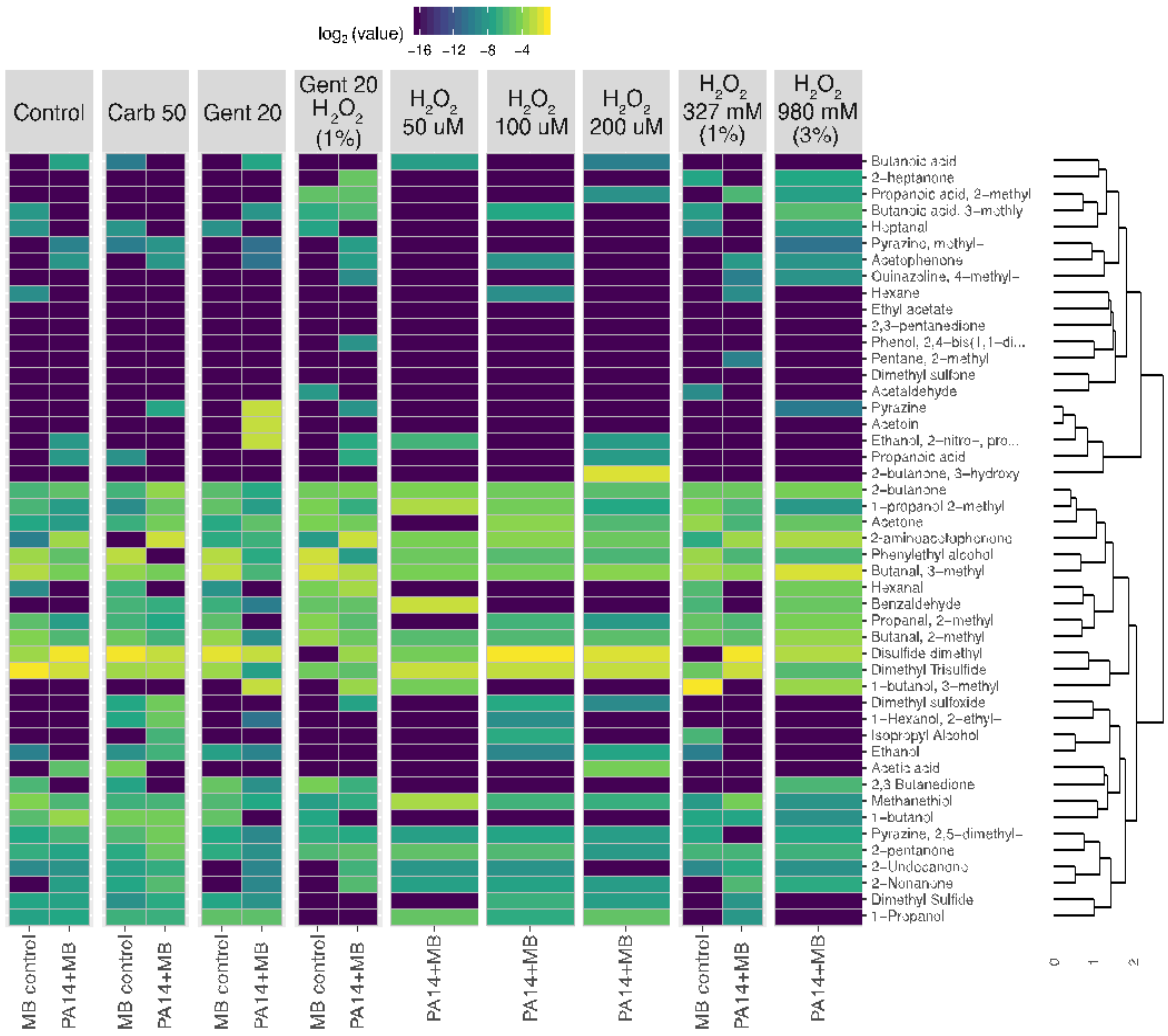

Figure 4.8- Heatmap showing clustering of relative abundances of volatile metabolites. PA14+MB represents the microbial community on a meat sample with both PA14 and MB(PA14) populations. The MB control community is a meat sample with only the meat microbial background. Metabolites were first normalized by total sample intensity. A Bray-Curtis distance matrix was generated for clustering with the unweighted pair group method with arithmetic mean (UPGMA) method.

Taking a closer look at the volatile molecules detected in each perfusion treatment condition, we saw that many highly abundant volatile metabolites were present across all conditions while some were more condition-specific (**Figure *4.8***). The classes of molecules we were able to detect included alcohols, aldehydes, aromatic compounds, carboxylic acids and esters, hydrocarbons, ketones, and sulfuric molecules. Acetophenone and 2-aminoacetophenone

were mostly present only in PA14+MB community treatments and had significantly higher relative abundances in the PA14+MB community compared to the MB control community (p value = $6x10^{-5}$ and p value = $4x10^{-6}$, respectively; **Figure *4.9***). Additional metabolites that were significantly more abundant in PA14+MB than MB control were 2-nonanone and 2-butanone (p value = 0.006 and p value = 0.029, respectively; **Figure *4.9***). Across antibiotic and H_2O_2 treatments applied to the PA14+MB community, 2-aminoacetophenone and 2-butanone were significantly more abundant with carbenicillin compared to control (p.adj = 0.0066 and p.adj = 0.0041) and 2-butanone was significantly more abundant with gentamicin + hydrogen peroxide treatment (p.adj = 0.03; **Figure *4.10***). As for the MB control community, butanal, 2-methyl; butanal, 3-methyl; heptanal; phenylethyl alcohol; and propanal,2-methyl were significantly more abundant in MB control than PA14+MB community (**Figure *4.9***). The MB control community had significant higher abundances of butanal, 3-methyl and propanal, 2-methyl in the gentamicin + hydrogen peroxide treatment compared to control (p.adj = 0.012 and p.adj = 0.042; **Figure *4.10***). Thus, in addition to the global changes shown in **Figure *4.6***, we were also able to detect changes in individual metabolites across treatments, suggesting a combination of metabolites are important for identifying responses to antibiotics and hydrogen peroxide.

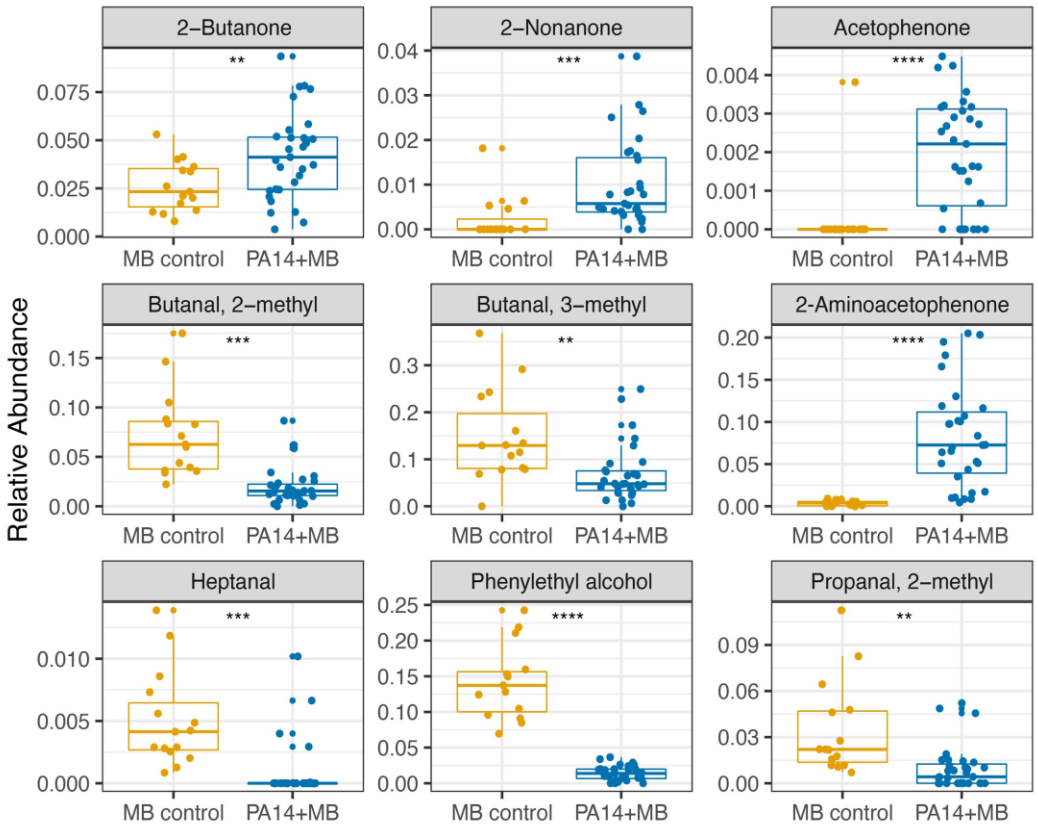

Figure 4.9 - *Relative abundances of metabolites significantly different between PA14+MB and MB control communities.* *PA14+MB represents the microbial community on a meat sample with both PA14 and MB(PA14) populations. The MB control community is a meat sample with only the meat microbial background. The relative abundances are values resulting from normalizing by total sample intensity. Each point represents a biological sample. All treatments are represented in this figure. Statistical testing was performed with T tests. Significance is indicated by asterisks. ** $p < 0.01$; *** $p < 0.001$; **** $p < 0.0001$.*

4.5. Discussion

The purpose of our study was to develop and test a novel three-dimensional *in vitro* perfusion meat model in order to study the effects of antimicrobials on polymicrobial communities in the presence of pathogens. The main questions this research addressed were: 1) how does the microbial community growth shift in response to antibiotics and hydrogen peroxide, molecules commonly present in a chronic wound and 2) how does metabolism change in response to these compounds? We investigated *P. aeruginosa* because of its widespread relevance in chronic infections. We were also interested in the native microbial community on the meat to model an infection in the context of a polymicrobial community and include the potential colonization of wounds by a background commensal population. We found that we were able to culture *P.*

aeruginosa in a perfused media model and that there were growth and metabolic consequences on the polymicrobial community in response to antibiotic and hydrogen peroxide treatments.

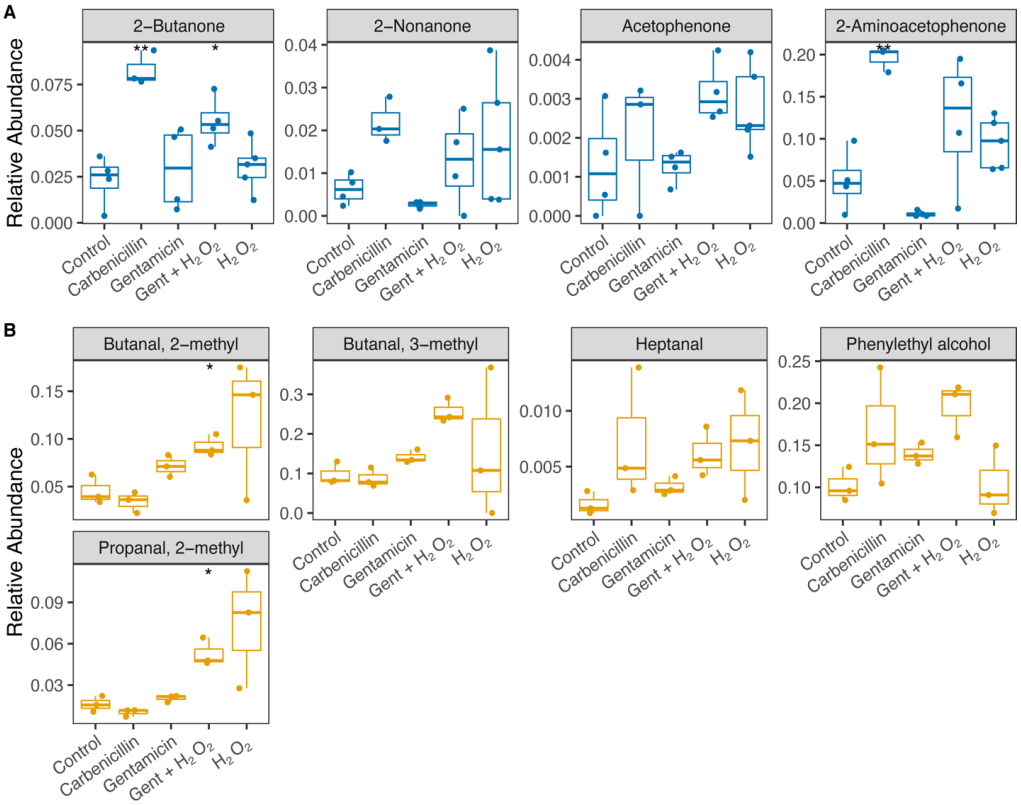

Figure 4.10-Metabolites significantly different in the PA14+MB and MB control communities across treatments. A) Metabolites with a significantly higher relative abundance in the PA14+MB community than MB control community. B) Metabolites with a significantly higher relative abundance in the MB control community than the PA14+MB community. The data included for hydrogen peroxide are from experiments with 327 mM (1%) hydrogen peroxide. Significance testing is performed by pairwise comparisons between the control treatment and the antibiotic and hydrogen peroxide treatments with T tests and Benjamini-Hochberg corrections for multiple comparisons. Significance is indicated by asterisks. The lack of an asterisk indicates no significance. * p<0.05; ** p<0.01.

To our knowledge, our perfusion meat model is the first *in vitro* model to include the combined elements of tissue, flow, polymicrobial community growth, and volatile metabolomics to investigate bacterial community development *in vitro*. Past and current *in vivo* and *in vitro* models have greatly contributed to the understanding of wound healing physiology and biofilm structure, yet there are some important factors that we should take into consideration. A new review by Thaarup et al. highlights the pros and cons of the different model characteristics of current *in vitro* chronic wound models [31]. Porcine skin is a widely used model for chronic wounds because it is more similar to human skin than rodent models [32]–[34]. However, physiological

differences between pig and human skin may confound results from pig skin models. For example, pig skin and hair follicles are less vascular, and the sweat glands differ [34].

Although wound infections that reach skeletal muscle are rare and understudied in *in vivo* models [35], [36], our choice of meat provides a novel framework which enables us to study microbial metabolism in a biologically relevant context *in vitro*. Examples of infections that reach muscle include abscess formation, trauma, or surgery are called infectious myositis [37], [38]. The types of agents in infectious myositis are bacteria, fungi, parasitic, and viral [37], [38]. There are currently no *in vitro* polymicrobial infection models in muscle tissue. Additionally, microbial biofilms are not studied widely in porcine skin models. The MB community in our model is a novel component as it likely comes from environmental contaminants and endogenous sources from the meat. One caveat of our study is the sequencing of the MB community from the static model, which identifies the microbes that grow on meat and the surrounding liquid. The microbes identified are likely to grow on the surface of the meat in the perfusion model, but further characterization by sequencing from the perfusion model and isolate sequencing will reveal the true microbial community. Another concern is that as the meat comes from a commercial source, we do not know what effect freezing has on the microbiome or structure of meat and should be considered in future studies.

Perfusion is an important biological process that may contribute to wound healing in infections. During the inflammatory phase in wound healing, essential cells (e.g. antibodies, white blood cells, growth factors, enzymes, and nutrients) reach the wounded area by blood vessel dilation. Following dilation, the tissue can receive oxygen and nutrients through the proliferation phase in which the network of blood vessels is restored by growth factors (angiogenesis) [39]. However, perfusion in chronic wounds is limited, resulting in low oxygenation and accumulation of harmful byproducts that delay healing [40]. Having control over the perfusion rate and perfusion media in our model would be a step towards recapitulating the physiological role blood vessels

play in mediating chronic infections. In addition, the model has throughput and research regulatory advantages over *in vivo* models. When comparing perfusion and static models, we observed significantly higher growth of the MB control population in the control, antibiotic, and hydrogen peroxide treatments under the perfusion model (**Figure *4.3***). A potential explanation for differences in growth in the MB control community is oxygen and nutrient availability in the perfusion model compared to the static model. As the static model was submerged in media, there was less oxygen and fewer nutrients available to the microbes underneath the surface of the liquid.

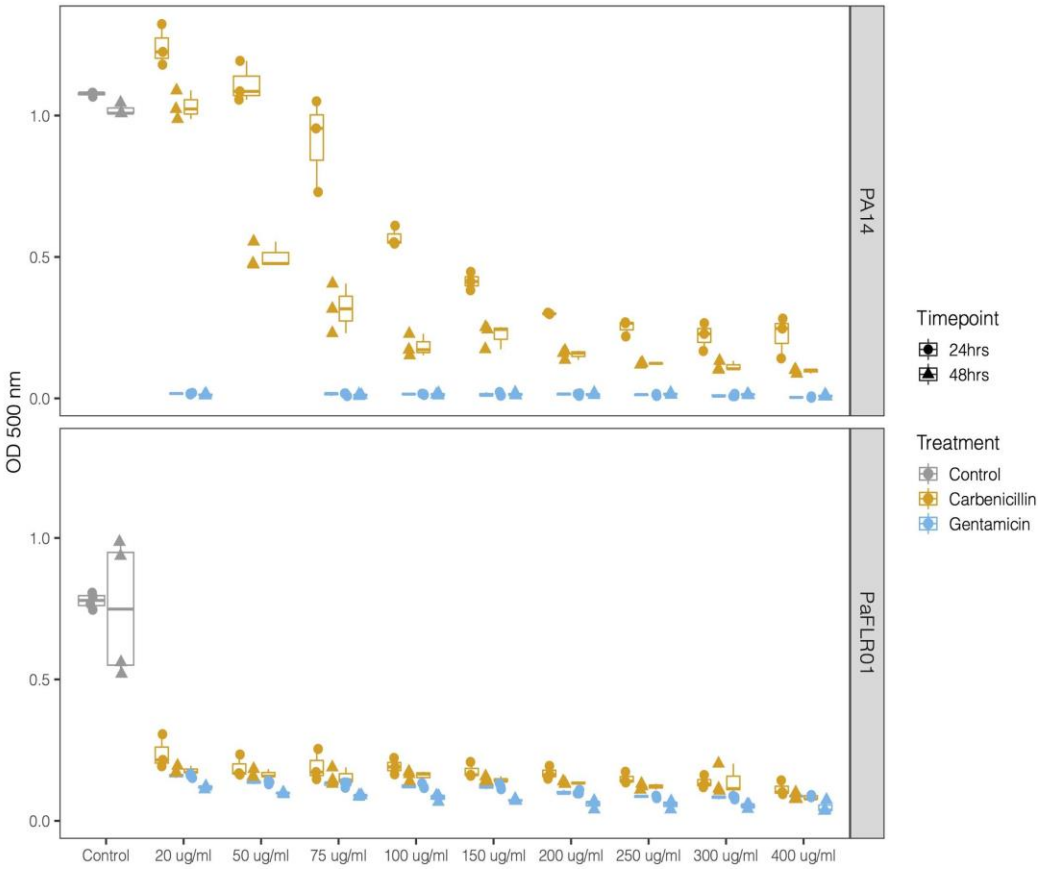

Figure 4.11- Minimum inhibitory curve endpoints for PA14 and PaFLR01. Fluorescent measurements for cell density were taken at 24 and 48 h timepoints. Experiments were performed in 96-well plates. PA14 was growing in LB. PaFLR01 was grown in TH.

The compounds perfused through our model are relevant molecules of interest in treating chronic wound infections. Antibiotics and hydrogen peroxide are routinely used against bacterial

infections, and hydrogen peroxide is also produced by the host during wound healing. Very early after injury, wounds with impaired healing contain increased levels of reactive oxygen and nitrogen species [5]. Low levels of reactive oxygen species (ROS) act as essential mediators of intracellular signaling and regulate numerous signal transduction and gene expression processes [16]. ROS at low concentrations lead to defense against invading pathogens and proper healing. In contrast, high levels of ROS clearly have the potential to complicate regeneration and remodeling of nascent tissue. ROS can cause damage by reacting with nucleic acids, protein and lipids and delay healing [5], [41]. In our perfusion model, we used physiological µM and therapeutic mM concentrations of hydrogen peroxide and observed that *P. aeruginosa* cell densities reached around 10^9-10^{10} CFU/mL. There was also a decrease in total ion intensity as concentrations of hydrogen peroxide increased (**Figure *4.6***), indicating a change in microbial metabolism in response to hydrogen peroxide exposure. The suppression of MB growth in the presence of both the lab-adapted PA14 and PaFLR01 clinical isolate of *P. aeruginosa*, and when exposed to antimicrobial compounds, suggests an interaction between the pathogen and MB populations that is triggered by exposure to the chemotherapeutics. Differences in MB growth inhibition in the presence of either PA14 or PaFLR01 depending on exposure to carbenicillin or gentamicin (**Figure *4.3***) may be due to differences in each strain's response to each antibiotic. PaFLR01 is sensitive to carbenicillin and gentamicin at 20 µg/mL (**Figure *4.11***). PA14 is resistant to carbenicillin at 20 µg/mL and sensitive to gentamicin at 20 µg/mL (**Figure *4.11***).

Metabolomic approaches have been extensively used to predict biomarkers of disease and bacterial colonization. The use of headspace metabolomics to capture volatile molecules is a powerful approach for capturing molecules that may act as important signals in a biological context and also as detectable biomarkers of the bacterial species and metabolic conditions. Common volatile compounds associated with *P. aeruginosa* that were detected in our study include acetophenone, 2-aminoacetophenone, dimethyl sulfide, dimethyl trisulfide, 2-butanone,

2-nonanone, and others [28]–[30], [42]. However, only a subset of the volatile molecules associated with *P. aeruginosa* (acetophenone, 2-aminoacetophenone, 2-nonanone, and 2-butanone) were significantly higher in the PA14+MB community compared to the MB control community (**Figure *4.10***) and 2-aminoacetophenone and 2-butanone were significantly different across treatments (**Figure *4.2***). 2-aminoacetophenone has been widely associated with a grape like odor in identifying *P. aeruginosa* [43]–[45], quorum sensing [46], [47], and oxidative stress [35]. In a murine skeletal muscle model, 2-aminoacetophenone produced by *P. aeruginosa* promotes mitochondrial dysfunction and reduced energy production [36] by inducing oxidative stress and apoptosis signaling pathways [35]. 2-aminoacetopheone has also been shown to alter the host epigenome, enabling higher bacterial burden tolerance [48] and promotes chronic infection [46]. Given the important role 2-aminoacetophenone plays in *P. aeruginosa* physiology, 2-aminoacetophenone could be an important biomarker for monitoring antibiotic efficacy in *P. aeruginosa*. The conditions that lead to the production of harmful microbially derived metabolites provide insight into wound physiology and outcome.

From a broader perspective of the volatile metabolome across all treatments, antibiotics had a greater influence on the volatile signature than hydrogen peroxide (**Figure *4.6***). The addition of carbenicillin, gentamicin, and gentamicin + hydrogen peroxide decreased the total volatile ion intensity detected in the PA14+MB community (**Figure *4.6***), while growth of the PA14 population was significantly higher than the MB(PA14) population for the carbenicillin treatment (**Figure *4.4***). This implies there was a diminished microbial metabolic response to the treatments for the MB(PA14) population, suggesting that the bulk of the volatile signal may be coming from the meat microbial community. *P. aeruginosa* may be thriving in the stressful environment generated by exposure to the chemotherapeutics, and it is outcompeting its corresponding MB community, especially in the case with carbenicillin, hydrogen peroxide (1 mM to 980 mM), and gentamicin + hydrogen peroxide for PA14, and gentamicin and 327 mM (1%) hydrogen peroxide

for PaFLR01 (**Figure *4.2*** and **Figure *4.4***). Lower concentrations (50 – 200 µM) of hydrogen peroxide, in the range of physiological concentrations, had higher ion intensities than the controls, suggesting increased microbial metabolism. In addition, there were no significant differences in CFU/mL values between PA14 and MB(PA14) populations for hydrogen peroxide conditions from 50-500 µM (**Figure *4.2***). Together with the use of multiple volatile molecules to serve as a fingerprint for *P. aeruginosa* metabolism, understanding which organisms contribute to the bulk of the volatile signal is also informative for identifying changes in community physiology.

The perfusion meat model is promising for the study of clinical wound isolates in more physiologically relevant conditions. In chronic infections treated with antibiotics, an individual pathogen such as *P. aeruginosa* comes to dominate over time. In the present model, lab-adapted and clinical *P. aeruginosa* strains reached higher cell densities than their respective MB populations when treated with carbenicillin, gentamicin, or hydrogen peroxide. The model may help us understand why common opportunistic pathogens thrive in infections despite treatment with antibiotics and reactive oxygen species. Furthermore, our goal of identifying microbial metabolism in response to different treatments is being realized with the use of volatile headspace analysis and metabolomics. For future studies aimed at identifying biomarkers for wound chronicity, it is important to utilize metabolomics to identify changes in metabolism for more targeted therapies. The use of biologically relevant models, such as our perfusion meat model, would also advance the field for understanding polymicrobial interactions and metabolisms within a chronic infection.

4.6. References

[1] J. M. Flynn, D. Niccum, J. M. Dunitz, and R. C. Hunter, “Evidence and Role for Bacterial Mucin Degradation in Cystic Fibrosis Airway Disease,” *Pathogens*, vol. 12, no. 8, pp. 1–21, 2016.

[2] E. M. Adamowicz, J. Flynn, R. C. Hunter, and W. R. Harcombe, “Cross-feeding

modulates antibiotic tolerance in bacterial communities," *ISME J.*, pp. 2723–2735, 2018.

[3] T. Dalton *et al.*, "An *in Vivo* Polymicrobial Biofilm Wound Infection Model to Study Interspecies Interactions," vol. 6, no. 11, 2011.

[4] A. Oates, S. Lindsay, H. Mistry, F. Ortega, and J. Andrew, "Modelling antisepsis using defined populations of facultative and anaerobic wound pathogens grown in a basally perfused biofilm model," *Biofouling*, vol. 7014, pp. 1–12, 2018.

[5] S. Dhall *et al.*, "A Novel Model of Chronic Wounds : Importance of Redox Imbalance and Biofilm-Forming Bacteria for Establishment of Chronicity," vol. 9, no. 10, 2014.

[6] F. Harrison, A. Muruli, S. Higgins, and S. P. Diggle, "Development of an Ex Vivo Porcine Lung Model for Studying Growth , Virulence , and Signaling of *Pseudomonas aeruginosa*," vol. 82, no. 8, pp. 3312–3323, 2014.

[7] E. Sweeney, M. M. Hassan, N. E. Harrington, A. R. Smyth, and N. Matthew, "An ex vivo cystic fibrosis model recapitulates key clinical aspects of chronic *Staphylococcus aureus* infection .," 2019.

[8] A. Dumigan *et al.*, "A Porcine Ex Vivo Lung Perfusion Model To Investigate Bacterial Pathogenesis," no. October, pp. 1–19, 2019.

[9] N. E. Harrington, E. Sweeney, and F. Harrison, "Bio fi lm Building a better bio fi lm - Formation of *in vivo* -like bio fi lm structures by *Pseudomonas aeruginosa* in a porcine model of cystic fi brosis lung infection," *Biofilm*, vol. 2, no. March, p. 100024, 2020.

[10] M. Ashrafi, L. Novak-frazer, M. Bates, and M. Baguneid, "Validation of biofilm formation on human skin wound models and demonstration of clinically translatable bacteria-specific volatile signatures," no. January, pp. 1–16, 2018.

[11] H. Byun, K. C. Persaud, and A. M. Pisanelli, "Wound-State Monitoring for Burn Patients

Using E-Nose / SPME System," *ETRI J.*, vol. 32, no. 3, pp. 440–446, 2010.

[12] T. R. Thomsen *et al.*, "The bacteriology of chronic venous leg ulcer examined by culture-independent molecular methods," *Wound Rep. Reg.*, vol. 18, pp. 38–49, 2010.

[13] J. Phan, S. Meinardi, B. Barletta, D. R. Blake, and K. Whiteson, "Stable isotope profiles reveal active production of VOCs from human-associated microbes Stable isotope pro fi les reveal active production of VOCs from human-associated microbes," *J. Breath Res.*, vol. 11, pp. 1–9, 2017.

[14] J. Phan, T. Gallagher, A. Oliver, W. E. England, and K. Whiteson, "Fermentation products in the cystic fibrosis airways induce aggregation and dormancy-associated expression profiles in a CF clinical isolate of *Pseudomonas aeruginosa*," *FEMS Microbiol. Lett.*, vol. 365, pp. 1–11, 2018.

[15] A. E. K. Loo *et al.*, "Effects of Hydrogen Peroxide on Wound Healing in Mice in Relation to Oxidative Damage," *PLoS One*, vol. 7, no. 11, 2012.

[16] S. Roy, S. Khanna, K. Nallu, T. K. Hunt, and C. K. Sen, "Dermal Wound Healing Is Subject to Redox Control," *Mol. Ther.*, vol. 13, no. 1, pp. 211–220, 2006.

[17] N. Ojha, S. Roy, G. He, S. Biswas, and M. Velayutham, "Assessment of wound-site redox environment and the significance of Rac2 in cutaneous healing," *Free Radic. Biol. Med.*, vol. 44, pp. 682–691, 2008.

[18] H. Lorentzen, F. Kallehave, H. J. Kolmos, U. Knigge, F. Gottrup, and J. Bu, "Gentamicin Concentrations in Human Subcutaneous Tissue," *Antimicrob. Agents Chemother.*, vol. 40, no. 8, pp. 1785–1789, 1996.

[19] K. H. Lee *et al.*, "Systemic Absorption of Gentamicin Irrigation in Joint Replacement Surgery: A cause of concern," *MAlaysian Orthop. J.*, vol. 2, no. 2, pp. 11–16, 2008.

[20] A. A. Hammond *et al.*, “An *in vitro* biofilm model to examine the effect of antibiotic ointments on biofilms produced by burn wound bacterial isolates,” *Burns*, vol. 37, no. 2, pp. 312–321, 2011.

[21] J. Fox *et al.*, “Package ‘car,’” 2020.

[22] Alboukadel Kassambara. 2018. “Ggpubr: ‘ggplot2’ Based Publication Ready Plots.” https://CRAN.R-project.org/package=ggpubr., “No Title.” 2018.

[23] A. J. Oksanen *et al.*, “The vegan Package,” pp. 1–182, 2009.

[24] A. Bunn, “An Introduction to dplR,” vol. 3, 2019.

[25] M. Eschbach, K. Schreiber, K. Trunk, J. Buer, D. Jahn, and M. Schobert, “Long-Term Anaerobic Survival of the Opportunistic Pathogen *Pseudomonas aeruginosa* via Pyruvate Fermentation,” *J. Bacteriol.*, vol. 186, no. 14, pp. 4596–4604, 2004.

[26] C. Vander Wauven, A. Pijrard, M. Kley-raymann, and D. Haas, “*Pseudomonas aeruginosa* Mutants Affected in Anaerobic Growth on Arginine : Evidence for a Four-Gene Cluster Encoding the Arginine Deiminase Pathway,” *J. Bacteriol.*, vol. 160, no. 3, pp. 928–934, 1984.

[27] K. J. P. Davies, D. Lloyd, and L. Boddy, “The Effect of Oxygen on Denitrification in Paracoccus denitrzfians and *Pseudomonas aeruginosa,*” *J. Gen. Microbiol.*, vol. 135, pp. 2445–2451, 1989.

[28] H. D. Bean, C. A. Rees, and J. E. Hill, “Comparative analysis of the volatile metabolomes of *Pseudomonas aeruginosa* clinical isolates Comparative analysis of the volatile metabolomes of *Pseudomonas aeruginosa* clinical isolates,” *J. Breath Res.*, vol. 10, pp. 1–10, 2016.

[29] J. N. Labows, K. J. Mcginley, G. U. Y. F. Webster, and J. J. Leyden, “Headspace

Analysis of Volatile Metabolites of *Pseudomonas aeruginosa* and Related Species by Gas Chromatography- Mass Spectrometry," *J. Clin. Microbiol.*, vol. 12, no. 4, pp. 521–526, 1980.

[30] V. Shestivska, K. Dryahina, K. Sovova, D. Smith, and A. Nemec, "Variability in the concentrations of volatile metabolites emitted by genotypically different strains of *Pseudomonas aeruginosa,*" *J. Appl. Microbiol.*, vol. 113, pp. 701–713, 2012.

[31] I. C. Thaarup and T. Bjarnsholt, "Current *in vitro* Biofilm-Infected Chronic Wound Models for Developing New Treatment Possibilities," *Wound Heal. Soc.*, vol. 00, no. 00, pp. 1–12, 2020.

[32] M. Seaton, A. Hocking, and N. S. Gibran, "Porcine Models of Cutaneous Wound Healing," *ILAR J.*, vol. 56, no. 1, pp. 127–138, 2015.

[33] W. J. Lindblad, "Considerations for selecting the correct animal model for dermal wound-healing studies," *J. Biomater. Sci. Polym. Ed.*, vol. 19, no. 8, pp. 1087–1096, 2008.

[34] W. Montagna, J. Yun, B. Ore, and V. Formisano, "Histology and Cytochemistry of Human Skin," *AMA Arch. Dermatology*, vol. 90, pp. 526–529, 1964.

[35] A. Bandyopadhaya *et al.*, "Bacterial-excreted small volatile molecule 2-aminoacetophenone induces oxidative stress and apoptosis in murine skeletal muscle," *Int. J. Mol. Med.*, vol. 37, pp. 867–878, 2016.

[36] A. A. Tzika *et al.*, "A Small Volatile Bacterial Molecule Triggers Mitochondrial Dysfunction in Murine Skeletal Muscle," *PLoS One*, vol. 8, no. 9, pp. 1–13, 2013.

[37] N. F. Crum-cianflone, "Bacterial, Fungal, Parasitic, and Viral Myositis," *Clin. Microbiol. Rev.*, vol. 21, no. 3, pp. 473–494, 2008.

[38] J. Bickels, L. Ben-Sira, A. Kessler, and S. Wientroub, "Primary Pyomyositis," *J. BONE Jt.*

Surg., vol. 84-A, no. 12, pp. 2277–2286, 2002.

[39] N. X. Landen, D. Li, and M. Stahle, “Transition from inflammation to proliferation: a critical step during wound healing,” *Cell. Mol. Life Sci.*, vol. 73, no. 20, pp. 3861–3885, 2016.

[40] K. Y. Woo, T. M. Brandys, and J. A. Marin, “Assessing chronic wound perfusion in the lower extremity: current and emerging approaches,” *Chronic Wound Care Manag. Res.*, vol. 2, pp. 149–157, 2015.

[41] C. K. Sen and S. Roy, “Redox signals in wound healing,” *Biochim. Biophys. Acta*, vol. 1780, pp. 1348–1361, 2008.

[42] M. Ashrafi, M. Bates, M. Baguneid, T. Alonso-rasgado, R. Rautemaa-richardson, and A. Bayat, “Volatile organic compound detection as a potential means of diagnosing cutaneous wound infections,” *Wound Rep. Reg.*, vol. 25, pp. 574–590, 2017.

[43] C. D. Cox and J. Parker, “Use of 2-Aminoacetophenone Production in Identification of *Pseudomonas aeruginosa*,” *J. Clin. Microbiol.*, vol. 9, no. 4, pp. 479–484, 1979.

[44] A. J. Scott-thomas *et al.*, “2-Aminoacetophenone as a potential breath biomarker for *Pseudomonas aeruginosa* in the cystic fibrosis lung,” *BMC Pulm. Med.*, vol. 10, no. 56, pp. 1–10, 2010.

[45] R. Pabary *et al.*, “Does mass spectrometric breath analysis detect *Pseudomonas aeruginosa* in cystic fibrosis ?,” *Eur. Respir. J.*, vol. 47, no. 3, pp. 994–997, 2016.

[46] M. Kesarwani *et al.*, “A Quorum Sensing Regulated Small Volatile Molecule Reduces Acute Virulence and Promotes Chronic Infection Phenotypes,” *PLoS Pathog.*, vol. 7, no. 8, pp. 1–12, 2011.

[47] I. Kviatovski, L. Chernin, T. Yarnitzky, I. Frumin, N. Sobel, and Y. Helman, “*Pseudomonas aeruginosa* activates the quorum sensing LuxR response regulator

through,” *Chem. Commun.*, vol. 51, no. 15, pp. 3258–3261, 2015.

[48] A. Bandyopadhaya, A. Tsurumi, D. Maura, K. L. Jeffrey, and L. G. Rahme, “A quorum-sensing signal promotes host tolerance reprogramming,” *Nat. Microbiol.*, vol. 1, no. December, pp. 1–9, 2016.

Chapter 5
Escherichia coli Induces Cross-protection Tolerance to Antibiotic through Osmotic Stress

5.1. Introduction

Like pH, temperature, oxidative, and osmotic stress, antibiotics are another type of stress which activate bacterial stress responses [1], [2]. By activating their stress response, bacteria protect critical proteins, membranes, RNA and DNA, or repair damages to these and other cellular components. These response pathways protect cells against higher levels of the same stressor, or against other stressors when the mechanisms of protection overlap. This behavior is known as cross-protection [3], [4], [5]. Cross-protection has been observed with different stressful environments against another stressor, especially for antibiotic. We are now facing a worrying era due to the increase in multidrug resistance among pathogenic bacteria [6]. Overpopulation, improper use of antibiotics in medical settings and in the livestock industry, enhanced global migration, and poor sewerage treatment systems are among the reasons for the increase in antibiotic-resistant bacterial strains [7]. It is estimated that 10 million lives are annually at risk due to the rise of resistance by 2050. If we do not find proactive solutions for antibiotic-resistant bacteria, 100 trillion USD of global economic output would be at risk [8]. As a result, global efforts are needed to minimize the pace of resistance by thorough study of emergent microorganisms, resistance mechanisms, and antimicrobial agents [9]. Cross-protection by non-antibiotic stressors decreases the effectiveness of antibiotic treatment [10], [11]. In this context, cross-protection is a promising target for reducing antibiotic resistance for which we need to deeply study the responsible mechanisms.

There are three contributing factors to bacterial survival of antibiotic treatment: resistance, tolerance, and persistence. Resistance to antibiotics is a dominant cause of infection treatment failure, but tolerance and persistence can enable the bacteria to survive the antibiotic treatment

and recolonize in the absence of the antibiotic. Also, this survival is able to affect adversely by providing time for bacterial cells to evolve resistance [12].

Resistance is the result of genetic changes which cause an inherited phenotype. Resistant cells experience the reduction in antibiotic effectiveness by decreasing drug binding to the target, and its penetration by lipopolysaccharide modification, alterations in the number of porins and antibiotic transporters, pumping antibiotic compounds out of the cell via efflux pumps, and production of beta-lactamase providing resistance to penicillins and cephalesporins which consequently increase the minimum inhibitory concentration (MIC) in a defined time window [13], [14], [15], [16]. The MIC value shows the sensitivity of the cell to the antibiotic over a specific exposure time. In healthcare, the resistance level to an antibiotic is quantified by the MIC to determine optimal therapies [17].

Tolerance may be acquired by dormant bacterial phenotypes, which are typically induced by stressful conditions such as essential nutrient deprivation [18]. As a result of this starvation, essential bacterial processes are slowed, and cells are protected by this dormancy against many types of antibiotics which require cell growth to act successfully on them. As a result, the survival time of the cells in lethal concentrations of antibiotic >> MIC) is increased [12], [19], [20]. This phenomenon will not change the MIC of the cells because it is not affecting the growth of the cells. Tolerance helps cells survive the bactericidal effect of antibiotic by a slower rate for being killed. Another characteristic of tolerant cells is the ability to start replication again once the antibiotic is removed from the growth environment [19], [17].

Persistence is the ability of a subset of the cell population which is metabolically inactive to survive bactericidal antibiotic exposure resulting in biphasic killing curve [12], [21]. Persistence is induced by a group of stress responses and serves as a reservoir of cells from which genetic adaptations of resistance can emerge [22]. persistence and tolerance are similar phenomena and regarding the molecular mechanisms, the two terms are interchangeable. However, the

persistence affects only part of the population, whereas tolerance is the general ability of a population to survive longer antibiotic exposure. So, persistence could also be called “hetero-tolerance”. Once the antibacterial agent is removed and fresh nutrients are supplied, persistent cells regrow. By re-exposing regrown cells to antibiotic, both susceptible and tolerant subpopulations which have different killing rates will be appeared in the population indicating that the slower killing rate is not a heritable change [17], [12]. However, genetic mutations can affect the size of tolerant or susceptible subpopulation [20]. Taken together, these studies suggest that targeting the physiological mechanisms of tolerance and/or persistence might be a promising strategy to reduce bacterial resistance. Medical diagnostics for tolerant and persistent phenotypes are not routine, but recent research indicates that distinguishing between resistant, tolerant, and persistent bacterial cells is critical to the selection of effective antibiotic treatment [17], [23].

Methods to measure tolerance and resistance:

Resistance to antibiotics is measured by a convenient metric, the MIC, which depends on measuring the minimum concentration of antibiotic to inhibit growth. Strains with higher MIC are considered more resistant to the tested antibiotic. Since tolerant and persistent cells have the same or similar MICs as resistant ones, these phenotypes are overlooked with such growth-based assays. Instead, survival assays must be used to characterize phenotypes associated with cell tolerance. Survival assays measure the fraction of viable cells remaining after antibiotic exposure as a function of exposure time. By counting the colony forming units (CFUs) before and after time, *t*, of antibiotic treatment and comparing the fraction of surviving cells from different populations, tolerant and persistent phenotypes can be identified and distinguished (**Figure *5.1***). The minimum duration for killing (MDK) of a specific percentage of the cells (e.g. MDK_{99} or $MDK_{99.99}$) is a metric complementary to MIC for distinguishing resistant, tolerant, and persistent phenotypes. The exposure time needed to kill tolerant cells is longer than susceptible cells at all times, but the persistent phenotype emerges from susceptible cells after some time of antibiotic exposure

(**Figure *5.1***). For this purpose, high concentrations of bactericidal antibiotics, typically several time the MIC or more, are used to make the killing effect insensitive to antibiotic concentration and only dependent on exposure time [17], [13].

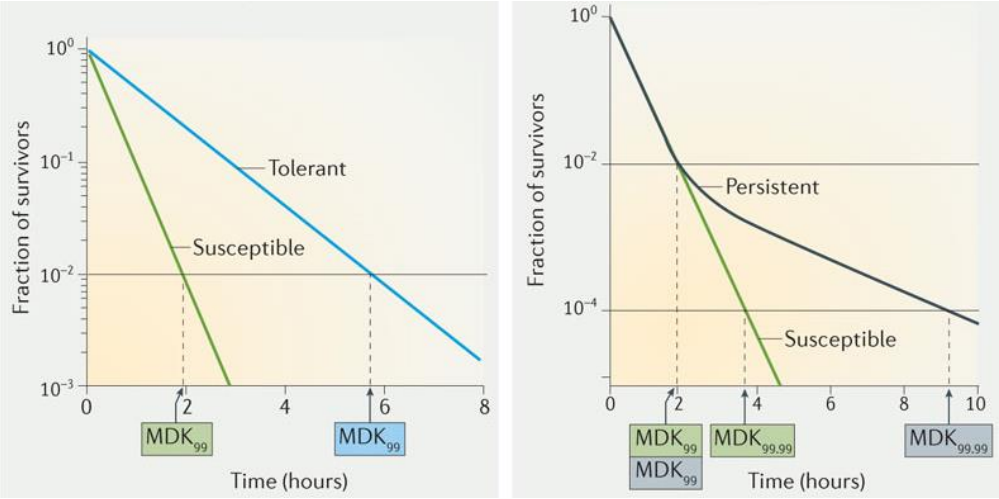

Figure 5.1 - Characteristic drug response of different forms of antibiotic susceptible and non-susceptible bacterial populations. Phenotypes of tolerant, susceptible, and persistent cells can be distinguished by tracking their fractional survival over time after antibiotic treatment (adopted from [17]).

Cells exposed to environmental stresses before getting exposed to antibiotic as the second stressor have shown only relatively moderate changes in their resistance. In a study on food-related pathogens, in the presence of low-pH or high-NaCl stress, *Staphylococcus aureus, Salmonella enterica* serovar Typhimurium displayed decreased susceptibility to antibiotics, with roughly four-fold increases in MIC observed in many cases [3]. In another study, osmotically stressed *E. coli* cells became resistant to antibiotic by 35% decrease in exponential growth rate of the bacteria [10]. *Listeria monocytogenes* is an organism with established stress responses to a number of stressors. It overcomes host defenses to colonize the gastrointestinal tract after gaining tolerance during food processing steps involving acid, heat, and salt [24]. Exposing *L. monocytogenes* cells to osmotic stress, acid stress, and cold stress also makes it more resistant (two to about four-fold increase in MIC) to different classes of antibiotics [25]. In these studies on cross-protection, several reasons for higher resistance against antibiotics such as increase in

efflux pump synthesis, and production of chaperones and proteases have been discussed [10], [25]. The cross-protection was quantified by measuring the growth rate or culture turbidity as indicators of MIC. The measured MIC mostly has between 2-4 fold increase which is considered as a moderate effect on the cells [10], [3]. Several studies have recently shown that tolerance phenotypes, on the other hand, exhibit orders of magnitude enhancements due to stress cross-protection [14], [26]. Tolerance enables cells to survive antibiotic exposure for longer times which increases the likelihood of developing resistance. Bacteria in the biofilm experience osmotic stress and 80% of bacterial infections are biofilm associated [27], [28]. So, osmotic stress effect on cross-protecting the cells through tolerance may contribute to the recalcitrance of the biofilms. The following study is the first to distinguish between resistance and tolerance response from the osmotically stressed cells while being exposed to different groups of antibiotics. The difference between these two phenomena might be the reason for having inconsistent results from different studies on investigating cross-protection from different groups of antibiotics through osmotic stress. For this purpose, the osmotic stress effects on cross-protection against different classes of antibiotics was studied through analyzing the survival rate of population to facilitate understanding of the mechanism underlying this phenomenon.

5.2. Materials and Methods

5.2.1. Bacterial Strains and Growth Culture

The bacterial strain used in this study was *E. coli* K-12 MC4100. Freezer stocks were streaked onto Lysogeny broth (LB) agar (1.5%) (both purchased from IBI Scientific) plates and grown overnight (O.N.). O.N. shaking cultures were inoculated from a single colony from the streaked plate into 3 mL of liquid LB (2%) and grown overnight at 37˚C on an orbital shaker at 250 rpm. The overnight culture was diluted into LB or LB supplemented with NaCl (Macron Fine Chemicals) or sucrose (Fisher Scientific) at the specified concentrations. The final OD was adjusted to 0.02 and cultures were re-grown for 6h (pre-incubation step). The pre-incubated

cultures were washed 3 times by centrifugation at 500g for 10 minutes and resuspended in 1x phosphate-buffered saline (Fisher Scientific). After the final wash, cells were diluted in M9 minimal medium and osmolyte added M9 (6 g/L Na_2HPO_4, 3 g/L KH_2PO_4, 0.5 g/L NaCl, 1 g/L NH_4Cl, 1 mL of filtered 1 M $MgSO_4$ and 0.1 M $CaCl_2$, and 10 mL of 10% glucose) (Fisher Scientific) to OD~0.2. To these bacterial cultures, 0-10 µL gentamicin (Fisher Scientific), kanamycin (Fisher Scientific), or ampicillin (VWR) was added to start the 4h antibiotic exposure. 200 µL of each inoculated solution was added to individual wells of a Corning 96-well flat-bottom microplate. Each condition was added to two different wells.

5.2.2. Minimum inhibitory concentration (MICs) measurement

The MICs were determined by recording the optical density at 600 nm of the wells in a microplate reader (Varioskan LUX-ThermoFisher). Cells were pre-incubated in LB, or NaCl/sucrose added LB. Pre-incubated cells were added to M9, and NaCl/sucrose added M9 to have the OD of 0.02 after addition of gentamicin. 200 µL of each solution was added to each well from 96-well plate and every 5 well were dedicated to one different antibiotic concentration as technical replicates (0-10 µg/mL). The optical density was measured by microplate reader every 30 minutes for 20 hours while shaking in 37°C. The border wells were filled with only Millipore water to control evaporation and only inner wells were used for samples. MIC_{50} values, the antibiotic concentration at which cultures grew to 50% of the cell density of the no-antibiotic control, were recorded for each sample.

5.2.3. Tolerance measurement

Survival assays were used to measure tolerance in differently stressed cell cultures. Colony Forming Units (CFU) were measured at the beginning and end of 4 h exposure to each antibiotic used in this study. For each time point, a 10 µL aliquot of each sample was added to the wells of the new 96 well microplate and the serial dilutions were done in sterile PBS. 5 µL from each dilution was spotted onto an LB-agar plate 4 times. These plates were incubated in 37°C

overnight then colonies were counted. CFU/mL values were calculated by dividing the number of the colonies by 5 µL and multiplying the results by dilution factor (e.g. 10^5) and 1000 as a unit conversion for µL to mL. The answer gave us the CFU/mL value for each read and the percent survival was calculated by 100 x the CFU/mL of remaining viable cells divided by the CFU/mL of the initial cultures. Tolerance measurement process for each condition was done for three biological replicates and 4-8 technical replicates for each.

5.3. Results

5.3.1. Comparing the effects of osmotic stress cross-protection on resistance and tolerance to antibiotics

In order to check the relative effects of osmotic stress-induced cross-protection against antibiotic susceptibility, we measured the MIC and survival rates of cells exposed to osmolytes and antibiotics. To induce osmotic stress, *E. coli* cells were exposed to two different classes of osmolytes, ionic (NaCl) and non-ionic (sucrose). Sucrose was chosen because *E. coli* K-12 strains cannot metabolize it effectively [29]. Osmotic stress was applied to cells by exposing liquid cultures to 0.5 M NaCl, 15% sucrose (0.5 M). These conditions were chosen because at these osmolyte concentrations, there is significant growth inhibition of *E. coli*, implicating the influence of osmotic stress on cells under these conditions (**Figure *5.2***). The osmolarity of these solutions is also similar: 1 and 0.5 osmol/L for the NaCl and sucrose media, respectively. To test the effects of osmotic stress on resistance and tolerance, cell cultures were pre-incubated for 6 h in osmolyte + LB or just LB media before exposure to the aminoglycoside antibiotic, gentamicin. For both

resistance and tolerance assays, cells were exposed to gentamicin in M9 minimal medium supplemented with the same concentrations of osmolytes in which they were pre-incubated.

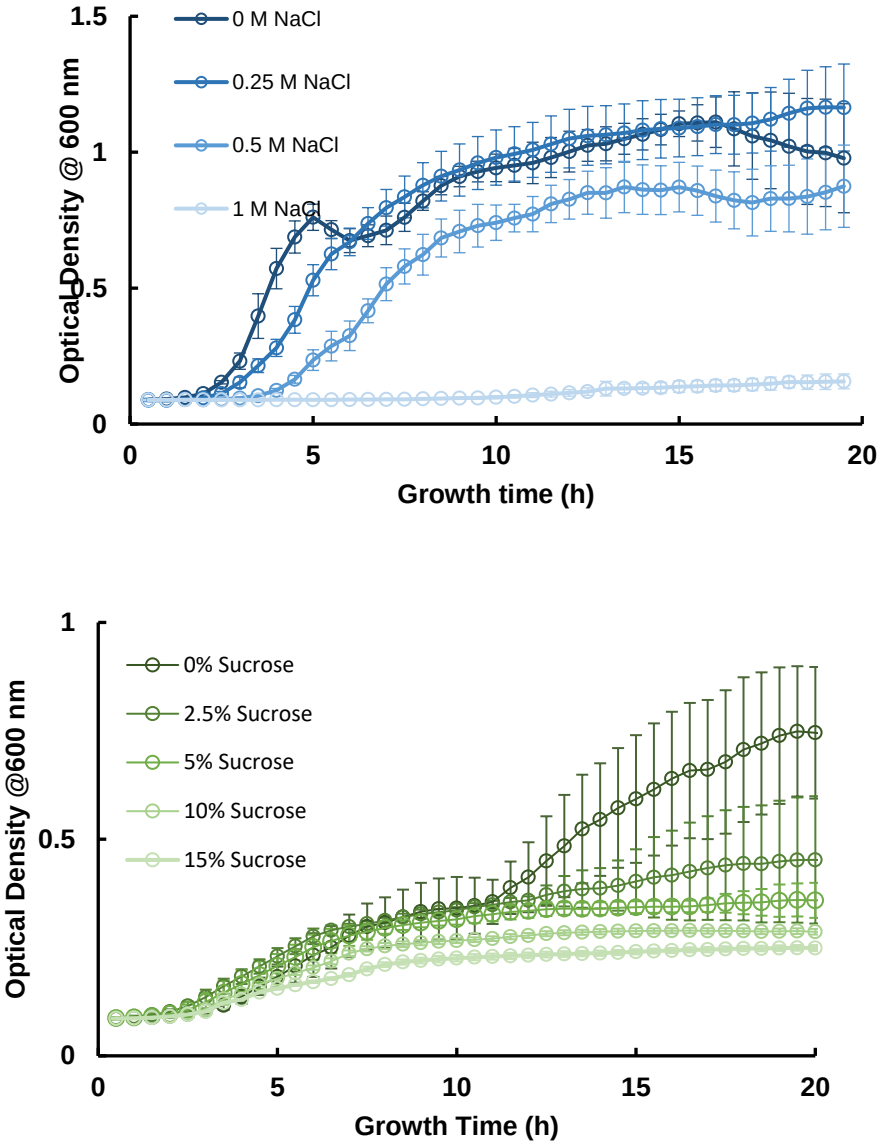

Figure 5.2 - *E. coli* growth is inhibited by high osmolyte concentration. 20 h growth of *E. coli* cell cultures were grown in the presence of: Top) LB + 0-1M NaCl, or Bottom) LB + 0-15% Sucrose. The optical density values are the average of 10 technical replicates and error bars represent standard deviations.

The effect of osmotic stress on resistance to gentamicin was measured using an MIC (growth based) assay. The effect of osmotic stress on tolerance to gentamicin was measured using a survival rate assay. In the induced resistance assays, the OD of cultures exposed to NaCl

and sucrose were lower at all concentrations of gentamicin, presumably due to osmotic stress-induced growth inhibition. Nevertheless, the MIC_{50} values for all three conditions were approximately 3 mg/mL (**Figure *5.3***), suggesting that the osmolytes had an insignificant effect on bacterial resistance to gentamicin.

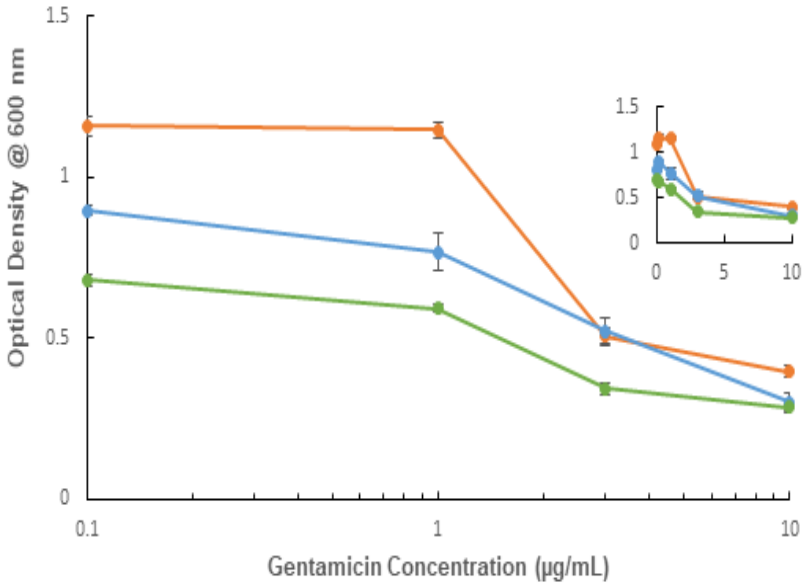

Figure 5.3 - Exposure to osmolytes does not significantly change *E. coli* resistance to gentamicin. The plot shows the ODs of *E. coli* cultures exposed to gentamicin in M9 (orange), M9 + 0.5 M NaCl (blue), or M9 + sucrose (green). Inset shows the same data on a linear concentration scale to include control samples exposed to 0 mg/mL gentamicin. The OD values after 20 h exposure to indicated gentamicin concentrations is averaged over 3 biological replicates and 5 technical replicates for each condition. Error bars represent the standard deviation. Inset is put to show a similar optical density of 0 mg/mL gentamicin with 0.1 mg/mL gentamicin.

In contrast, the induced tolerance assays showed a substantial effect of osmolyte exposure on cell survival in antibiotic media. After 4 h exposure to 10 mg/mL gentamicin (about 3x MIC_{50}) in M9, only 0.005% of cells in the control culture survived the treatment. In cultures exposed to NaCl or sucrose, on the other hand, 260% and 0.35%, respectively, survived (**Figure *5.4***). The survival rates in NaCl and sucrose represent 52,000x and 70.0x factor increases in *E. coli* tolerance to gentamicin, respectively. In fact, in M9 + NaCl, the bacteria not only survived but grew by 2.6-fold increase in viable cell density.

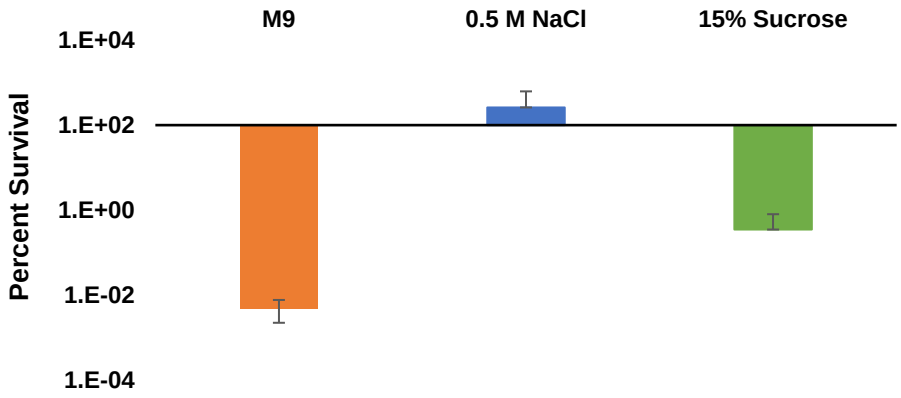

Figure 5.4 - Exposure to osmolytes significantly increases *E. coli* tolerance to gentamicin. The plot shows percent survival of cells exposed to gentamicin in M9, M9 + NaCl, and M9 + sucrose. All percent survival values are averages of viable cell densities after 4 h exposure to 10 mg/mL gentamicin in 3 biological replicates and 6-8 technical replicates for each biological replicate in each condition. Error bars represent standard deviations.

5.3.2. Does pre-incubation in osmotic stress matter for cross-protection against antibiotics?

Application of high degree osmotic stress inhibits the cell growth. To study the effect of osmotic stress on preparing the cells before introducing the antibiotic reagent, cells were challenged with inhibiting concentrations of sucrose and NaCl before antibiotic treatment. Pre-incubation in salt and sugar for 6 hours made cells more tolerant than the cells pre-incubated with the background growth media (LB) only (**Figure *5.5***). These results suggest that pre-incubation cross-protects the cells more than non-pre-incubated cells for antibiotic treatment. However, this is not a statistically significant higher effect on cross-protection.

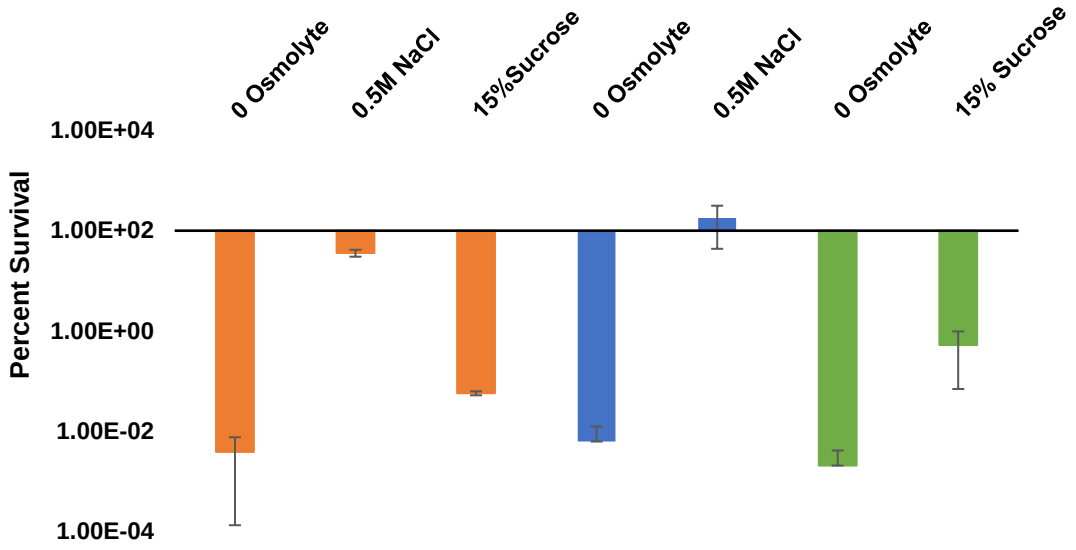

Figure 5.5 - Pre-incubation with osmolytes has a slight but not statistically significant effect on degree of cross-protection. O.N. *E. coli* cells are pre-incubated in fresh LB with 0.5 M NaCl (Blue), 15% sucrose (Green) and without osmolyte (Orange). Cells were exposed to M9 + 10 µg/mL gentamicin with and without 0.5 M NaCl and 15% sucrose. All percent survival values are the averages of viable cell counts from3 biological replicates and 6-8 technical replicates for each biological replicate in each condition. Error bars represent standard deviations.

5.3.3. The effect of osmolyte type and concentration on cross-protection level

Even though NaCl and sucrose have different molecular structures, they are both able to apply osmotic stress to the cells. In order to investigate the extent of cross-protection generated by these two osmolytes, 0.25-1 M NaCl and 5%-20% sucrose was added to background media to apply different osmolarity levels during pre-incubation and antibiotic treatment steps. These two osmolytes cross-protect the *E. coli* against gentamicin differently. Cells experienced the highest survival rates with 1 M concentration of NaCl (~28%) and with 15% sucrose (~0.34%) (**Figure *5.6*).** NaCl selection as an osmolyte not only made cells more tolerant but also made cells

grow around 3-times higher during 4 h gentamicin treatment. This difference in osmolytes' effects might be an indication for the different triggered systems by these two molecules.

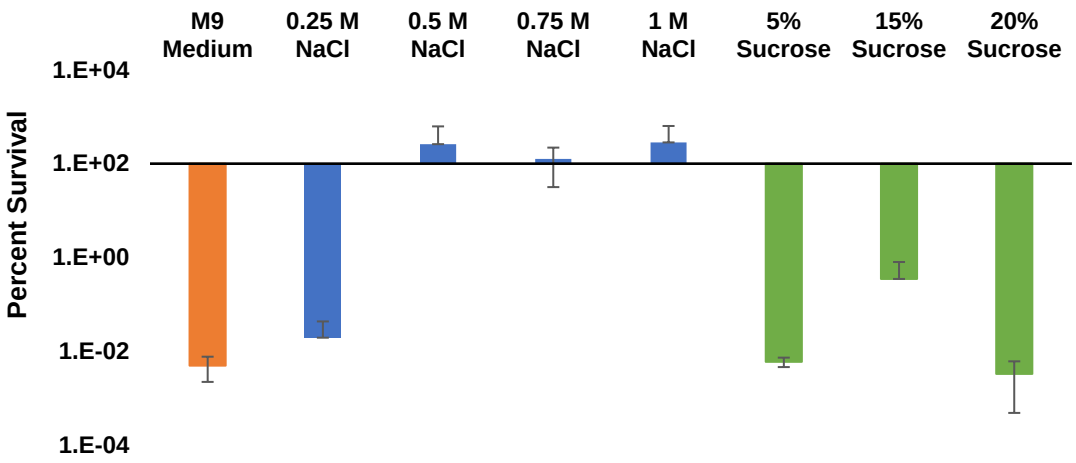

Figure 5.6 - *E. coli* Pre-incubation in different concentrations of sucrose and NaCl changes the level of cross-protection against gentamicin. O.N. cells were pre-incubated in fresh LB with different concentrations of NaCl (Blue) and sucrose (Green), and only LB (Orange). Cells were to 10 µg/mL gentamicin in M9 + the same concentration of the same osmolyte for 4 hours. All percent survival values are the average from viable cell densities of 3 biological replicates and 4-8 technical replicates for each. Error bars represent standard deviations.

5.3.4. The effect of antibiotic class on degree of cross-protection

According to variant background structures and mode of actions for different classes of antibiotics, we decided to study cross-protection effect against other antibiotics in the aminoglycoside (same) class and penicillin (other) class which have bactericidal effect. Osmotically stressed cells by NaCl and sucrose were challenged by 10 µg/mL (~3x MIC) kanamycin and showed higher survival in compare with cells grown in only background media (**Figure *5.7***)**.**The level of cross-protection against kanamycin was very similar to the one against gentamicin observed in **Figure *5.6***. Study of both kanamycin and gentamicin which are from the same sub-class of aminoglycosides, having similar MIC, shows similar effect on osmotically stressed cells. On the other hand, osmotically stressed cells treated with 5 (~2x MIC), and 10 µg/mL (~4x MIC) of ampicillin, an antibiotic from penicillin class, showed higher survival rate in compare with control (non-osmotically stressed cells). However, cross-protection level from same

concentration of sucrose and NaCl was exactly the opposite of what was observed for aminoglycosides. 15% sucrose protected more cells (8.2% and 0.34% survival) than NaCl (4.62% and 0.03% survival) while stressed *E. coli* was exposed to 5, and 10 µg/mL of ampicillin for 4 hours (**Figure *5.8***). NaCl and sucrose have different structures (ionic and non-ionic) and similarly antibiotics of different classes. So, it is interpreted that the variability of osmolytes and antibiotics might differently activate stress response systems of *E. coli*. Consequently, levels of tolerance induced by these two osmolytes cross-protection effects is different using different classes of antibiotics.

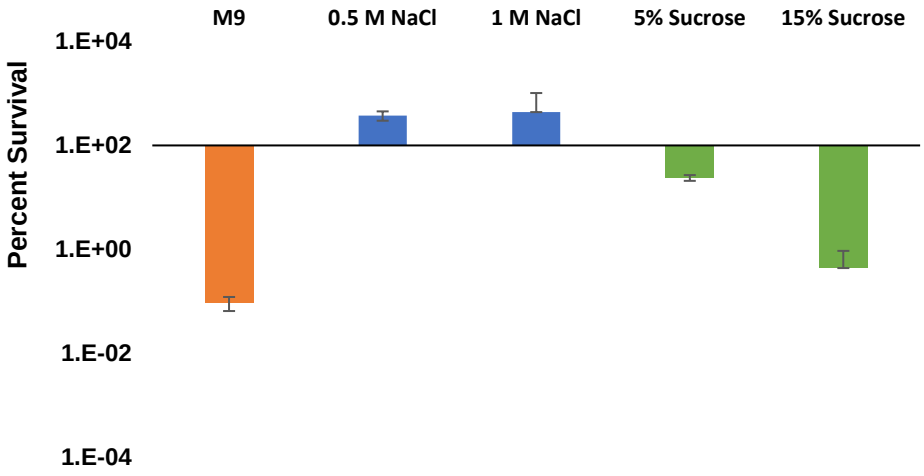

Figure 5.7 - Use of sucrose and NaCl cross-protect *E. coli* against kanamycin. O.N. cells were pre-incubated in LB + different concentrations of NaCl (blue), LB+ different concentrations of sucrose (green), or only LB (orange) and exposed to 10 µg/mL kanamycin in M9+ the same concentration of same osmolyte for 4 h. All percent survival values are the average from 3 biological replicates and 6-8 technical replicates for each. Error bars represent standard deviations.

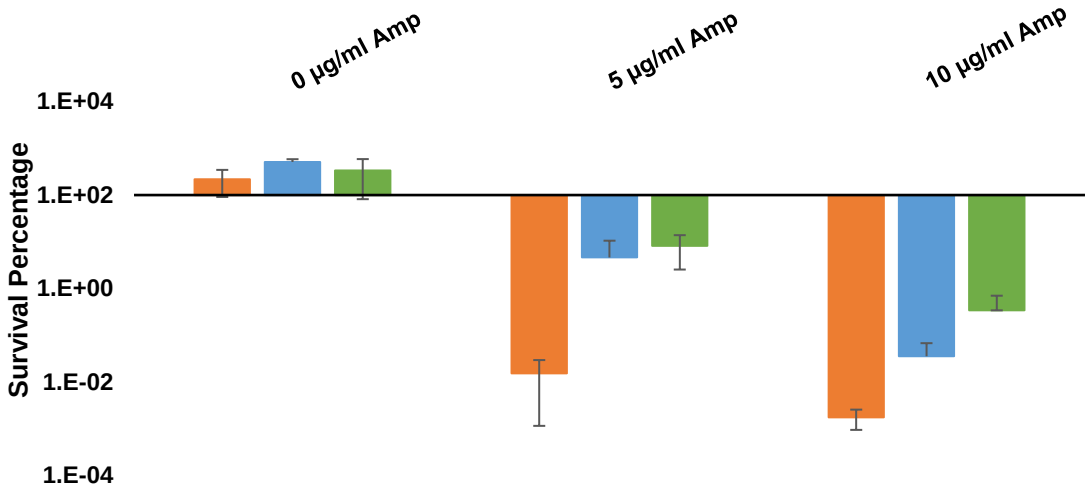

Figure 5.8 - Use of sucrose and NaCl cross-protect *E. coli* against ampicillin. O.N. cells were pre-incubated in LB + 0.5 M NaCl (blue), LB + 15% sucrose (green), or only LB (orange) and exposed to 0, 5, and 10 µg/mL ampicillin in M9+ the same concentration of the same osmolyte for 4 hours. All percent survival values are the average from 3 biological replicates and 3-4 technical replicates for each. Error bars represent standard deviations.

5.4. Discussion

Our results indicate that osmotic stress cross-protects *E. coli* cells against antibiotics. This cross protection is not evident in resistance (growth) assays, but rather in enhanced bacterial tolerance (cell survival) to antibiotic treatment. The osmolyte type and antibiotic affected the magnitude of the induced tolerance phenotype. Even though the concentrations of NaCl and sucrose used in this study apply similar osmotic stress (around 1 Osm/Kg), the cross-protection effect from these two molecules against different antibiotics was different (**Figure *5.6***, **Figure *5.7***, and **Figure *5.8***). We hypothesize that the difference between the stress response systems activated by sucrose and NaCl causes the difference in induced tolerance against aminoglycosides and penicillins which exhibit distinct killing mechanisms.

Among 300 genes which are significantly up- or down-regulated by osmotic stress in *E. coli*, 43% of the genes showed specific behavior by addition of high concentrations of NaCl and 37% of the genes showed specific behavior by the high sucrose treatment. Different effects on the cross-protection from these two osmolytes may be due to their different behavior on membrane polarization. Transcriptional responses affect K^+ flux and consequently the membrane

potential. Addition of high concentrations of NaCl to the growth media causes K^+ leakage from the cell and simultaneously, accumulation of Na^+ inside the cell, resulting in a depolarization effect. In contrast, sugar addition stimulates K^+ uptake and a hyperpolarization effect [30]. Aminoglycosides are hydrophilic, polycationic antibiotics with three to five ionizable amine groups. Membrane depolarization caused by NaCl addition may be reducing the cationic aminoglycoside entry through the membrane. Based on this lower permeation, it is expected to have lower antibiotic molecules inside the cell which reduces antibiotic effect on killing the cells. This behavior can explain the observation of higher cross-protection from NaCl molecules in compare with sucrose.

Another potential cause of the difference in cross protection level is the regulated stress response both osmolytes trigger within the cells. Both antibiotics and osmolytes activate stress response systems in the bacteria [31], [32]. Aminoglycosides act by binding the 30S ribosomal subunit, inhibiting part of the protein translation process [33]. In *E. coli*, the lethal mode of action of aminoglycosides is the complete inhibition of ribosome function or insertion of mistranslated proteins into the inner membrane and the periplasm [34]. These antibiotics, along with pH, osmolarity, and attachment to hydrophobic surfaces are among the diverse stimuli which modulate cell stress receptor module known as the Cpx two component system [35]. Protein misfolding in response to defective translational process or stressful environment can cause aggregation in the cell. Aggregation of one protein in the cell can increase the aggregation of other proteins by depleting the factors essential for proper protein folding. This phenomenon in most of the cases can lead cells to the death due to loss of function of the several proteins.

Bacteria have different strategies to be protected from aggregations and perform a protein quality control via ATP-dependent mechanisms and protease/chaperones synthesis [36]. This network is controlled by stress response pathways such as Cpx by inducing protease/chaperones synthesis such as DegP and DsbA (**Figure *5.10***) [37]. Direct interaction of the misfolded proteins

such as pilus subunits with the hydrophobic cleft on CpxP results in the release of CpxP from CpxA and CpxR phosphorylation to switch the Cpx system “on” (**Figure *5.9***) [38]. As a result of cells’ exposure to aminoglycosides, protein misfolding will activate Cpx system to express chaperones/proteases. Chaperones will prevent the aggregation of the misfolded proteins and proteases are able to degrade them [39].

It has been shown that gentamicin exposure also induces Cpx response due to misfolding of mistranslated proteins, though this exposure alone does not induce resistance, perhaps due to the competition between Cpx induction and cell killing [40]. On the other hand, recombinant expression of CpxA above basal levels did induce resistance to gentamicin exposure [40]. Similar to the gentamicin effect on Cpx induction for *E. coli* cells, transcriptional profiling and phenotypic analysis of *Pseudomonas aeruginosa* showed that the Amg system, a homolog of the Cpx system, is responsible for cells’ survival against aminoglycosides [41]. Moreover, in the absence of stressors, CpxP blocks the CpxA receptor from dimerizing and triggering a response. High salt concentrations activate the Cpx system in a partially CpxP-dependent manner by blocking the inhibition of the membrane-bound CpxA sensing domain by CpxP. CpxA then dimerizes, phosphorylating CpxR and initiating a stress signaling pathway. High NaCl concentrations, for example, trigger such a response by screening the electrostatic interaction between the positively charged patch on the convex surface of CpxP and the negatively charged sensing domain of CpxA [38], [42], [43], which switches the Cpx system “on” via CpxA phosphorylation activity (**Figure *5.9*-A**) [38]. Non-ionic sucrose, on the other hand, is not expected to screen the CpxP-CpxA interaction (**Figure *5.9*-B**).

In this context, we hypothesize that the higher cross-protection effect of NaCl compared to sucrose against aminoglycosides is due to the overlap of Cpx activation by NaCl as an ionic osmolyte and the similarity of gentamicin and kanamycin as aminoglycosides (**Figure *5.4***, **Figure *5.5***, **Figure *5.6*** and **Figure *5.7***). Additionally, there are efflux pumps such as AcrD specific for

aminoglycosides which have been shown to get highly expressed by Cpx activation (**Figure *5.10***) [44], [45]. Based on this information, we expect that higher activity of Cpx system through NaCl increases the synthesis of such efflux pumps and help higher survival during aminoglycoside treatment.

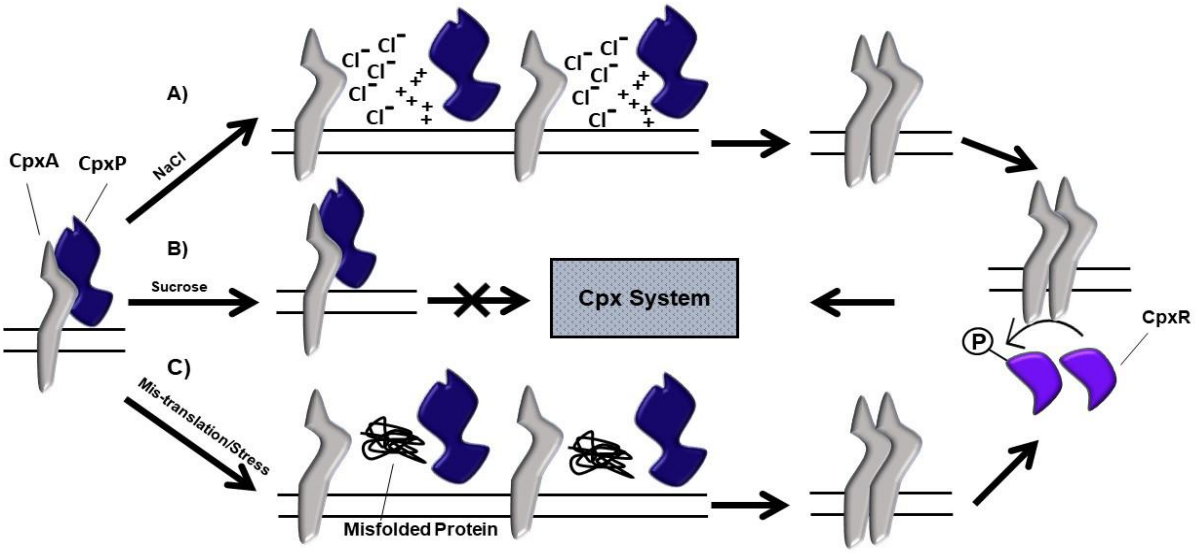

Figure 5.9 - Cpx activation mechanism. CpxP is an inhibitor molecule for Cpx system. CpxP should be dissociated from CpxA molecule to let it phosphorylate CpxR and activate the Cpx system. There are different ways of titrating CpxP from CpxA molecule. **A)** Presence of NACl molecules will make Cl^- ions to interact with positively charged patch on the concave surface of the CpxP. **B)** sucrose presence will not help the CpxA and CpxP dissociation and cannot activate the Cpx system. **C)** Presence of misfolded proteins and hydrophobic interaction between CpxP and hydrophobic parts of them leads to Cpx activation through CpxA dimerization and subsequent phosphorylation of CpxR.

The relative cross protection effects of NaCl and sucrose, however, were reversed for ampicillin, a beta-lactam related to penicillin class of antibiotics. While a molecular mechanism for this effect remains uncharacterized, sucrose induces cross-protection in *E. coli* at higher levels than NaCl [46]. In our study, we observed the similar behavior for the osmotically stressed cells treated with ampicillin (**Figure *5.7***). Even though the addition of sucrose and NaCl to the background media help cells survival more than non-stressed media, this cross-protection was higher with sucrose.

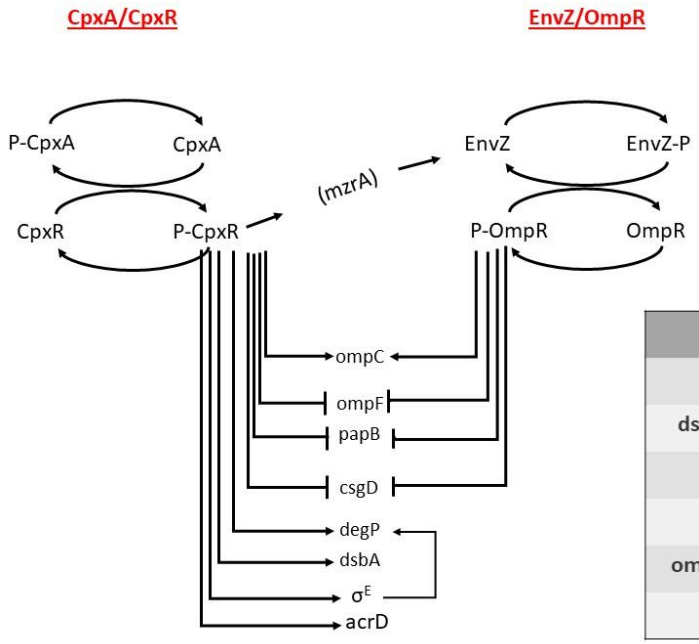

Gene	Role
σ^E	Extra-cytoplasmic stress response
dsbA/degP	Chaperone/Protease
csgD	Flagella synthesis (motility)
papB	Pilus synthesis (adhesion)
ompC/ompF	Outer membrane porins
acrD	Efflux pump

Figure 5.10 - A brief summary on the genes activated by Cpx and the cross-talk between CpxA/CpxR and EnvZ/OmpR. Several genes are regulated by CpxA/CpxR system to provide different functions for protecting cell membrane against stressors. Some of the genes are regulated by EnvZ/OmpR system as well. The table on the side shows the function of each gene which lead to cell protection in different situations.

Different cross-protection effects from these two osmolytes can be due to the difference in the extent of the stress response systems induced by them and consequently the overlap between the mechanism of their action with different antibiotics.

According to the obtained results, stress application to the cells prepares them for the second stressor due to the activation of the stress response mechanisms. Here, we found very limited information on tolerance/resistance of the cells. According to the previous studies and our findings in this study, we found out that the cross-protection against antibiotic through resistance phenotype is only a few folds but its effect on cell tolerance is around 2-3 log folds. This observation indicates the importance of study on the tolerance phenotype and distinguishing the responsible systems for resistance and tolerance. Also, as observed in this study, the cross-protection effect differs according to the type/concentration of the osmolyte and concentration of the antibiotic. This variable effect in the body is usually reflected by delivery methods of the drugs and the final concentration and environment they ended up with in different organs of the host.

Therefore, antibiotic tolerance/resistance of different pathogens all over the body is affected not only by the used antibiotic, but also by the varied environment of the host which may provide niches to activate different stress responses with variable intensities. As a result, cross-protection against heterogenous concentrations of antibiotics emerges through host-derived stresses with variable levels of survival. By performing gene-sequencing and getting more information on the specific stress response systems for responding to sucrose and NaCl we can find the main systems which manifest different degrees of cross-protection. By targeting those genetic mechanisms causing tolerance phenotypes we can inhibit the emergence of genetic resistance and enhance the antibiotic effectiveness for infections formed by antibiotic-resistant/tolerant pathogens.

5.5. References

[1] K. Mitosch and G. Rieckh, “Noisy Response to Antibiotic Stress Predicts Subsequent Single-Cell Survival in an Acidic Article Noisy Response to Antibiotic Stress Predicts Subsequent Single-Cell Survival in an Acidic Environment,” *Cell Syst.*, vol. 4, no. 4, pp. 393-403.e5, 2017.

[2] S. Galdiero *et al.*, “Microbe-Host Interactions: Structure and Role of Gram-Negative Bacterial Porins,” *Curr. Protein Pept. Sci.*, vol. 13, pp. 843–854, 2012.

[3] M. A. S. Mcmahon *et al.*, “Environmental Stress and Antibiotic Resistance in Food-Related Pathogens,” *Appl. environmen*, vol. 73, no. 1, pp. 211–217, 2007.

[4] D. E. N. Rangel, “Stress induced cross-protection against environmental challenges on prokaryotic and eukaryotic microbes,” *World. J. Microbiol. Biotechnol.*, vol. 27, pp. 1281–1296, 2011.

[5] D. R. Andrade-linares, A. Lehmann, and M. C. Rillig, “Microbial stress priming: a meta-analysis,” *Environ. Microbiol.*, vol. 18, no. 4, pp. 1277–1288, 2016.

[6] S. Galdiero *et al.*, “Microbe-Host Interactions : Structure and Role of Gram-Negative Bacterial Microbe-Host Interactions : Structure and Role of Gram-Negative Bacte- rial Porins,” no. December, 2012.

[7] U. S. Centers and D. Control, “Antibiotic Resistance Threats in the United States, 2019,” 2019.

[8] J. O’Neill, R. on Antimicrobial Resistance, and E. Wellcome Trust (London, *Tackling Drug-resistant Infections Globally: Final Report and Recommendations*. Review on Antimicrobial Resistance, 2016.

[9] W. Wang *et al.*, “Antibiotic resistance: a rundown of a global crisis,” *Infect. Drug Resist.*, vol. 11, pp. 1645–1658, 2018.

[10] M. Zhu and X. Dai, “High Salt Cross-Protects *Escherichia coli* from Antibiotic Treatment through Increasing Efflux Pump Expression,” *mSphere*, vol. 3, no. 2, pp. 1–8, 2018.

[11] X. Liao *et al.*, “Interplay of antibiotic resistance and food-associated stress tolerance in foodborne pathogens,” *Trends Food Sci. Technol.*, vol. 95, no. July 2019, pp. 97–106, 2020.

[12] T. R *et al.*, “Mechanisms of Bacterial Tolerance and Persistence in the Gastrointestinal and Respiratory Environments,” *Clin. Microbiol. Rev.*, vol. 31, no. 4, pp. 1–46, 2018.

[13] A. Brauner, N. Shoresh, O. Fridman, and N. Q. Balaban, “An Experimental Framework for Quantifying Bacterial Tolerance,” *Biophysj*, vol. 112, no. 12, pp. 2664–2671, 2017.

[14] J. Liu, O. Gefen, I. Ronin, M. Bar-meir, and N. Q. Balaban, “Effect of tolerance on the evolution of antibiotic resistance under drug combinations,” *Science (80-.).*, vol. 367, no. 6474, pp. 200–204, 2020.

[15] F. Corona and J. L. Martinez, “Phenotypic Resistance to Antibiotics,” *Antibiotics*, vol. 2, pp.

237–255, 2013.

[16] D. M. Livermore and D. F. J. Brown, “Detection of beta-lactamase-mediated resistance,” *J. Antimicrob. Chemother.*, vol. 58, pp. 59–64, 2001.

[17] A. Brauner, O. Fridman, O. Gefen, and N. Q. Balaban, “Distinguishing between resistance, tolerance and persistence to antibiotic treatment,” *nrmicro*, vol. 14, pp. 320–330, 2016.

[18] E. Tuomanen, D. T. Durack, and A. Tomasz, “Antibiotic Tolerance among Clinical Isolates of Bacteria,” *Antimicrob. Agents Chemother.*, pp. 521–527, 1986.

[19] B. R. Levin and D. E. Rozen, “Non-inherited antibiotic resistance,” *Nat. Rev.* | *Microbiol.*, vol. 4, no. July, pp. 556–562, 2006.

[20] I. Levin-reisman, A. Brauner, I. Ronin, and N. Q. Balaban, “Epistasis between antibiotic tolerance , persistence , and resistance mutations,” *PNAS*, vol. 116, no. 4, pp. 14734–14739, 2019.

[21] N. Q. Balaban *et al.*, “Definitions and guidelines for research on antibiotic persistence,” *Nat. Rev. Microbiol.*, vol. 17, no. July, pp. 441–448, 2019.

[22] N. R. Cohen, M. A. Lobritz, and J. J. Collins, “Microbial Persistence and the Road to Drug Resistance,” *Cell Host Microbe*, vol. 13, no. 6, pp. 632–642, 2013.

[23] L. Fernández-García *et al.*, “Relationship between Tolerance and Persistence Mechanisms in Acinetobacter baumannii Strains with AbkAB Toxin- Antitoxin System,” *Antimicrob. Agents Chemother.*, vol. 62, no. 5, pp. 1–7, 2018.

[24] M. Begley, C. G. M. Gahan, and C. Hill, “Bile Stress Response in Listeria monocytogenes LO28: Adaptation, Cross-Protection , and Identification of Genetic Loci Involved in Bile Resistance,” *Appl. Environ. Microbiol.*, vol. 68, no. 12, pp. 6005–6012, 2002.

[25] A. A. Al-nabulsi *et al.*, “Effects of osmotic pressure , acid , or cold stresses on antibiotic susceptibility of Listeria monocytogenes,” *Food Microbiol.*, vol. 46, pp. 154–160, 2015.

[26] D. E. Jenkins, J. E. Schultz, and A. Matin, “Starvation-Induced Cross Protection against Heat or H202 Challenge in *Escherichia coli*,” *J. Bacteriol.*, vol. 170, no. 9, pp. 3910–3914, 1988.

[27] A. C. Graf *et al.*, “Virulence Factors Produced by *Staphylococcus aureus* Biofilms Have a Moonlighting Function Contributing to Biofilm Integrity Authors Virulence Factors Produced by *Staphylococcus aureus* Biofilms Have a Moonlighting Function Contributing to Biofilm Integrity,” *Mol. Cell. Proteomics*, vol. 18, pp. 1036–1053, 2019.

[28] U. Romling and C. Balsalobre, “Biofilm infections, their resilience to therapy and innovative treatment strategies,” *J. Intern. Med.*, vol. 272, pp. 541–561, 2012.

[29] J. W. Lee, S. Choi, J. H. Park, C. E. Vickers, L. K. Nielsen, and S. Y. Lee, “Development of sucrose-utilizing *Escherichia coli* K-12 strain by cloning β -fructofuranosidases and its application for L-threonine production,” *Appl. Microbiol. Biotechnol.*, vol. 88, pp. 905–913, 2010.

[30] L. Shabala, J. Bowman, J. Brown, T. Ross, T. Mcmeekin, and S. Shabala, “Ion transport and osmotic adjustment in *Escherichia coli* in response to ionic and non-ionic osmotica,” *Environ. Microbiol.*, vol. 11, no. 1, pp. 137–148, 2009.

[31] E. Batchelor, D. Walthers, L. J. Kenney, and M. Goulian, “The *Escherichia coli* CpxA-CpxR Envelope Stress Response System Regulates Expression of the Porins OmpF and OmpC The *Escherichia coli* CpxA-CpxR Envelope Stress Response System Regulates Expression of the Porins OmpF and OmpC,” *J. Bacteriol.*, vol. 187, no. 16, pp. 5723–5731, 2005.

[32] K. Mitosch and G. Rieckh, “Noisy Response to Antibiotic Stress Predicts Subsequent Single-Cell Survival in an Acidic Article Noisy Response to Antibiotic Stress Predicts Subsequent Single-Cell Survival in an Acidic Environment,” *Cell Syst.*, vol. 4, no. 4, pp. 393–403, 2017.

[33] E. Cudic, K. Surmann, G. Panasia, E. Hammer, and S. Hunke, “The role of the two-component systems Cpx and Arc in protein alterations upon gentamicin treatment in *Escherichia coli*,” *BMC Micorbiology*, vol. 17, no. 1, pp. 1–17, 2017.

[34] M. A. Kohanski, D. J. Dwyer, J. Wierzbowski, G. Cottarel, and J. J. Collins, “Mistranslation of Membrane Proteins and Two-Component System Activation Trigger Antibiotic-Mediated Cell Death,” *Cell*, vol. 135, pp. 679–690, 2008.

[35] P. Hoernschemeyer and S. Hunke, “New insights into stimulus detection and signal propagation by the Cpx-envelope stress system,” in *Stress and Environmental Regulation of Gene Expression and Adaptation in Bacteria, I&II*, 2016, pp. 1025–1030.

[36] N. G. Bednarska, J. Schymkowitz, F. Rousseau, and J. Van Eldere, “Protein aggregation in bacteria: the thin boundary between functionality and toxicity,” *Microbiology*, vol. 159, pp. 1795–1806, 2013.

[37] C. L. Hews, T. Cho, G. Rowley, and T. L. Raivio, “Maintaining Integrity Under Stress: Envelope Stress Response Regulation of Pathogenesis in Gram-Negative Bacteria,” *Front. Cell. Infect. Microbiol.*, vol. 9, no. 313, pp. 1–25, 2019.

[38] X. Zhou, R. Keller, R. Volkmer, N. Krauss, P. Scheerer, and S. Hunke, “Structural Basis for Two-component System Inhibition and Pilus Sensing by the Auxiliary CpxP Protein,” *J. Biol. Chem.*, vol. 286, no. 11, pp. 9805–9814, 2011.

[39] J. Pogliano, A. S. Lynch, D. Belin, E. C. C. Lin, and J. Beckwith, “Regulation of *Escherichia*

coli cell envelope proteins involved in protein folding and degradation by the Cpx two-component system," *Genes Dev.*, vol. 11, pp. 1169–1182, 1997.

[40] T. F. Mahoney and T. J. Silhavy, "The Cpx Stress Response Confers Resistance to Some, but Not All, Bactericidal Antibiotics," *J. Bacteriol.*, vol. 195, no. 9, pp. 1869–1874, 2013.

[41] S. Lee *et al.*, "Targeting a bacterial stress response to enhance antibiotic action," *PNAS*, vol. 106, no. 34, pp. 14570–14575, 2009.

[42] S. Hunke, R. Keller, and V. S. Mu, "Signal integration by the Cpx-envelope stress system," *FEMS Microbiol. Lett.*, vol. 326, pp. 12–22, 2012.

[43] K. Tschauner, P. Hornschemeyer, V. S. Muller, and S. Hunke, "Dynamic Interaction between the CpxA Sensor Kinase and the Periplasmic Accessory Protein CpxP Mediates Signal Recognition in E . coli," *PLoS One*, vol. 9, no. 9, 2014.

[44] T. L. Raivio, "Everything old is new again: An update on current research on the Cpx envelope stress response," *Biochim. Biophys. Acta*, vol. 1843, no. 8, pp. 1529–1541, 2014.

[45] H. Hirakawa, K. Nishino, T. Hirata, and A. Yamaguchi, "Comprehensive Studies of Drug Resistance Mediated by Overexpression of Response Regulators of Two-Component Signal Transduction Systems in *Escherichia coli*," *J. Bacteriol.*, vol. 185, no. 6, pp. 1851–1856, 2003.

[46] D. Greenwood and F. O. Grady, "The effect of osmolality on the response of *Escherichia coli* and *proteus mirabilis t*o penicillins," *Br. J. Exp. Pathol.*, vol. 53, no. 4, pp. 457–464, 1972.

Chapter 6
Conclusion and future work

6.1. Conclusion

Absolute numbers of infections due to resistant microbes are increasing globally and become problematic. So, it is required to find new strategies to combat infection and aim for new diagnostic tools to determine susceptibility of the microbes causing infection. As a result, my PhD thesis studied mechanisms used by bacteria to survive in stressful environments by developing new tools and new strategies to understand and combat these natural survival mechanisms.

Results of *in vitro* experiments are not often relevant to bacterial infections *in vivo* [1], [2].. Better experimental methods that more accurately recapitulate *in vivo* observations are required. Dynamic biofilm studies *in vitro* promise to bridge this gap because biofilm phenotypes more closely resemble those found *in vivo* than experiments on conventional planktonic cultures [3], [4]. In addition, *in vitro* biofilm models can also provide environments of reduced complexity compared to the *in vivo* host environment, allowing for detailed studies of molecular mechanisms and microbial interactions not possible *in vivo*. For example, Chapter 2 describes iron competition between *Escherichia coli* Nissle and *Salmonella enterica* serovar Typhimurium during infection in the gut. This competition has been studied in murine models, but the chemical complexity of animal models precludes some specific insights into chemical mechanisms of this competition. As a complementary method, using microfluidic devices model to study iron competition between *E. coli* and *S. enterica* in coculture biofilms gave us similar competition outcomes as animal models while also elucidating inter-species interactions that highlighted the role of microcin concentrations and siderophore piracy in mediating this competition. Our biofilm model showed that, once secreted, siderophores are taken up bidirectionally by *E. coli* and *S. enterica*, which enhances *S. enterica* competitiveness in the gut, but is also exploited by *E. coli* Nissle to outcompete *S. enterica.* Based on these results, the capability of exploiting microcin piracy for treating specific pathogens seems a promising therapeutic strategy.

The ability to separate signaling and metabolite-based interactions is another advantage of these *in vitro* chemostatic and dynamic models in comparison with *in vivo* models. Chapter 4 describes another *in vitro* model applied to understand the interactions between host microbiomes and pathogens during wound infections. The perfusion meat model exhibits similar benefits of using a dynamic liquid flow environment for *in vitro* experiments. This biologically relevant model supported the growth of a multispecies biofilm and interactions between host microbiota and pathogens. Metabolomic analysis after standard anti-infective treatments represent initial steps towards identifying biomarkers of effective or ineffective therapies. These results showed higher similarity to the physiologically relevant conditions than the static models, presumably due to the morphological complexities and dynamic nature of the perfused meat environment. This perfusion meat model could substitute for *in vivo* experiments in a more cost effective and high throughput manner and provides important information on the effect of different antibacterial treatments on each member of the community, such as host microbiota and pathogens. Such models can be used to correlate *in vitro* therapy outcomes with specific biomarkers or metabolic fingerprints that will pave the way for the development of more effective treatments of wound infections.

The morphological complexity of biofilms is one of the main causes of antibiotic resistance due to the creation of niches that support the development of resistance [5], [6]. For example, cells in biofilms experience osmotic stress [7], which may be due to the presence of concentrated osmolytes in the biofilm extracellular matrix. In chapter 3 we studied a specific biosynthetic and molecular mechanism that bacteria use to survive this osmotic stress. As a result of growth inhibition by the presence of osmotic stress in the cell environment, inhibiting the stress response mechanism of *E. coli* cells can be helpful in preventing *E. coli* biofilm growth. This strategy can be used for preventing other pathogens causing infection by growing as a biofilm on wound or medical device interfaces. The inhibitor molecule used in this study is a potential drug for

combating *E. coli* biofilms. More generally, this work shows that targeting stress response pathways is a promising strategy for the development of new anti-biofilm and antimicrobial drugs.

While the major focus of antimicrobial therapies is on finding an effective treatment while avoiding antibiotic resistance, tolerance phenotypes significantly contribute to treatment failure and represent an under-studied area of direct clinical relevance. Tolerance is triggered by a group of common stress response mechanisms and supports the emergence of resistance in bacterial cells [6]. Our studies in Chapter 5 showed that by activating a bacterial stress response, such as to osmotic stress, cells become more tolerant to antibiotics and survival rate is increased by orders of magnitude, even though the conventional resistance is relatively unchanged. The osmolyte selection for applying osmotic stress and the class of antibiotic applied both affect the degree of induced tolerance. Finding the induced stress response systems for each stressor through gene sequencing is the next step to identifying the cross-protection mechanism. Additionally, identifying the genetic mechanisms causing tolerance phenotypes will inform strategies to inhibit them and potentially suppress the emergence of genetic resistance, which is inherited to the new cells. Genetic markers of tolerance will also be helpful in identifying environmental niches, such as in biofilms, which induce cross-protection and support tolerant phenotypes. The pharmacokinetics of antimicrobial compound distribution in the body suggest that one should expect a broad distribution of antibiotic concentrations and gradients throughout the host. Consequently, pathogens may have different susceptibilities to applied therapeutics. The varied environment of the host may provide niches that induce cross-protection against antibiotics, the heterogeneous distribution of antibiotics themselves may cross-protect pathogens against higher concentrations of the same or related drugs, or they may induce cross-protection against host-derived stresses. My work provides critical preliminary information on mechanisms and phenotypes of tolerance that will inform design of new antimicrobial treatments in this emerging area of research.

6.2. References

[1] C. B. Ibberson *et al.*, “Co-infecting microorganisms dramatically alter pathogen gene essentiality during polymicrobial infection,” vol. 17079, no. May, pp. 1–6, 2017.

[2] D. M. Cornforth, J. L. Dees, C. B. Ibberson, H. K. Huse, I. H. Mathiesen, and K. Kirketerp-møller, “*Pseudomonas aeruginosa* transcriptome during human infection,” vol. 115, no. 22, 2018.

[3] D. Lindsay and A. Von Holy, “Bacterial biofilms within the clinical setting : what healthcare professionals should know,” 2006.

[4] K. K. Jefferson, “What drives bacteria to produce a biofilm ?,” vol. 236, pp. 163–173, 2004.

[5] O. Ciofu and T. Tolker-nielsen, “Tolerance and Resistance of *Pseudomonas aeruginosa* Biofilms to Antimicrobial Agents — How *P . aeruginosa* Can Escape Antibiotics,” vol. 10, no. May, 2019.

[6] I. Levin-reisman, I. Ronin, O. Gefen, and I. Braniss, “Antibiotic tolerance facilitates the evolution of resistance,” vol. 830, no. February, pp. 826–830, 2017.

[7] P. S. Stewart, M. J. Franklin, K. S. Williamson, J. P. Folsom, L. Boegli, and A. James, “Contribution of Stress Responses to Antibiotic Tolerance in P*seudomonas aeruginosa* Biofilm,” vol. 59, no. 7, pp. 3838–3847, 2015.